

To my family.

## ACKNOWLEDGEMENTS

First of all, I want to thank my advisor Doctor Pedro Bouchon for his guidance, his patience, his advices, and most of all, for believing in me. I really appreciate his concern at the academic level, but also his commitment with me as a person, always encouraging me to be better in every sense, giving me support when I most needed.

I am also very grateful to Doctor Christopher Brown. He gave me valuable advice during my visits to his lab at the Worcester Polytechnic Institute. He was incredibly warm and he took care of me beyond his obligations. Thank you professor for sharing your experiences and your knowledge with me, and for making me feel at home during the periods that I spent away from my family.

To the members of the Committee, Doctor Sergio Almonacid, Doctor Claudio Gelmi, Doctor Franco Pedreschi and Doctor Cristián Vial, thank you for your comments and for helping me to improve my work.

To all my friends from the University, Anita Gazmuri, Verónica Dueik, Mariel Farfán, Loreto Muñoz, Rommy Zúñiga, Wenceslao Medina, Cecilia Aguilera, Rossmery Cuadros, Pablo Cortés, Nicolás Ovalle, Salomé Mariotti, Fabián Reyes, Fredy Urrego, Gonzalo Núñez, Tere Molina and Trini. Thank you all for our discussions and for your camaraderie.

To the secretaries Hilda Agurto, Verónica Armijo, María Inés Valdebenito, Debbie Meza and Danisa Herrera, thank you for being always available to help me and for been so efficient. To the staff from the Chemical and Bioprocess Engineering Department, Samuel Torres, Ricardo Cayupe, Ulises, Rosa, Jacky and José, thank you for helping me every time that I needed.

To my father, Oscar, thank you for your advices, your wisdom, for our long talks and for having always the right words for me. To my mother, Laura, thank you for your unconditional love, for being always so concerned about me and for trying to help me in every sense. I hope to make you both proud.



To my brother Oscar, thank you for your love and concern, and for our talks. To my sister Francisca, thank you for all the times that you helped me with the babies. To my sister Alejandra, her husband Carlos Andrés, and his mother in law Marta, thank you for receiving me and spent time with me during my visits to Colombia and the US.

To my husband, Pablo, he has been so perceptive, patient and supportive. He took full care of our three babies, Pablo, Héctor and Oscar, so I could finish my studies. I really appreciate his effort and his love and I will be always grateful.

I honestly believe that the most difficult part of carrying out a PhD is not the research itself nor the publications, not even the thesis, the real challenge goes beyond that, and is the test of the strength of the person, its perseverance and its persistence. The most valuable learning that PhD students can acquire is to realize what are they made off and who they really are. During my studies I pass through excellent moments, but also through difficult ones, and without all the help and support that I received from all the above mentioned people, I would not have being able to get to the end.

From the bottom of my heart,

Thank you all!

Carito

Financial support:

I really appreciate the financial support of the National Commission for Scientific and Technological Research (CONICYT), the School of Engineering at Pontificia Universidad Católica de Chile, and the Research Vicerectory (VRI) of Pontificia Universidad Católica de Chile.

## LIST OF CONTENTS

ACKNOWLEDGEMENTS .....	ii
FIGURES INDEX.....	1
TABLES INDEX .....	8
RESUMEN.....	9
ABSTRACT.....	13
LIST OF PAPERS .....	17
PROCEEDINGS .....	18
AWARDS .....	19
NOMENCLATURE AND ABBREVIATIONS.....	20
I. Introduction.....	22
I.1. Hypothesis and objectives.....	27
I.2. Outline of the thesis .....	28
II. Evaluating the Ability of Different Characterization Parameters to Describe the Surface of Fried Foods .....	31
II.1. Introduction.....	31
II.2. Materials and Methods.....	34
II.2.1. Sample Preparation .....	34
II.2.2. Moisture Content Measurement.....	34
II.2.3. Surface Texture Measurement .....	35
II.2.4. Surface Image Acquisition .....	36
II.2.5. Surface Analysis .....	36
II.2.5.1. Conventional Parameters .....	36
II.2.5.2. Area-Scale Fractal Analysis.....	36
II.2.5.3. Analysis of the Size of the Measured Region .....	37
II.2.6. Statistical Analysis.....	38
II.3. Results.....	38

II.4.	Discussion .....	44
II.5.	Conclusions .....	45
III.	Effect of food surface roughness on oil uptake by deep-fat fried products .....	46
III.1.	Introduction .....	46
III.2.	Materials and methods .....	49
III.2.1.	Materials .....	49
III.2.2.	Product formulation .....	49
III.2.3.	Sample preparation .....	50
III.2.4.	Frying .....	51
III.2.5.	Analytical methods .....	51
III.2.6.	Surface analysis .....	52
III.2.6.1.	Surface measurement .....	52
III.2.6.2.	Surface characterization .....	53
III.2.7.	Digital image acquisition .....	54
III.2.8.	Statistical analysis .....	54
III.3.	Results and discussion .....	55
III.3.1.	Surface topography .....	56
III.3.2.	Total oil content .....	59
III.3.3.	Penetrated and surface oil contents .....	64
III.4.	Discussion and Conclusions .....	67
IV.	Microstructural characterization of deep-fat fried formulated products using confocal scanning laser microscopy and a non-invasive double staining procedure .....	68
IV.1.	Introduction .....	68
IV.2.	Materials and methods .....	72
IV.2.1.	Materials .....	72
IV.2.2.	Product formulation .....	72
IV.2.3.	Product preparation .....	73
IV.2.4.	Microstructural observation .....	75
IV.2.5.	Image restoration .....	75
IV.2.6.	Image visualization .....	76

IV.2.7.	Image segmentation .....	76
IV.2.8.	Image analysis .....	78
IV.2.9.	Porosity by pycnometry.....	79
IV.2.10.	Statistical analysis .....	79
IV.3.	Results and discussion .....	80
IV.3.1.	Fluorescent labeling .....	80
IV.3.2.	Qualitative analysis of inner microstructure.....	81
IV.3.3.	Quantitative analysis of inner microstructure.....	85
IV.4.	Conclusions .....	91
V.	Understanding the relationship of structural, textural and wetting related parameters with oil uptake in deep-fat fried formulated products .....	93
V.1.	Introduction .....	93
V.2.	Materials and methods .....	99
V.2.1.	Materials.....	99
V.2.2.	Product preparation.....	99
V.2.3.	Geometry measurement.....	100
V.2.4.	Texture measurement .....	101
V.2.5.	Contact angle measurement.....	102
V.2.6.	Digital image sequence acquisition of the frying process .....	104
V.2.7.	Statistical analysis and variables normalization.....	104
V.3.	Results and discussion .....	104
V.3.1.	Expansion kinetics and product geometry .....	104
V.3.2.	Texture .....	110
V.3.3.	Contact Angle .....	111
V.4.	Conclusions .....	115
VI.	Discussion and Conclusions.....	117
References	.....	123

## FIGURES INDEX

<b>Figure I.1:</b> Schematic diagram of simultaneous heat transfer (left hand side of the figure) and mass transfer (right hand side of the figure) during deep-fat frying .....	23
<b>Figure I.2:</b> Diagram showing the 3 locations of oil in the product microstructure after deep-fat frying adapted from Bouchon et al. (2003).....	25
<b>Figure I.3:</b> Schematic diagram describing product formulation by an engineering approach. ....	26
<b>Figure I.4:</b> Thesis general structure .....	30
<b>Figure II.1:</b> Scanning laser microscope setup.....	35
<b>Figure II.2:</b> Photograph of the surface of products A, B, and C. The size of the photographed region of each product is $2 \times 2 \text{ cm}^2$ .....	38
<b>Figure II.3:</b> Coefficient of variation (COV) of conventional parameters ( $S_q$ and $S_{ku}$ ) and area-scale fractal parameters (SRC and fractal dimension) for the surface of product A as a function of the size of the measured region. ....	39
<b>Figure II.4:</b> Conventional surface parameters $S_q$ and $S_{ku}$ of products A, B, and C. Mean values of six measures $\pm$ standard deviation are shown. The charter inside each bar indicates significant differences.....	40
<b>Figure II.5:</b> Area scale plot of products A, B, and C. Mean values of relative areas of six measures $\pm$ standard deviation are shown. ....	41
<b>Figure II.6:</b> Results of scale-based F-test of significance with 95% confidence when comparing six measures of products A and B. The mean square ratio (MSR) is plotted as a function of the scale. The threshold of differentiation between the surfaces is	

determined by a MSR of 4.26. The scales over which both surfaces are different are shown in the plot. ....42

**Figure II.7:** Results of scale-based F-test of significance with 95% confidence when comparing six measures of products A and C. The mean square ratio (MSR) is plotted as a function of the scale. The threshold of differentiation between the surfaces is determined by a MSR of 4.26. The scales over which both surfaces are different are shown in the plot. ....42

**Figure II.8:** Results of scale-based F-test of significance with 95% confidence when comparing six measures of products B and C. The mean square ratio (MSR) is plotted as a function of the scale. The threshold of differentiation between the surfaces is determined by a MSR of 4.26. The scales over which both surfaces are different are shown in the plot. ....43

**Figure II.9:** Area-scale fractal parameters SRC and fractal dimension of products A, B, and C. Mean values of six measures  $\pm$  standard deviation are shown. The charter inside each bar indicates significant differences. ....44

**Figure III.1:** : Diagram showing a sequence of three tiling exercises on a gluten-based product (12G) measured at 10  $\mu$ m sampling interval over a 5x5 mm<sup>2</sup> surface region. From the bottom to the top, the size of the triangular patch, or scale, decreases progressively, and the relative area increases. ....53

**Figure III.2:** Photographs of the surface (left) and representation of the measured topography (right) of deep-fat fried potato-flake-based product (PF on top) and gluten-based product (12G at the bottom). Each surface measure was acquired with a 10 lm sampling interval on x and y directions. Note that the color scales that represent the z dimension are different in the two products.....56

**Figure III.3:** Area-scale plots of gluten-based products. Relative area values correspond to the mean of six measures  $\pm$  standard deviation at each scale of observation. Larger relative areas indicate greater surface roughness. ....57

**Figure III.4:** Area-scale plots of potato-flake-based products. Relative area values correspond to the mean of six measures  $\pm$  standard deviation at each scale of observation. Larger relative areas indicate greater surface roughness. ....59

**Figure III.5:** Total oil (TO) content of formulated products after two cooling times, 2 s and 10 min. Values correspond to the mean of 5 measures  $\pm$  standard deviation. The same letter inside two bars indicates no significant differences in TO content between G-based products (lowercase letters) and between PF-based products (uppercase letters). 60

**Figure III.6:** Results of scale-based correlation test applied to potato-flake-based products and gluten-based products. Least squares regression coefficients ( $R^2$ ) for relative area as a function of total oil content are plotted versus the scale of observation. Possible scales of interaction for each product category are indicated in the plot. ....62

**Figure III.7:** Total oil content vs. relative area of potato-flake-based products and gluten-based products at candidate scales of interaction of  $1793 \mu\text{m}^2$  and  $19,920 \mu\text{m}^2$ , respectively. Least squares regression coefficients ( $R^2$ ) are shown. ....63

**Figure III.8:** Penetrated oil (PO) content of formulated products, at two cooling times, expressed as a fraction of total oil (TO) content after 10 min of cooling, or final TO content. Values correspond to the mean of 5 measures  $\pm$  standard deviation. The same letter inside two bars indicates no significant differences in PO content between G-based products (lowercase letters) and between PF-based products (uppercase letters). ....66

**Figure III.9:** Surface oil (SO) content of formulated products, at two cooling times, expressed as a fraction of total oil (TO) content after 10 min of cooling, or final TO content. Values correspond to the mean of 5 measures  $\pm$  standard deviation. The same

letter inside two bars indicates no significant differences in SO content between G-based products (lowercase letters) and between PF-based products (uppercase letters). .....66

**Figure IV.1:** Dough preparation and staining protocol.....74

**Figure IV.2:** Example of image segmentation procedure performed in a focal plane of a 12G product: (A) Original image, (B) Empty pores outlined after segmentation using “L” coordinate thresholding, (C) Pores filled with oil outlined after segmentation using “a” coordinate thresholding, (D) Segmented solid matrix. In this image:  $PO_{ia} = 20.4\%$  and  $\epsilon_{ia} = 30.4\%$ .....77

**Figure IV.3:** Digital photographs of unstained 8G+MC (left) and PF+NS (right) fried products (170°C). .....81

**Figure IV.4:** Focal planes of G-based products where the solid matrix (green), the oil (red) and the empty pores (black) can be observed.....83

**Figure IV.5:** Focal planes of PF-based products where the solid matrix (green), the oil (red) and the empty pores (black) can be observed.....84

**Figure IV.6:** Penetrated oil content determined by soxhlet extraction ( $PO_{soxhlet}$ ) v/s porosity determined by image analysis ( $\epsilon_{ia}$ ) of fried products. Least squares regression coefficient ( $R^2$ ) is shown for G-based products. Oil content values were taken from Moreno et al. (2010). Mean values  $\pm$  standard deviation are presented. ....86

**Figure IV.7:** Mean values of porosity determined by image analysis ( $\epsilon_{ia}$ ) v/s mean values of porosity determined by pycnometry ( $\epsilon_p$ ) Least squares regression coefficients ( $R^2$ ) for all 7 formulated products are shown. Mean values  $\pm$  standard deviation are presented for  $\epsilon_{ia}$ . Mean value together with maximum and minimum measurements are presented for  $\epsilon_p$ .....87

**Figure IV.8:** Mean values penetrated oil determined by image analysis ( $PO_{ia}$ ) v/s PO determined by soxhlet extraction ( $PO_{soxhlet}$ ) of formulated products. The values of PO by



soxhlet extraction were taken from Moreno et al. (2010). Least squares regression coefficients ( $R^2$ ) for all 7 formulated products (green) and G-based products (blue) are shown. Mean values  $\pm$  standard deviation are presented. ....88

**Figure IV.9:** Cumulative pore area fraction v/s pore size of pores filled with oil (Filled) and empty pores (Empty) of G-based products. Results include all the pores measured for 9 focal planes. ....89

**Figure IV.10:** Cumulative pore area fraction v/s pore size of pores filled with oil (Filled) and empty pores (Empty) of PF-based products. Results include all the pores measured for 18 focal planes. ....90

**Figure IV.11:** Three-dimensional rendition of PF (left) and G (right) based products. A and C: Upper view of the solid matrix (green) showing the porous structure without oil. B and D: Oil (red) located inside the pore structure of the solid matrix. ....91

**Figure V.1:** Schematic diagram showing the capillary penetration phenomena when having different arrangements. Left: Upward configuration, the action of gravity restricts capillary penetration. Right: Downward configuration, the action of gravity enhances capillary penetration; from Bouchon and Pyle (2005). ....94

**Figure V.2:** Definition of geometrical parameters used to characterize product geometry; e1: minimum thickness, e2: maximum thickness, a: length, b: width. ....100

**Figure V.3:** Three point bending test set-up. ....101

**Figure V.4:** Protocol used to measure the contact angle between the oil and the fried formulated matrix. ....103

**Figure V.5:** Image sequence of a G-based product during frying at 170°C. The maximum thickness of the products determined by image analysis is also shown in each picture. ....105

<b>Figure V.6:</b> Image sequence of a PF-based product during frying at 170°C. The maximum thickness of the products determined by image analysis is also shown in each picture.....	106
<b>Figure V.7:</b> Digital images of: (A) 8G fried product, (B) 8G interior and (C) 8G external crust. ....	107
<b>Figure V.8:</b> Cross sections of: (A) 12G, (B) 12+MC and (C) PF fried products.....	107
<b>Figure V.9:</b> Mean values $\pm$ standard deviation (n=10) of geometrical parameters of fried formulated products. Side views of the products were illustrated by keeping the proportions to the actual measured geometrical parameters. Lowercase letters indicate significant differences in thickness (minimum and maximum thicknesses were compared together). Uppercase letters indicate significant differences in length. ....	108
<b>Figure V.10:</b> Maximum force of fracture and total oil content of fried formulated products. Oil content values were taken from Moreno et al. (2010). Mean values of 5 measurements $\pm$ standard deviation are shown for oil content. Mean values of 10 measurements $\pm$ standard deviation are shown for maximum force. Different letters inside each bar indicate significant differences. ....	110
<b>Figure V.11:</b> (A) Photograph of the flat surface of a 12G defatted formulated product. (B) Advancing oil drop before reaching equilibrium. (C) Oil drop at equilibrium. (D) Segmented oil drop at equilibrium. The contact angle between solid-oil and oil-air interfaces is outlined and measured. ....	112
<b>Figure V.12:</b> Contact angle of fried formulated products. Mean values of 6 measurements $\pm$ standard deviation are shown. Different letters inside each bar indicate significant differences. ....	113
<b>Figure VI.1:</b> Spider map showing most important factors analyzed in Chapters II, III, IV and V. Each parameter was normalized between 0 and 1 with respect to the	

maximum and minimum value. Acronyms stand for their composition in a dry basis: PF (100% PF), PF+MC (90% PF + 10% MC), PF+NS (90% PF + 10% NS), 8G (8% G + 92% NS), 12G (12 G + 88% NS), 8G+MC (90% 8G mixture + 10% MC) and 12G+MC (90% 12G mixture + 10% MC).....121

## TABLES INDEX

<b>Table III-1:</b> Dry mixture blends of G- and PF-based products categories, expressed in terms of the components' proportions (proportions exclude ingredients' water content). The formulation of gluten-based products consisted of wheat vital gluten (G) and NS blends to emulate wheat flour, and MC as additional ingredient. The formulation of potato-flake-based products consisted of potato flakes (PF) as the main ingredient and native wheat starch (NS) and methylcellulose (MC) as additional ingredients. ....	50
<b>Table III-2:</b> Scales of discrimination of G- and PF-products categories determined by scale-based F-test of significance with 99% confidence when comparing six measures of two surfaces for each pair-wise comparison. ....	58
<b>Table IV-1:</b> Composition of raw formulated products and relevant parameters of the fried dough (170°C), including: porosity determined by pycnometry ( $\epsilon_p$ ), porosity determined by image analysis ( $\epsilon_{ia}$ ) and penetrated oil content determined by image analysis ( $PO_{ia}$ ). ....	73
<b>Table V-1:</b> Dry basis formulations and nomenclature used throughout the study .....	100

PONTIFICIA UNIVERSIDAD CATOLICA DE CHILE

ESCUELA DE INGENIERIA

## **MICROESTRUCTURA Y FENÓMENOS DE TRANSPORTE EN FRITURA DE PRODUCTOS FORMULADOS**

Tesis enviada a la Dirección de Investigación y Postgrado en cumplimiento parcial de los requisitos para el grado de Doctor en Ciencias de la Ingeniería.

**MARÍA CAROLINA MORENO CONSTENLA**

### **RESUMEN**

Los productos fritos son apetecidos y consumidos en grandes cantidades en todo el mundo. Durante el proceso de fritura, el alimento retiene aceite, el cual puede llegar a ser uno de los principales componentes del producto final. Desafortunadamente, el consumo de grasas y aceites se considera un factor de riesgo para la salud de la población. Debido a eso, el fenómeno de absorción de aceite en alimentos fritos ha sido objeto de varios estudios. Pese a ello, aún no ha sido completamente elucidado.

Se ha establecido que los esfuerzos deben orientarse a entender lo que ocurre a nivel microscópico, ya que la microestructura de los alimentos podría ser de vital relevancia para la absorción de aceite. Es por ello que existe la necesidad de caracterizar matrices alimentarias fritas a través de la utilización de parámetros microestructurales para dilucidar el efecto real de la microestructura en el fenómeno de transporte de aceite. Este conocimiento permitiría mejorar el diseño de los futuros alimentos fritos. Para ello, un enfoque ingenieril sustentado en la construcción de estructuras controladas a través de la formulación de productos, mediante la comprensión de la funcionalidad de los elementos estructurales, o ingredientes, podría permitir comprender con mayor precisión este fenómeno.

En concordancia, la hipótesis de esta tesis es que a través del conocimiento de la funcionalidad de los ingredientes alimentarios y su comportamiento durante el procesamiento, es posible generar alimentos con microestructuras controladas para ser fritos, con diferentes propiedades físicas y capacidades de absorción de aceite, para mejorar la comprensión de la relación que existe entre la microestructura y los fenómenos de transporte involucrados, especialmente el de absorción de aceite.

En consecuencia, el objetivo principal de este trabajo es generar diferentes microestructuras controladas en base de la formulación de productos y fritura por inmersión, con el fin de comprender y describir la relación entre la microestructura desarrollada y la absorción de aceite.

Para ello se generó diferentes microestructuras mediante formulación de productos. Dos categorías de productos fueron desarrolladas, una basada en hojuelas de papa (productos en base a PF), y otra en gluten de trigo y almidón (productos en base a G). Ambos tipos de productos se elaboraron con un contenido de humedad de 40% (base húmeda), fueron laminados, fritos a 170 ° C hasta un contenido de humedad de 2% (base húmeda) y fueron analizados. Las formulaciones no solamente se basaron en PF y G, sino que también se utilizó metilcelulosa (MC) y se añadió almidón nativo de trigo (NS).

La cinética de absorción de aceite fue analizada. Dos fracciones de aceite, aceite penetrado y aceite superficial, se determinaron en diferentes etapas después de la fritura, y se encontró que los productos en base a G absorben la mayor parte del aceite durante la fritura, mientras que los productos en base PF absorben el aceite principalmente durante el enfriamiento.

Con el objetivo de entender mejor el rol de las características superficiales, la relación entre la rugosidad superficial y la absorción de aceite se estudió midiendo la topografía de la superficie de los productos utilizando un microscopio láser de barrido (SLM). Se obtuvo diferentes parámetros derivados de un análisis fractal sensible a la escala, tales como el límite liso-rugoso y la dimensión fractal, sin embargo, el parámetro denominado área relativa fue seleccionado para caracterizar las topografías medidas, ya que es

sensible a la escala de observación y se demostró que permite discriminar entre diferentes superficies. Los principales resultados obtenidos indican que, dentro de cada categoría de productos, los productos con mayor rugosidad superficial retuvieron más aceite. Sin embargo, los productos basados en PF eran más rugosos que los productos basados en G, pero no retuvieron más aceite.

Con el objetivo de entender mejor la relación entre la microestructura interna y la absorción de aceite, se examinó la microestructura interna mediante microscopía confocal de barrido láser (CSLM). Se desarrolló un procedimiento no invasivo de doble tinción para llevar a cabo una observación de dos canales en el microscopio. Las masas se tiñeron directamente durante la preparación con fluoresceína-5-isotiocianato (FITC), se laminaron y se frieron en aceite teñido con rojo Nilo. Posteriormente, las muestras se observaron sin intrusión adicional. Mediante la utilización de análisis de imágenes se determinó tamaño de poro, porosidad y contenido de aceite. Se detectó una relación directa entre la porosidad y la absorción de aceite en los productos basados en G, pero no se detectó relación alguna en los basados en PF. Además, los productos basados en G eran menos porosos que los productos basados en PF, pero no retuvieron menos aceite.

Ciertamente, la rugosidad superficial y la microestructura interna son factores clave en la absorción de aceite, pero otras propiedades relacionadas a los alimentos pueden explicar las diferencias entre diferentes categorías de productos. Para entender mejor las diferencias, los productos se caracterizaron adicionalmente a través de su geometría, su afinidad química con el aceite (medida a través del ángulo de contacto), y su dureza (por mediciones de fuerza de fractura). Adicionalmente, se desarrolló un protocolo de captura de imágenes digitales, a través del cual se demostró que la expansión de los productos ocurre durante los primeros 15-20 s en ambas categorías de productos. Sin embargo, los productos en base a G desarrollan una delgada costra externa, la cual se puede distinguir claramente del interior del producto, mientras que los productos en base a PF desarrollan una costra gruesa que engloba al producto completo. No existe una relación clara entre la cantidad de aceite retenido por los productos y su geometría, pero algunos cambios durante la fritura podrían ser relevantes para la dinámica de penetración de aceite. Puede

haber una relación entre la dureza de los productos y el mecanismo de absorción de aceite, ya que productos más duros tienden a retener menos aceite. La medición del ángulo de contacto permitió discriminar entre los productos bajo estudio, y ayudó a explicar por qué los productos en base a PF retienen menos aceite a pesar del ser más rugosas y más porosas, pues tenían menor afinidad química con el aceite.

En general, se desarrollaron diferentes técnicas no-invasivas de análisis microscópico, las cuales en conjunto con métodos analíticos permitieron entender los parámetros más importantes para la absorción de aceite. Como se muestra a lo largo de este trabajo, fue posible distinguir de forma adecuada la mayoría de los factores importantes que afectan a la absorción de aceite, dentro de una categoría específica de producto o cuando se comparan diferentes categorías, a la luz de ecuaciones fenomenológicas, que ayudan a comprender el comportamiento de diferentes formulaciones.

#### **Miembros de la Comisión de Tesis Doctoral**

Pedro Bouchon

Sergio Almonacid

Claudio Gelmi

Franco Pedreschi

Christopher A. Brown

Cristián Vial

Santiago, noviembre 2012



PONTIFICIA UNIVERSIDAD CATOLICA DE CHILE  
ESCUELA DE INGENIERIA

**MICROSTRUCTURE AND TRANSPORT PHENOMENA IN DEEP-FAT  
FRIED FORMULATED PRODUCTS**

Thesis submitted to the Office of Research and Graduate Studies in partial fulfillment  
of the requirements for the Degree of Doctor in Engineering Sciences by

**MARIA CAROLINA MORENO CONSTENLA**

**ABSTRACT**

Fried products are desired and consumed in large amounts worldwide. During the frying process, oil is retained by the food and may become one of the main components of the final product. Unfortunately, the consumption of fats and oils is considered an important health risk factor. For that reason, the understanding of oil absorption in deep-fat fried foods has been the focus of intensive research in the food domain. However, it still remains unclear.

It has been stated that efforts should be oriented to understand what happens at the microscopic level, since food microstructure should play a key role. In this respect, there is a need to characterize fried matrices using relevant microstructural parameters to elucidate the actual effect of food microstructure in oil transport phenomena, to improve the design of fried foods. To do so, an engineering approach based in the development of controlled structures through product formulation, through the understanding of structural elements or ingredients functionality, could allow an accurate design.

In accordance, the hypothesis of this thesis was that through the knowledge of the functionality of food ingredients and their behavior during processing, it was possible to

generate controlled food microstructures to be fried, with different physical properties and oil absorption capacities, to improve the understanding of the relationship between product microstructure and transport phenomena, particularly oil absorption.

Consequently, the main objective of this work was to generate different controlled microstructures based on product formulation and deep-fat frying, in order to understand and describe the relationship between the developed microstructure and oil absorption.

To do so, different microstructures were generated by means of product formulation. Two product categories, which were either based on potato-flakes (PF-based products), or wheat gluten and starch (G-based products) with 40% moisture content (wet basis) were laminated, fried at 170°C until 2% moisture content (wet basis) and analyzed. Formulations were based on PF and G, but also the use of methylcellulose (MC) and added native wheat starch (NS) were included.

Oil absorption kinetics was analyzed. Two oil fractions, penetrated oil and surface oil, which corresponds to the fraction that remains on the surface, were determined after 2 s or 10 min after frying. This was done to understand the importance of oil drainage upon frying. Interestingly, it was found that G-based products absorbed most of the oil during frying, whereas PF-based products mostly absorbed oil during cooling. These results gave an important clue about the relevance of product microstructure and oil absorption phenomenon.

To better understand the key role of product surface, the relationship between surface roughness and oil uptake was studied, measuring the surface topography of the different products using a scanning laser microscope (SLM). Several parameters derived from area-scale fractal analysis were obtained, such as the smooth-rough crossover and the fractal dimension; however, the relative area was selected since it was scale-sensitive and allowed adequate discrimination of fried surfaces through a range of relevant scales. Most important results showed that within each product category, products with higher surface roughness retained more oil. However, PF-based products were rougher than G-based products, but did not retain more oil.

To get a better understanding between oil absorption and the microstructure of both product categories, the inner microstructure was examined using confocal scanning laser microscopy (CSLM). A non-invasive double staining protocol was developed, which allowed performing a two channel observation using CSLM. The dough was directly stained during preparation with fluorescein-5-isothiocyanate (FITC), laminated and fried in oil stained with Nile red. Thereafter, samples were observed without further intrusion. Pore size, porosity and oil were quantified using image analysis. Results showed a direct relationship between porosity and oil absorption in G-based products, but, no relationship was detected in PF-based ones. Further, G-based products were less porous than PF-based products, but did not retain less oil.

Certainly, surface roughness and inner microstructure are key factors in oil absorption, but other food-related properties were thought to explain differences among product categories. To get a better understanding of such differences, additional aspects, such as the understanding of the chemical affinity between the oil and the food matrix (contact angle measurement), as well as product expansion and texture (maximum breaking force) in oil absorption, were also examined. In addition, an in situ examination protocol using digital recording was set-up, which demonstrated that product expansion occurred during the first 15-20 s in both product categories. However, in G-based products an external crust layer was formed, which could be clearly identified from the interior, whereas in PF-products a thicker global crust was obtained. Overall, no clear relationship between oil absorption and product geometry was determined. In relation to texture, it was found that hardest products tended to retain less oil. The measurement of contact angle allowed a good discrimination between products. It was concluded that the tendency of PF-based products to retain less oil despite the higher surface roughness and porosity could be related to some extent to its lower wetting.

Overall, different non-invasive microscopy techniques were developed, which can be used in different domains and, together with analytical methods, allowed a good understanding of most important parameters affecting oil absorption. As shown along this work, it was possible to have a good distinction of key parameters affecting oil

absorption, within a specific product category or when comparing different product categories, in the light of phenomenological equations, which help understanding the behavior of different formulations.

**Members of the Doctoral Thesis Committee:**

Pedro Bouchon

Sergio Almonacid

Claudio Gelmi

Franco Pedreschi

Christopher A. Brown

Cristián Vial

Santiago, November 2012.

## LIST OF PAPERS

This thesis is based on the following papers, referred in the text by respective chapter:

Chapter 3: María Carolina Moreno, Pedro Bouchon and Christopher A. Brown. (2010). **Evaluating the Ability of Different Characterization Parameters to Describe the Surface of Fried Foods.** *Scanning*, 32, 212-218.

Chapter 4: María Carolina Moreno, Christopher A. Brown and Pedro Bouchon (2010). **Effect of food surface roughness on oil uptake by deep-fat fried products.** *Journal of Food Engineering*, 101,179-186.

Chapter 5: María Carolina Moreno and Pedro Bouchon (2012). **Microstructural characterization of deep-fat fried formulated products using confocal scanning laser microscopy and a non-invasive double staining procedure.** *Journal of Food Engineering*. Submitted.

Chapter 6: María Carolina Moreno and Pedro Bouchon (2012). **Understanding the relationship of structural, textural and wetting related parameters with oil uptake in deep-fat fried formulated products.** To be submitted.

## PROCEEDINGS

Parts of this work have also been presented at international congresses under the following references:

- Moreno, M.C. **Effect of freeze, air and osmotic drying on tissue composition, oil absorption and location during potato frying.** International Congress on Engineering and Food-ICEF10, Viña del Mar, Chile, 2008. Poster.
- Moreno, M.C. and Bouchon, P. **Relationship between surface topography and oil suction in deep-fat fried restructured food matrixes built from wheat gluten, native wheat starch and methylcellulose.** Congreso Iberoamericano de Ingeniería de Alimentos (CIBIA-7), Bogotá, Colombia, 2009. Oral and poster expositions.
- Moreno, M.C. and Bouchon, P. **Relationship between oil uptake and surface topography during deep-fat frying of controlled food systems.** International Conference on Surface Metrology, Worcester, Massachusetts, USA, 2009. Oral exposition.
- Moreno, M.C., Dueik, V. and Bouchon, P. **Effect of frying pressure on oil uptake, surface roughness and texture of fried potato-flake based fabricated products.** International Conference of Food Innovation-FoodInnova, Valence, Spain, 2010. Poster exposition.
- Moreno, M.C. and Bouchon, P. **Microstructural analysis of deep-fat fried formulated products by Confocal Laser Scanning Microscopy (CLSM) and fluorescent labeling.** International Congress on Engineering and Food-ICEF11, Athens, Greece, 2011. Oral exposition.
- Moreno, M.C. and Bouchon, P. **Relationship between oil absorption and inner microstructure of fried formulated products.** Conference of Food Engineering-COFE. Leesburg, Virginia, USA, 2012. Oral exposition.

## **AWARDS**

After the exposition of partial results of this work, the following awards were received:

- International Congress on Engineering and Food-ICEF10, Viña del Mar, Chile, 2008. One of the 10 best posters among 300 participants.
- Congreso Iberoamericano de Ingeniería de Alimentos-CIBIA7, Bogotá, Colombia, 2009. One of the 4 best posters among 400 participants.
- International Conference of Food Innovation-FoodInnova, Valence, Spain, 2010. Best presented poster for young researcher.
- Second place in the Congress of Graduate Students of the Engineering School, Pontificia Universidad Católica de Chile, 2010.

## NOMENCLATURE AND ABBREVIATIONS

### Abbreviations:

FITC: Fluorescein-5-isothiocyanate  
G: vital wheat gluten  
COV: Coefficient of variation  
CSLM: Confocal scanning laser microscope  
MC: Methylcellulose  
MSR: Mean square ratio  
NA: Numerical aperture  
NS: Native wheat starch  
PF: Potato flakes  
PO: Penetrated oil  
 $R^2$ : Least squares regression coefficient  
SEM: Scanning electron microscopy  
Sa: Average roughness  
Sku: Surface Kurtosis  
SLM: Scanning laser microscope  
SO: Surface oil  
Sq; Root mean square roughness  
SRC: smooth–rough crossover  
Ssk: Surface skewness  
TO: Total oil

### Nomenclature:

$g$  = Acceleration due to gravity, [m.s<sup>-2</sup>]  
 $h$  = Oil penetration distance, [m]  
 $P_2^*$  = Piezometric pressure at the bottom of the capillary, [Pa]  
 $P_1^*$  = Piezometric pressure at the liquid side of the meniscus, [Pa]



$P_v$  = Vapour pressure, [Pa]

$P_{atm}$  = Atmospheric pressure, [Pa]

$P_{pore}$  = Pore's pressure, [Pa]

$r$  = Radius of the capillary, [m]

$\theta$  = Contact angle (between oil and solid inner pore wall), [Rad]

$\alpha$  = Angle between normal and vertical axes, [rad]

$\rho$  = Oil density, [kg.m-3]

$\sigma_{sg}$  = Interfacial tension between solid and gas [N/m]

$\sigma_{so}$  = Interfacial tension between solid and the oil [N/m]

$\sigma_{og}$  = Interfacial tension between oil and gas [N/m]

$\theta$  = Contact angle (between liquid drop and solid surface) [rad]

**Subscripts:**

b: Bulk

ia: Image analysis

o: oil

g: gas

p: Pycnometry

s: Solid

## **I. Introduction**

Fried products are desired and consumed in large amounts worldwide because of their unique characteristics of color, taste, texture and mouthfeel that are acquired during the deep-fat frying process, one of the oldest cooking methods (Varela et al., 1988). The process basically consists in the immersion of a food piece in an edible oil or fat at temperatures above the boiling point of water (Farkas et al., 1996). Frying temperatures typically range between 150 and 200 °C, in the case of atmospheric frying. In the case of vacuum frying, a newer and lower spread technology, which takes place at pressures well below atmospheric levels, the temperature usually, does not exceed 120 °C.

Deep-fat frying is a complex unit operation involving high temperatures, significant microstructural changes both to the surface and the body of the food, and simultaneous heat and mass transfer resulting in flows in opposite directions of water vapor (bubbles) and oil at the surface of the piece, as depicted in Figure I.1 (Bouchon et al, 2003). The high temperatures of the frying oil lead to the evaporation of water at the surface of the food. Due to evaporation, water in the external layers of the product leaves the food to the surrounding oil and surface drying occurs, inducing to crust formation. Additionally, oil is absorbed by the food, replacing part of the water (Mellema, 2003). Most of the desirable characteristics of fried foods are derived from the formation of a composite structure: a dry, porous, crisp and oily outer layer, or crust, and a moist cooked interior (Bouchon and Aguilera, 2001).

During the frying process, the oil retained by the food may become one of the main components of the final product. In terms of palatability, this is beneficial, since fat provides taste, smell and texture, conferring the attributes that distinguish fried food from baked products. In terms of health, this is negative, since the consumption of oils and fats, particularly saturated ones, is considered as a risk factor in the increment of heart disease, cancer, diabetes and hypertension among the population (Minihane and Harland, 2007).

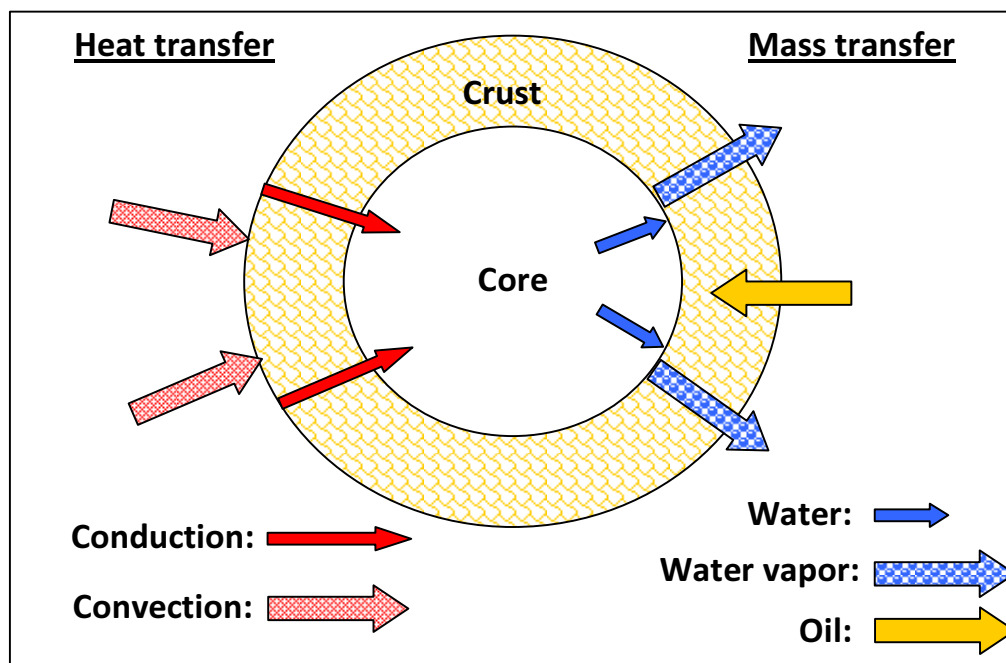


**Figure I.1:** Schematic diagram of simultaneous heat transfer (left hand side of the figure) and mass transfer (right hand side of the figure) during deep-fat frying

Several studies have been conducted in order to understand the oil migration phenomenon within fried foods. When, how and where the oil penetrates into the food have been the main questions that several researchers have tried to answer (Ufheil and Escher, 1996; Aguilera and Gloria, 1997; Moreira et al., 1997; Bouchon et al., 2001; Bouchon et al. 2003; Mellema, 2003).

Even though it is not fully understood when and how the oil penetrates into the food structure, it has been shown that most of the oil is confined to the surface region of the fried product (Farkas et al., 1992; Saguy et al., 1997; Bouchon et al., 2001) and there is strong evidence that it is mostly absorbed during the cooling period (Ufheil and Escher, 1996; Moreira et al., 1997; Bouchon et al., 2003). For that reason, it is believed that during frying, after initial heating occurs, the vigorous escape of water vapor would generate a barrier to prevent oil migration into the porous crust and as a consequence oil absorption would be limited during most of the immersion period. As a result, oil uptake

would mainly result from the competition between drainage and suction into the porous crust once the food is removed from the oil and cools down, being essentially a surface-related phenomenon. It has been suggested that the largest amount of oil is pulled into the product when it is removed from the fryer because of the vacuum effect due to steam condensation. Accordingly, it has been suggested that oil absorption depends on the amount of water removed and on the way moisture was lost.

In 1996, Ufheil and Escher studied the dynamics of oil uptake during deep-fat frying of potato slices, using a fat-soluble and heat-stable dye (Sudan Red B). They determined that most of the oil was absorbed when the product was removed from the oil bath and proposed that oil uptake was primarily a surface phenomenon, involving equilibrium between adhesion and drainage of oil upon removal of the product from the oil. In 1997, Moreira et al. determined that only 20% of the total oil content of tortilla chips was absorbed while they were immersed in the oil bath and that almost 64% of the total oil content was absorbed during post-frying cooling, the rest remaining on the surface (outer layers of the product). Later, Bouchon et al. (2003) combined and adapted the methods developed by Ufheil and Escher (1996) and Moreira et al. (1997) and were able to distinguish 3 different oil fractions when frying potato cylinders, that is: i) structural oil (STO) which represents the amount of oil absorbed during frying, ii) penetrated surface oil (PSO) which represents the amount of oil suctioned into the food during cooling, following its removal from the fryer and iii) surface oil (SO), that is, the oil that remains on the surface. A schematic diagram showing these oil fractions is presented in Figure I.2.

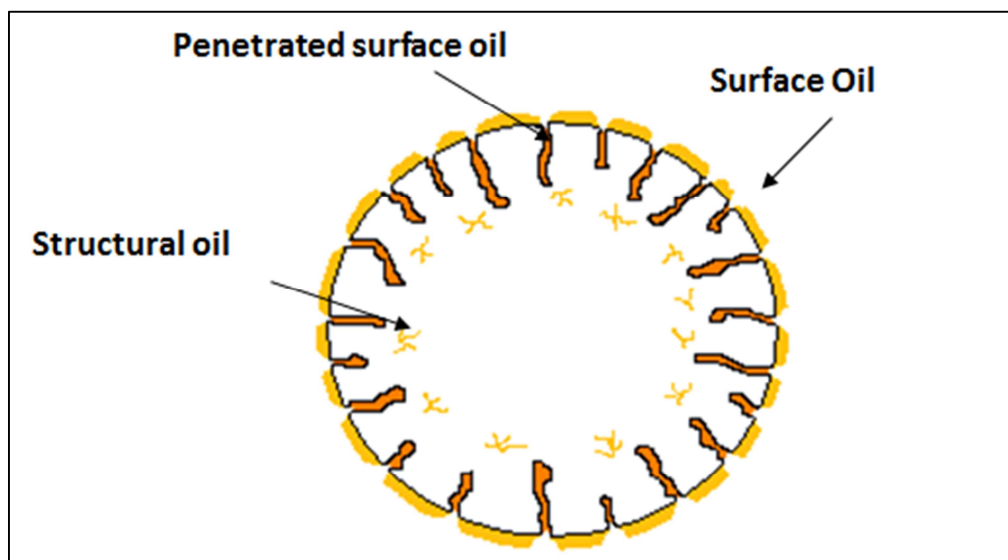


**Figure I.2:** Diagram showing the 3 locations of oil in the product microstructure after deep-fat frying adapted from Bouchon et al. (2003).

Results showed that only a small amount of oil was able to penetrate during frying since most of the oil was picked up at the end of the process, suggesting that oil uptake and water removal were not synchronous phenomena. After cooling, oil was located either on the surface of the product or was suctioned into the porous crust microstructure, with an inverse relationship between them for increasing frying times. According to experimental facts, several approaches have been used to describe and model oil absorption. Moreira and Barrufet (1998) explained the mechanism of oil absorption during cooling in tortilla chips in terms of capillary forces. This hypothesis was supported by experimental results, where they determined that oil uptake occurred during the first 20s of cooling, that is, when the temperature was still above the condensation temperature.

The main conclusions point out that most of the oil would penetrate within the structure during the cooling period, after frying, and would be determined by the competition between oil drainage from the surface of the food and porous oil suction. The mechanism of oil penetration is related to steam condensation upon cooling, which

would suck the oil into the porous network, and is strongly related to capillary suction. In accordance, it has been shown that oil is mostly located in the crust region.

Despite the considerable amount of oil contained in fried food and the increase concern of consumers about the relationship between food, nutrition and health, frying remains as one of the most common cooking methods (Saguy and Dana, 2003). In accordance, an important need of the food industry is to be able to generate products with a low fat content that are able to maintain the desirable characteristics of fried food, in line with current food trends, to provide safe and high quality products, contributing to health and welfare of consumers (Aguilera, 2006). In practical terms, this vision requires the need to design and create new products using an engineering approach, which may be achieved by building controlled structures from food ingredients (food building blocks), considering their functionality, their assembly, together with the effect of processing conditions. Figure I.3 presents schematically the concept building structures through an engineering approach.

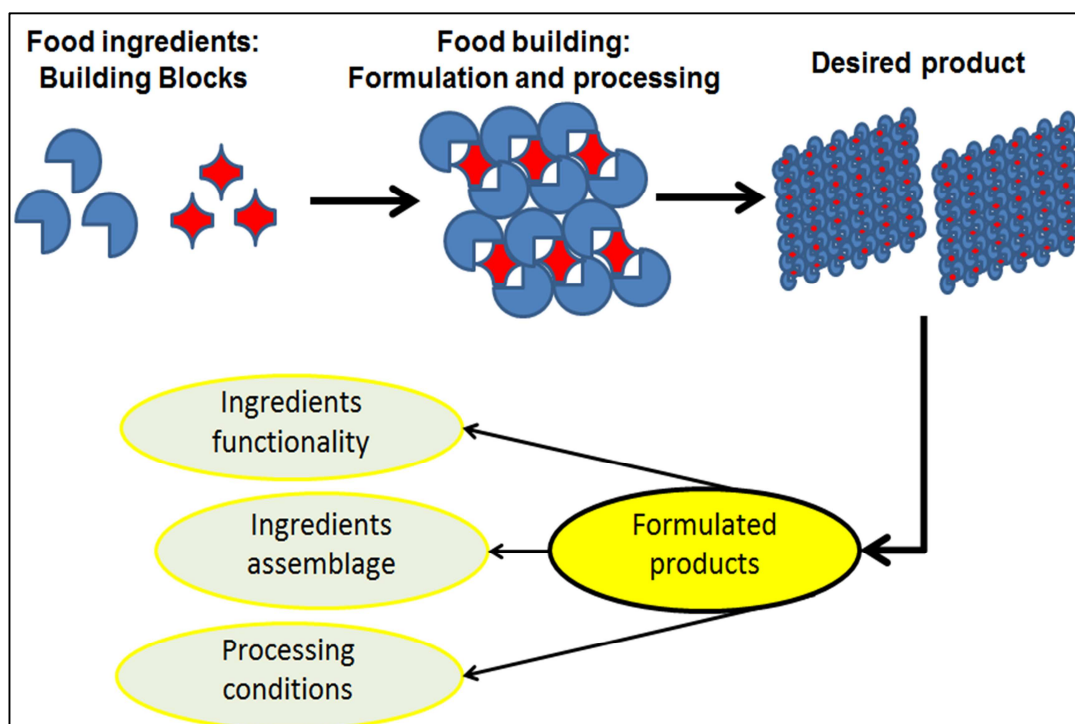


**Figure I.3:** Schematic diagram describing product formulation by an engineering approach.

In accordance, efforts should be oriented to understand what happens at the microscopic level, since transport properties in food, as well as physical and sensory attributes depend on the architecture formed by the elementary components, which are usually below 100 microns, that is, below eye resolution (Aguilera, 2005). In relation to deep-fat frying, the microstructure of the food matrix and the microstructural changes occurring during processing will define the characteristics of the final product, including oil absorption. As a consequence, there is a need to characterize fried matrices using microstructural parameters to elucidate the actual effect of microstructure in oil transport phenomena in order to improve the design fried foods with a healthier profile and desired quality attributes.

As mentioned, this product-driven engineering approach requires building controlled right structures and therefore, understanding the functionality of the structural elements prior to or formed during processing. The snack industry is profoundly directed by this product-driven process engineering era. New product developments and processing procedures are under constant evolution. In this respect, snack formulated products are getting importance as a good alternative to the use of traditional raw materials because of the advantages of reproducibility, uniformity and lack of defects, which make them suitable to fit consumer demands. In fried products, these may be an option for the production of tailor-made snacks with improved quality and lower oil content, a key issue in nowadays diet.

### **I.1. Hypothesis and objectives**

The hypothesis of this thesis is that through the knowledge of the functionality of food ingredients and their behavior during processing, it would be possible to generate controlled food microstructures to be fried, with different physical properties and oil absorption capacities, to improve the understanding of the relationship between product microstructure and transport phenomena, particularly oil absorption.

Accordingly, the main objective of this work is to generate different controlled microstructures based on product formulation and deep-fat frying, in order to understand and describe the relationship between the developed microstructure and oil absorption.

The specific objectives are:

- To generate different microstructures by means of product formulation, with markedly different surface topographies, porosity and oil absorption capacities, to be further analyzed.
- To characterize the different microstructures using non-invasive microscopy tools, developing tailor-made microscopy protocols, which allow surface topography and inner microstructure analysis and discrimination, avoiding artifacts incorporation.
- To study and understand the relationship between product microstructure (surface roughness and inner microstructure) and oil uptake in fried formulated products with a wide range of oil absorption capacities.
- To determine and understand the effect of most important factors affecting oil absorption during deep-fat frying.

## **I.2. Outline of the thesis**

This thesis is divided in 6 chapters.

**Chapter 1** presents an overall introduction to the topic, which is needed to understand the hypothesis and the objectives of the thesis.

The aim of **Chapter 2** is to develop a surface topography measurement protocol using a non-invasive tool (laser scanning microscopy) and to identify surface topography characterization parameters that are able to discriminate the surfaces of different formulated fried foods, using both conventional parameters and area-scale fractal analysis.



**Chapter 3** studies the relationship between surface roughness and oil absorption in different fried formulated matrices, which are either based on potato-flakes or wheat gluten, that is, ingredients with a strong structure-development potential. To do so, two oil fractions, penetrated oil and surface oil, are determined at the beginning and at the end of the cooling period after frying, and the surface is characterized using area-scale fractal analysis.

In **Chapter 4** the relationship between inner microstructure and oil absorption capacity of potato-flakes and gluten-based product categories is analyzed. A protocol to carry out non-invasive confocal scanning laser microscopy observation is developed, which is based on product staining with a fluorescent probes prior to processing, allowing distinguishing the solid matrix from the oil and the empty space at microscopic level. Pore size, porosity and penetrated oil are quantified using image analysis, and are later related to the actual oil content of the different products.

**Chapter 5** studies different characteristics of the two groups of fried formulated products to understand their importance to the amount of oil retained after deep-fat frying and their influence in the mechanism of oil migration into the products. The fried products were characterized by their geometrical features, their chemical affinity with oil (by contact angle measurements in their restructured surfaces), and their hardness (by fracture force measurements).

Finally, **Chapter 6** presents the main conclusions of the thesis together with a discussion of some future challenges.

In order to better understand the relationship between the different sections of the document, the general structure of this thesis is schematically presented in Figure I.1:

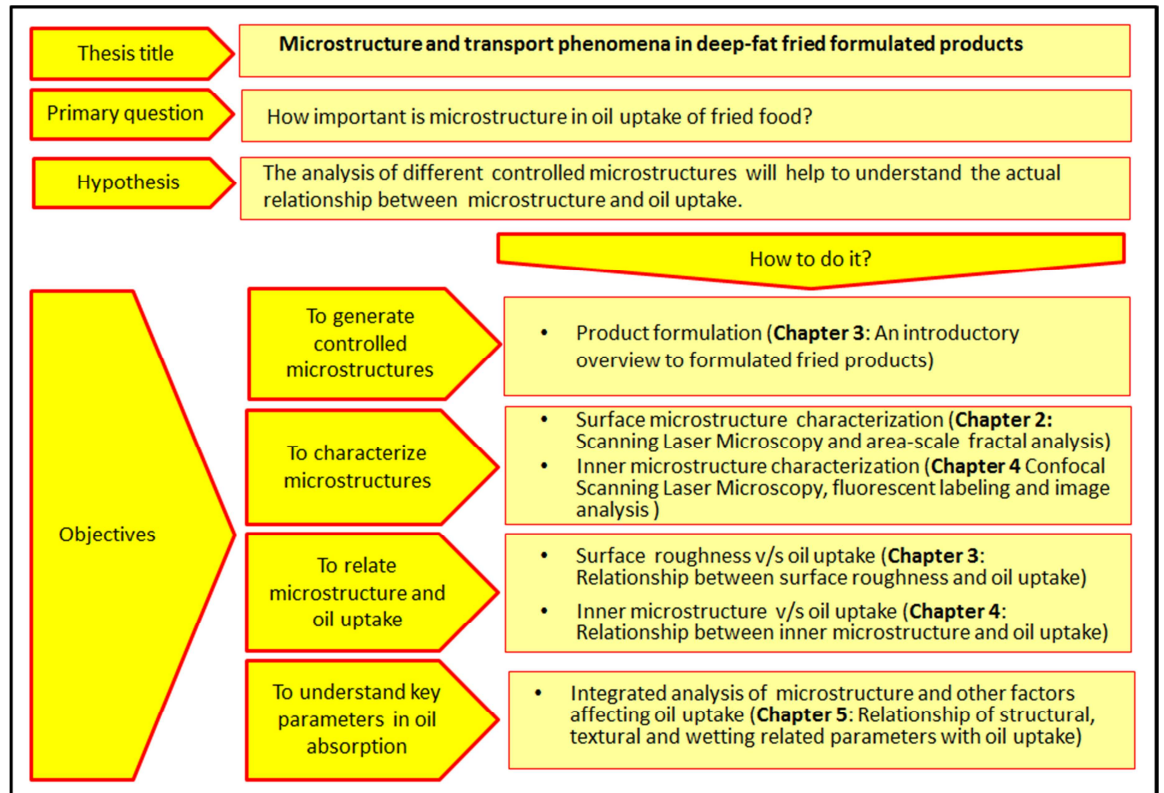


**Figure I.4:** Thesis general structure

## **II. Evaluating the Ability of Different Characterization Parameters to Describe the Surface of Fried Foods**

### **ABSTRACT**

The objective of this work is to identify surface topography characterization parameters that are capable of discriminating the surfaces of different fried foods. Three fried food model systems with clearly different surfaces were formulated from vital wheat gluten, native wheat starch, and potato flakes. The surfaces were measured with a scanning laser microscope (SLM), and the ability of several parameters to discriminate between them was tested. Two conventional parameters, the root mean square roughness (Sq) and the surface Kurtosis (Sku), were calculated, along with parameters derived from area-scale fractal analysis: smooth-rough crossover (SRC), fractal dimension, and relative area as a function of scale. The coefficient of variation (COV) of Sq, Sku, and SRC and fractal dimension of different sizes of measurement regions were calculated for the surface of the roughest product in order to specify a measurement region that would be sufficiently large to be representative. The size of the representative region was found to be 25 mm<sup>2</sup>. Among the parameters evaluated in this study, the most reliable parameter for discriminating the surfaces of fried foods is the relative area calculated from area-scale fractal analysis.

Keywords: Food, deep-fat frying, surface metrology, fractal analysis.

### **II.1. Introduction**

Fried foods are consumed all around the world because of their unique characteristics of flavor, color, and texture that are acquired by the process of deep-fat frying. During this process, the food is submerged in an edible oil or fat at temperatures well above the boiling point of water (Farkas et al., 1996). The heat transferred from the oil cooks and dehydrates the food. Part of the frying oil also is transferred to the food and can be one of the main components of the final product.

One of the most important indications of the quality of fried food is the amount of oil absorbed during the process (Moreira et al., 1999). Oil content is counter to recent trends toward creating healthy foods and low-fat products (Minihane and Harland, 2007) and many researchers have tried to understand the oil absorption phenomenon on fried products.

Despite the progress that has been made, the oil adsorption process is not fully understood, and it is difficult to predict the final oil content of fried products. Studies indicate that oil absorption is a surface-related phenomenon. It is there, at the surface of the product, that the oil uptake occurs (Bouchon et al., 2001; 2003; Moreira et al., 1997; Ufheil and Escher, 1996). Consequently, the surface characteristics of the fried product could be significant factors affecting oil uptake, especially at the end of the frying process, and this requires further study.

Food surfaces are complex, and their effect on transport phenomena is related to several characteristics that involve both chemical and physical aspects of the product. In the frying processes particularly, several factors of the fried product surface should be considered when determining its characteristics including hydrophobic behavior, strength, porosity, and topography. Each of them needs to be measured, parameterized, analyzed, and related to oil uptake. The current work is focused on the measurement and analysis of fried food's surface geometrical irregularities, also described as texture, topography, or roughness.

The selection of measurement conditions and texture characterization parameters for identifying and differentiating the texture of surfaces that are prepared or that perform differently is a fundamental problem in surface metrology (Jordan and Brown, 2006). There are few measurement and characterization procedures in the literature that describe the surfaces of fried foods and relate them to oil uptake. These include scanning electron microscopy (SEM) image acquisition with fractal dimension calculations (Rubnov and Saguy, 1997; Thanatuksorn et al., 2005) and reflective confocal scanning laser microscopy (CSLM) surface measurements, with conventional height parameters

calculation (Bouchon and Pyle, 2004). Both of the above microscopy techniques require special sample preparation methods, such as microtome cutting before contour observations by SEM and gold coating before CSLM measurements. No discussion was found regarding the characterization parameters employed to describe the surfaces of fried products, although it is an important issue, as different parameters could lead to variant conclusions.

An accurate analysis of the surface of fried foods demands the utilization of non-intrusive measurement techniques and the selection of appropriate topographic characterization parameters. Pedreschi et al. (2000) measured the surface of different food products with a scanning laser microscope (SLM) and demonstrated that this device makes topographic measurements that are capable of discrimination. They measured the surfaces of bread, chocolate, raw potatoes, and fried potatoes at a spatial resolution of 25  $\mu\text{m}$  without any special sample preparation. The SLM provides a quantitative representation of the measured surfaces as relative heights in an elevation map, with a high vertical resolution (up to 2  $\mu\text{m}$ ) and no intrusive sample preparation, which makes it a good instrument for the study of the surfaces of fried foods.

Several texture characterization methods and parameters could be applied to topographic data in order to describe surface roughness. The current work will compare standardized conventional height parameters (ASME B46.1, 2002; ISO 25178, 2007) as well as standardized parameters derived from area-scale fractal analysis (fractal dimension, smooth-rough crossover, and relative area) (ASME B46.1, 2002).

The objective of this work is to determine surface topography parameters that are capable of discriminating fried foods by their surface topographies. Three fried foods with markedly different surface topographies were prepared by means of product formulation. Their surfaces were measured by SLM, and the ability of different analysis methods to discriminate between them was tested.

## **II.2. Materials and Methods**

### **II.2.1. Sample Preparation**

Three dough-like products were formulated in order to generate different surface topographies after deep-fat frying. The test products included potato flakes (PF; Alimentos Unisur, Chile), native wheat starch (NS), and vital wheat gluten (G; Asitec S.A., Chile). The dry components (100% PF for product A; 8% G and 92% NS for product B; 12% G and 88% NS for product C) were mixed for 2 min in a food mixer (K50-KPM50; KitchenAid, St Joseph, MI). Distilled water was added until a moisture content of 40% wet basis (w.b.) was reached, and the dough was formed. When product A was formulated, all the water was added at 15°C, but when products B and C were formulated, half of the water was added at 15°C, and the other half was added at 90°C. The formed doughs were wrapped in a plastic bag for 1 h at room temperature (20°C), then kneaded and laminated to a thickness of approximately 2 mm using a dough sheeter (DOYONLSB516, Saint Come Liniere, Quebec, Canada), and finally cut into 4x4 cm<sup>2</sup> square-shaped samples.

The samples were fried in high oleic sunflower oil (Camilo Ferrón, Chile) at 170±2°C until they reached a final moisture content of 2% w.b. in a deep-fryer (Somela-535T, Santiago, Chile) with an external temperature control system (PID+Autotuning, Veto, Chile). When frying was completed, the products were removed from the fryer and immediately submerged in petroleum-ether for 30 s, thus removing the oil adhered to the surface.

### **II.2.2. Moisture Content Measurement**

The moisture content of the samples before (40% w.b.) and after frying (2% w.b.) was verified gravimetrically by air drying 3 g of minced sample at 105°C during 24 h (AOAC, 1995).

### **II.2.3. Surface Texture Measurement**

The texture measurements were made using a UBM (Solarius Development, Sunnyvale, CA) SLM mounted on an air table. This equipment basically consists of two positioning tables that move the sample under a height sensor (see Figure II.1). A Keyence LC-2210 (Osaka, Japan) triangulation laser height sensor was used on the UBM to measure the heights on the surface. This sensor has a fast measurement rate (40 kHz), which improves the resolution of an individual height measurement during the measurement of the topographies of objects moving at a high speed. The measurements consisted of heights,  $z$  ( $\mu\text{m}$ ), at 10- $\mu\text{m}$  sampling intervals in  $x$  and  $y$  directions. The positioning tables moved the samples at a tracing speed of 0.5 mm/s, giving a measurement rate of 50 point/s at the specified lateral resolution.

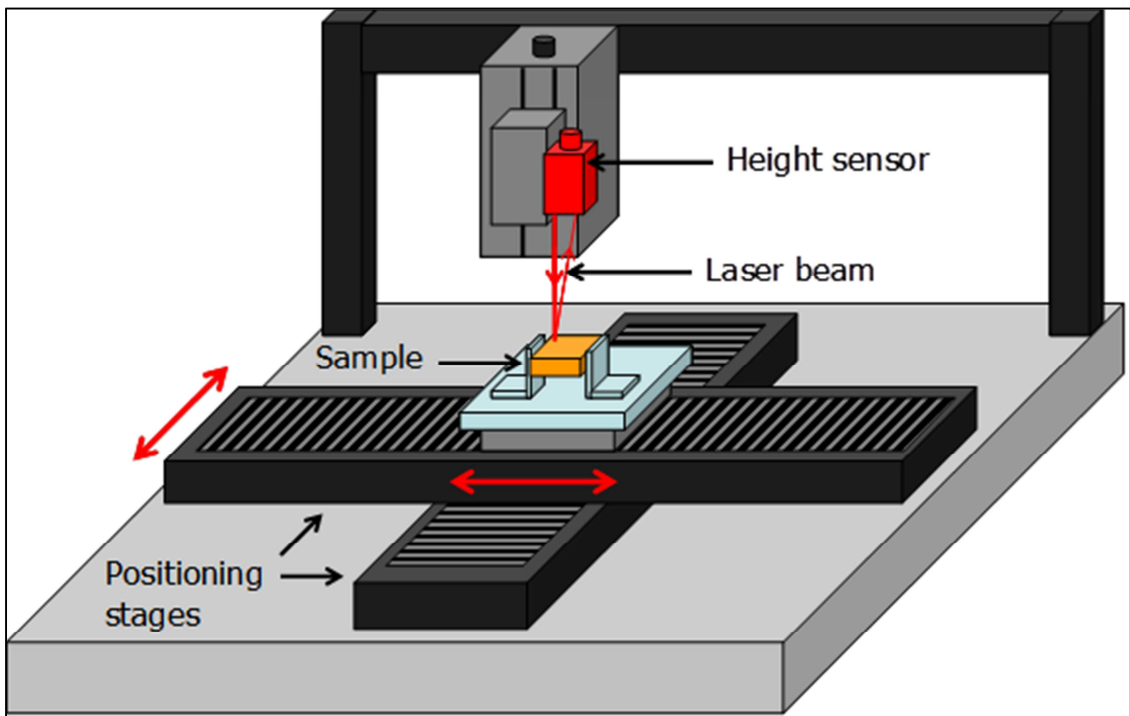


**Figure II.1:** Scanning laser microscope setup.

Six measurements were made on each product over squared regions of  $5 \times 5 \text{ mm}^2$ . In addition, six measurements of  $2.5 \times 2.5$ ,  $1.7 \times 1.7$ , and  $1.3 \times 1.3 \text{ mm}^2$  of product A were

made in order to evaluate the size of the measurement region. The acquired topographic data were stored digitally for later analysis.

#### **II.2.4. Surface Image Acquisition**

A color digital camera (PowerShot A70; Canon, Newport News, VA) was mounted inside a box impervious to light with internal black surfaces and a uniform light system. One digital image of each fried product was acquired in order to observe their macroscopic characteristics.

#### **II.2.5. Surface Analysis**

Surface texture measurements were analyzed according to the following procedures.

##### **II.2.5.1. Conventional Parameters**

Two conventional parameters were calculated using the software Mountains 3.1.6 Digital Surf ([www.digitalsurf.fr](http://www.digitalsurf.fr), Besancon, France), the root mean square roughness ( $S_q$ ), and the surface kurtosis ( $S_{ku}$ ). Both of them involve the statistical distribution of height values along the z axis (ASME B46.1, 2002; ISO 25178, 2007). The  $S_q$  equals the root mean square average of the measured height deviations from the mean surface, and the  $S_{ku}$  equals the kurtosis of the height distribution. ASME B46 (2002) makes a distinction between height and shape parameters. According to that classification, it was decided to evaluate one parameter of each category. Among the height parameters,  $S_q$  and the average roughness ( $S_a$ ) were found to be the most frequently used in the reviewed literature. Only one of them was selected because both of them ranked the surfaces under study in the same way. Among shape parameters,  $S_{ku}$  and the surface skewness ( $S_{sk}$ ) could be used.  $S_{sk}$  was discarded as its coefficient of variation (COV) was too high (up to 50%).

##### **II.2.5.2. Area-Scale Fractal Analysis**

Area-scale fractal analysis was conducted by SFRAX® software ([www.surfact.com](http://www.surfact.com)). This method is described extensively by Brown et al. (1993) and



consists basically of a series of virtual tiling exercises, achieved by covering the measured surface in a patchwork fashion with triangular patches. The area of the patches corresponds to the scale of observation, and the tiling exercises are performed with patches of progressively smaller areas. The apparent area at each scale is calculated as the number of triangular patches times the area of the patches. The apparent area is normalized by dividing it by the projected area of the tiled region to determine a relative area; therefore, the minimum relative area is one. The range of scale of observation over which the relative areas were calculated went from half of the nominal area of the measured region to the square of the sampling interval divided by two.

An area-scale plot is constructed as a log-log plot of the relative area versus the scale of observation. Two parameters can be calculated from this plot, the smooth-rough crossover (SRC) scale and the area-scale fractal dimension (ASME B46, 2002). The SRC is the scale above which the relative areas are close to one, and the surface appears to be smooth, and below which the relative area changes dramatically with the scale, and the surface appears to be rough. In order to determine the SRC from the area-scale plot, a threshold value of relative area was set at 5% of the greatest calculated relative area. The area-scale fractal dimension is calculated from the slope of the area-scale plot in the scale range below the SRC and equals 2 minus 2 times the value of the slope. Also, the relative areas at each scale were considered as surface characterization parameters, with the additional benefit that these relative areas allow for scale-based discrimination.

#### **II.2.5.3. Analysis of the Size of the Measured Region**

As explained by Pedreschi et al. (2000), for sufficiently large measured regions, relatively small variations of the characterization parameters from region to region are expected. For smaller measured regions, the COV of the parameters could increase when the size of the measured region approaches the size of distinctive features on the surface. The COV of  $S_q$ ,  $S_{ku}$ , SRC, and fractal dimension of different sizes of measurement regions was calculated for the surface of product A. The COV is the standard deviation

divided by the mean. The intent is to select a measurement region that is large enough to include a good statistical sample of the features on the surface.

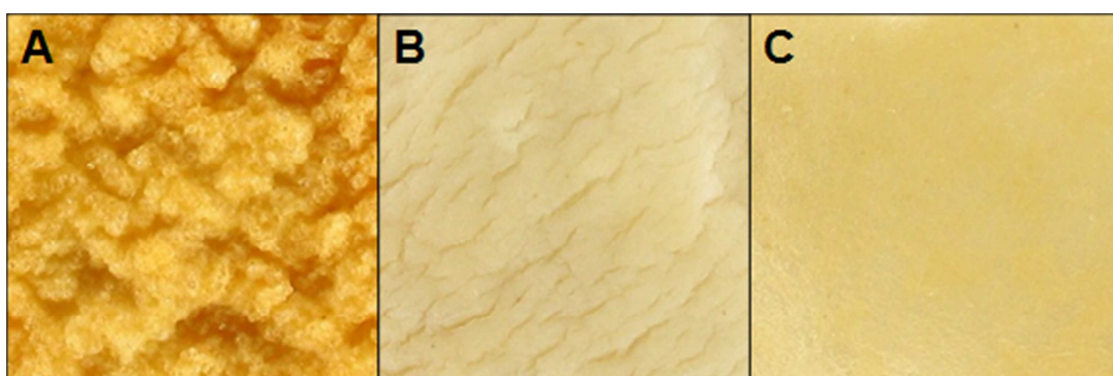
### **II.2.6. Statistical Analysis**

Conventional parameters, SRC, and fractal dimension were compared by implementing a Duncan's multiple-range test with a confidence level of 95%, using Statgraphics Plus software version 5.1 (Manugistic Inc., Rockville, MD).

The comparison of relative areas at each scale was achieved by a scale-based F-test of significance, performed by SFRAX® software (Surfract, [www.surfract.com](http://www.surfract.com), Worcester, MA). This method allows the comparison of two product surfaces by considering the relative areas at each scale as two samples from two populations (Jordan and Brown, 2006). At each scale, the mean square ratio (MSR) of the six measurements of the compared surfaces was computed, and a MSR threshold value of 4.26 was determined for a confidence level of 95%. The two surfaces are different to that level of confidence, over those scales where the MSR exceeds the threshold value.

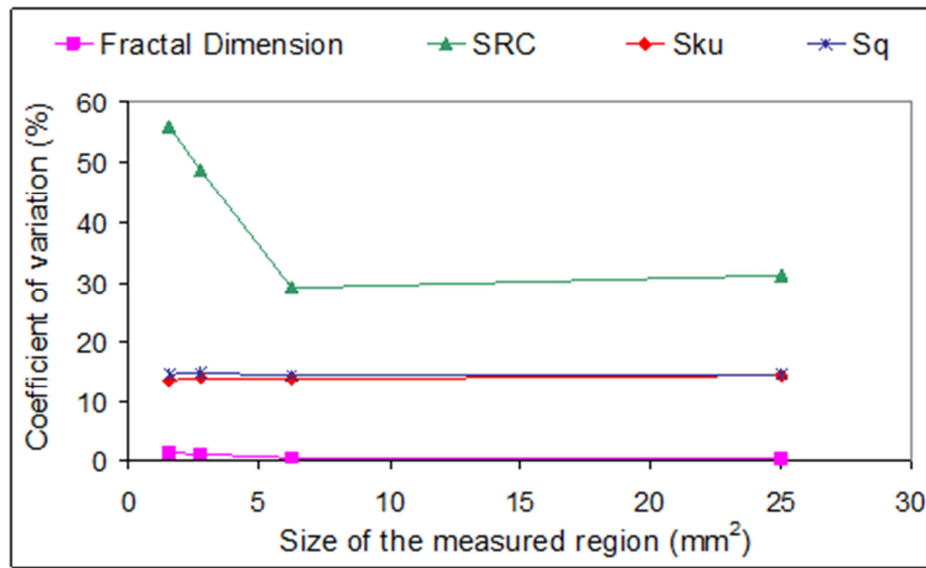
### **II.3. Results**

Figure II.2 shows photographs of the surfaces of the three fried products. The differences between the surfaces are evident: A appears to be the roughest, followed by B, and then C.



**Figure II.2:** Photograph of the surface of products A, B, and C. The size of the photographed region of each product is 2x2 cm<sup>2</sup>.

The COVs of  $S_q$ ,  $S_{ku}$ , SRC, and the fractal dimension determined for different measurement sizes of the surface of product A, the rougher surface, are shown in Figure II.3. No variation is observed for  $S_q$ ,  $S_{ku}$ , or the fractal dimension, when the size of the measurement region is diminished from 25 to 1.6 mm<sup>2</sup>. The SRC presents almost the same COV between measured regions of 25 and 6.3 mm<sup>2</sup>, but at smaller measurement sizes the COV increases significantly.



**Figure II.3:** Coefficient of variation (COV) of conventional parameters ( $S_q$  and  $S_{ku}$ ) and area-scale fractal parameters (SRC and fractal dimension) for the surface of product A as a function of the size of the measured region.

The means and standard deviations of the root mean square height and skewness parameters, i.e., first and second statistical moments,  $S_q$  and  $S_{ku}$ , are shown in Figure II.4. According to the Duncan's multiple-range test with a confidence level of 95%,  $S_q$  is capable of discriminating A from B and C but not B from C; also,  $S_{ku}$  discriminates A from B but not C from A and B.

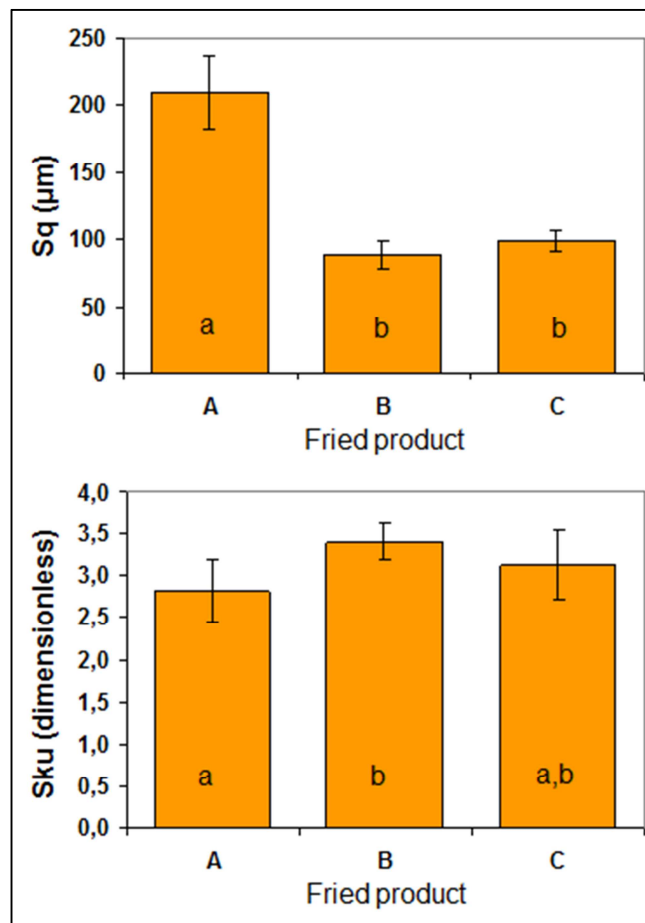


**Figure II.4:** Conventional surface parameters  $S_q$  and  $S_{ku}$  of products A, B, and C. Mean values of six measures  $\pm$  standard deviation are shown. The charter inside each bar indicates significant differences.

The area-scale fractal analysis results are shown in Figure II.5. The mean value of relative area, with the corresponding standard deviation, of the six surface measurements of 25 mm<sup>2</sup> from each fried product is plotted against the scale of observation. As is expected, all the fried products show relative areas near 1 at the larger scales. At smaller scales, the differences between them can be clearly identified. The surface of product A shows relative areas considerably higher than B and C, and the relative areas of product B are higher than those of product C. The ranges of scales over which the relative areas of the products are different are shown in Figures II.6-II.8, where the MSR was plotted against the scale of observation for the comparison between products A and B (Figure II.6), A and C (Figure II.7), and B and C (Figure II.8). When product A is compared with products B or C, the range of scales of discrimination goes from 1,500,000 m<sup>2</sup> to the finest scale. When products B and C are compared, the range of scales of discrimination is smaller, going from 200,000 mm<sup>2</sup> to the finest scale.

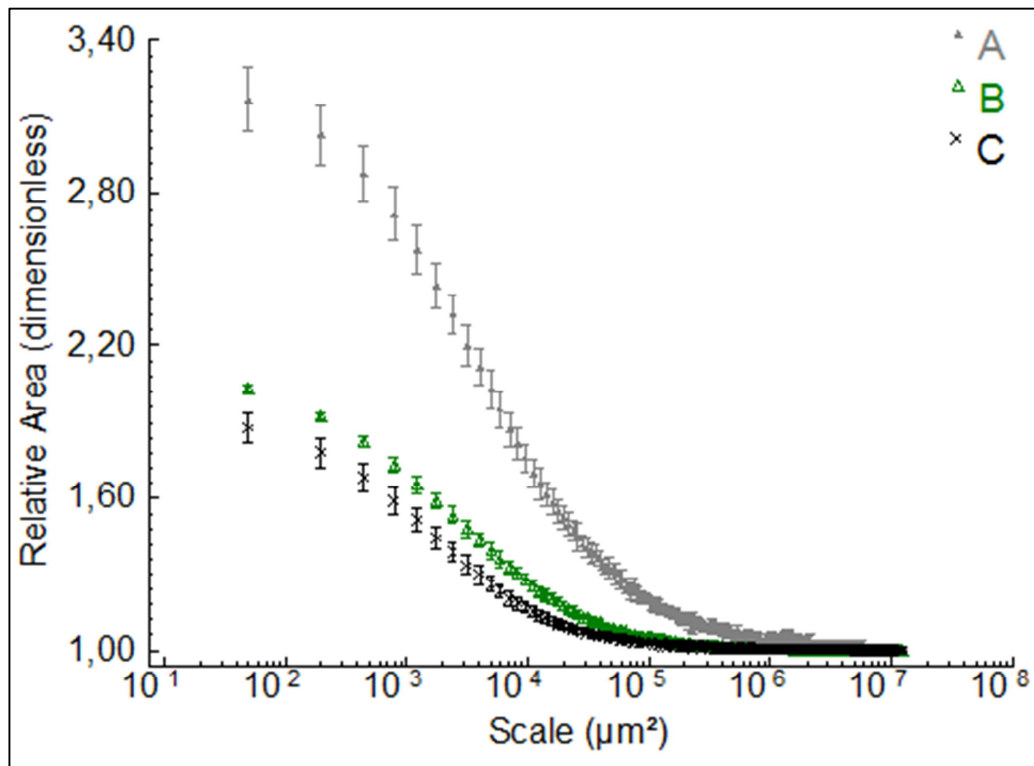


**Figure II.5:** Area scale plot of products A, B, and C. Mean values of relative areas of six measures  $\pm$  standard deviation are shown.

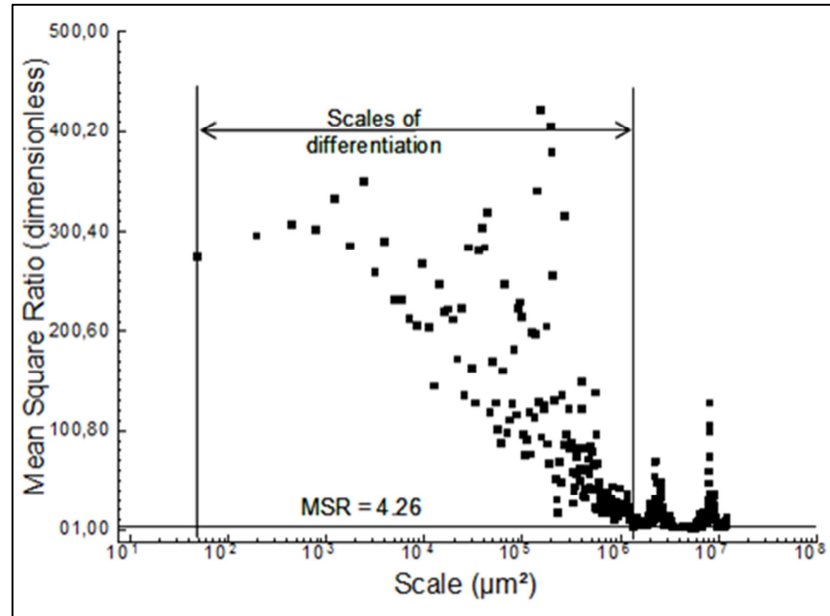


**Figure II.6:** Results of scale-based F-test of significance with 95% confidence when comparing six measures of products A and B. The mean square ratio (MSR) is plotted as a function of the scale. The threshold of differentiation between the surfaces is determined by a MSR of 4.26. The scales over which both surfaces are different are shown in the plot.

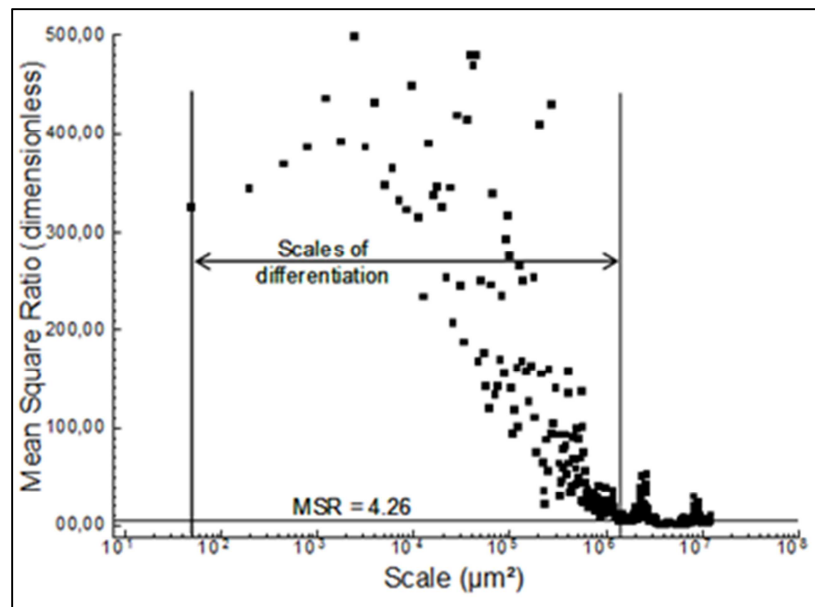


**Figure II.7:** Results of scale-based F-test of significance with 95% confidence when comparing six measures of products A and C. The mean square ratio (MSR) is plotted as a function of the scale. The threshold of differentiation between the surfaces is determined by a MSR of 4.26. The scales over which both surfaces are different are shown in the plot.

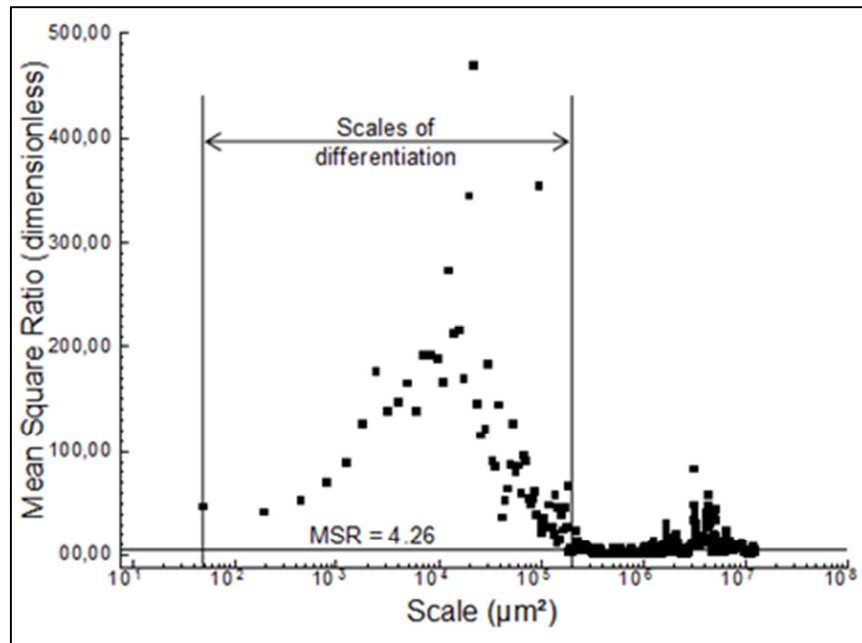


**Figure II.8:** Results of scale-based F-test of significance with 95% confidence when comparing six measures of products B and C. The mean square ratio (MSR) is plotted as a function of the scale. The threshold of differentiation between the surfaces is determined by a MSR of 4.26. The scales over which both surfaces are different are shown in the plot.

The SRC and the fractal dimension, which are derived from area-scale plots, are shown in Figure II.9. The mean values of the six measurements of 25 mm<sup>2</sup> of the surface of each fried product are presented in bar plots, and the statistical differences between the parameters are symbolized inside each bar. The SRC can discriminate the surfaces of the three products. The surface of product A shows a value of SRC considerably higher than those of products B and C, and the SRC of product B is higher than that of product C. The fractal dimension can discriminate the surface of product A from B and C but it cannot discriminate B and C.

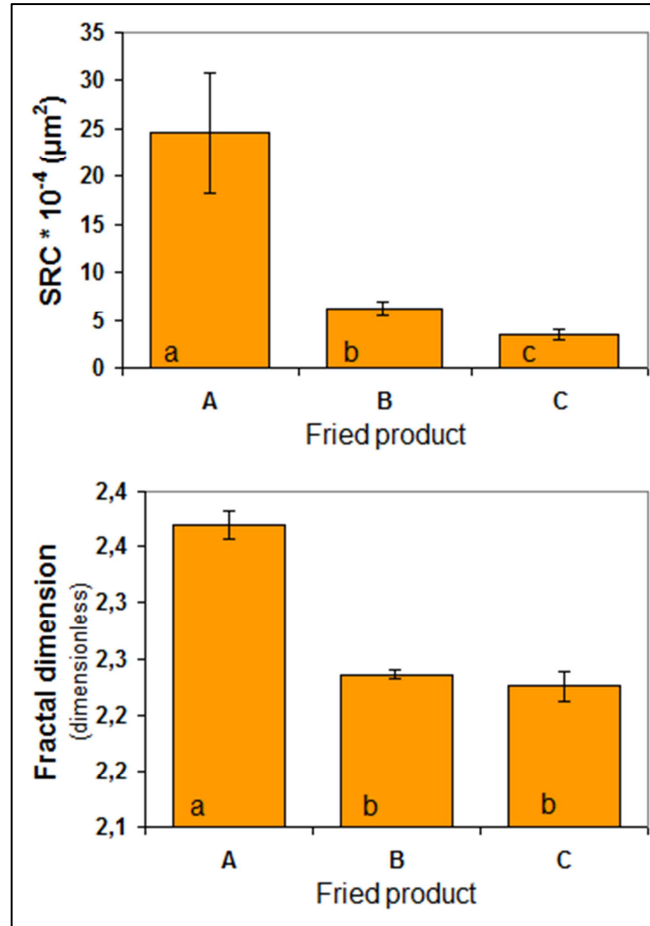


**Figure II.9:** Area-scale fractal parameters SRC and fractal dimension of products A, B, and C. Mean values of six measures  $\pm$  standard deviation are shown. The charter inside each bar indicates significant differences.

#### II.4. Discussion

An appropriate selection of the size of the measurement is a key factor for surface characterization. In this work, the size of measurement was determined by evaluating changes of the COV of several parameters on the surface of the rougher product. No changes of COV were observed in any parameter for measurement regions larger than 6.25 mm<sup>2</sup>, and a measurement region of 25 mm<sup>2</sup> was sufficiently large to ensure the determination of representative parameters to all the studied surfaces. Also, the lateral resolution is an important factor to be considered when measuring a surface. This



parameter was not evaluated in this study; however, it is important to mention that it was selected based on the ability to discriminate between the different surfaces.

Among the analyzed parameters, the fractal dimension and the  $S_q$  ranked the surfaces of the three fried products in the same manner. The information contained in these two parameters is different, but both are commonly employed to symbolize surface roughness, and neither of them was able to discriminate B and C. Therefore, they are not appropriate descriptors for the surfaces studied in the current work. The  $S_{ku}$  parameter did not discriminate the surfaces of the studied products and is also inadequate for analytical purposes.

The SRC and the relative area successfully discriminate the surfaces products A, B, and C. Regarding the SRC, high variation is observed in the rougher product, which has a COV of 31%. High variations indicate a need for more measurements, which makes this parameter less convenient for discriminating the surfaces of fried foods.

The relative area is the most reliable parameter for discriminating surfaces of the fried products studied in this work. This parameter is scale-sensitive and allows determination of the scales over which two surfaces are different, thereby giving information about the relevant scales of interaction on topographically related phenomena. This could lead to an understanding of the role of the surface from a phenomenological perspective; moreover, it is less arbitrary than describing the surfaces only with one number.

## **II.5. Conclusions**

Testing the ability to discriminate is a means of selecting topographic characterization parameters for use in food studies. Among the parameters evaluated in this study, the most reliable parameter for discriminating the surfaces of fried foods is the relative area, calculated from area-scale fractal analysis. This parameter is scale-sensitive and allows the discrimination of the surfaces through a range of scales.

### **III. Effect of food surface roughness on oil uptake by deep-fat fried products**

#### **ABSTRACT**

The aim of this work is to examine the relationship between surface roughness and oil uptake in fried fabricated products. Two product categories were studied, using formulations based either on potato flakes or wheat gluten. Products were deep-fat fried at 170°C and two oil fractions, penetrated oil and surface oil, were determined at the beginning and at the end of cooling period. The surface of fried products was measured using a scanning laser microscope and characterized by an area-scale fractal analysis. Within each product category, products with higher surface roughness retained more oil. However, this relationship could not be extended when comparing products of different categories. Potato-flake-based products were rougher than gluten-based products, but did not retain more oil. Further, gluten-based products absorbed most of the oil during frying, whereas potato-flake-based mostly absorbed oil during cooling. Certainly, surface roughness is a key factor in oil absorption, but other food-related properties, such as the micro-structure of the crust, may explain differences among product categories and should be examined in future studies.

Keywords: Deep-fat frying, oil uptake, fabricated products, formulated products, surface roughness.

#### **III.1. Introduction**

Deep-fat frying is a process of cooking foods by immersing them in edible oils and fats at elevated temperatures to induce fast dehydration. One of the most important quality changes during the process is the amount of oil retained inside the product, which is incompatible with current health trends. Several studies have shown that oil is mainly retained in the crust region (Aguilera and Gloria, 1997; Bouchon et al., 2001; Keller et al., 1986; Pedreschi et al., 1999), which mostly penetrates during the post-frying cooling period (Bouchon et al., 2001; 2003; Mellema, 2003; Moreira et al., 1997; Ufheil and Escher, 1996). Research has demonstrated that during frying the vigorous

escape of water vapor and related inner pressure precludes oil migration into the crust and therefore, oil penetration is limited during most of the immersion period. As a result, oil absorption would be essentially a surface-related phenomenon, which is determined by the equilibrium between surface drainage and suction during post-frying cooling (Bouchon et al., 2003).

Previous information suggests that the surface characteristics of fried products and particularly the geometrical irregularities, or roughness, are highly important in oil absorption kinetics. However, the equilibrium between drainage and suction still remains unclear. Rubnov and Saguy (1997) studied the relationship between oil absorption and surface roughness in fried restructured potato products formulated from a potato-flake-based dough and fructose. They derived an apparent fractal dimension from the silhouettes of scanning electron microphotographs of sample contours, using image analysis, and found a direct relationship between oil absorption and surface roughness. However, using the same approach in wheat-flour-based products, Thanatuksorn et al. (2005) did not determine any direct effect of surface roughness on oil uptake. Bouchon and Pyle (2004) characterized the surface of restructured potato chips using reflective confocal laser scanning microscopy. They determined conventional, statistical surface roughness descriptors, such as the root mean square roughness ( $S_q$ ), which was higher for products with higher total oil content. Both the fractal dimension and the conventional parameters allow, in some cases, to discriminate between surfaces with different oil absorption capacity. However, such parameters do not provide a clear physical interpretation of the role of surface roughness on oil absorption.

In order to clarify the effect of surface roughness on oil uptake mechanisms, controllable and uniform food systems with different oil absorption capacities should be used. Model structures may be obtained using ingredients with strong structure-development potential. Wheat flour and potato-flakes fulfill this requirement and have been previously used to develop food model systems to understand oil uptake mechanisms during deep-fat frying (Bouchon and Pyle, 2004; Gazmuri and Bouchon, 2009; Pinthus et al., 1992; Rubnov and Saguy, 1997; Thanatuksorn et al., 2005). Wheat

flour is a valuable food building block because of the functionality of gluten, a highly hydrophobic viscoelastic protein with film-forming and water-binding capacities (Day et al., 2006). Similarly, potato flakes provide adequate stickiness and a high water-holding capacity, due to the high level of extra-cellular gelatinized starch (Bouchon and Pyle, 2004). Other ingredients such as native and pre-gelatinized potato starch (Bouchon and Pyle, 2004), fructose (Rubnov and Saguy, 1997), cellulose, cellulose derivatives and gums (Annapure et al., 1999; Pinthus et al., 1993) have been successfully added in the formulated products in low quantities to modify oil absorption capacity. In addition, the surface topography of the fried product should be precisely measured and characterized. The scanning laser microscope (SLM) is a profiling, non-contact instrument, that measures set of heights as function of position (height elevation matrix; ASME B46, 2002) that can be used to construct a topographic maps. The instrument has been previously used to measure food surface successfully because of its minimal intrusion and satisfactory resolution (Briones et al., 2006; Pedreschi et al., 2000). Topographical measurements can be analyzed by either using conventional statistical methods or more recent methods, such as area-scale fractal analysis (ASME B46.1, 2002) that provides a better description for discrimination between some surfaces (Jordan and Brown, 2006). This method was developed by Brown et al. (1993) and is based on the fact that the area of a rough surface varies with the scale of measurement as indicated by fractal geometry. It can be used to determine the scales over which two surfaces are different, giving information about the relevant scales of interaction of topographically related phenomena. The objective of this work is to study the relationship between surface roughness and oil uptake in fried formulated products with a wide range of oil absorption capacities. Two oil fractions were determined: surface oil and penetrated oil (Moreno and Bouchon, 2008), which were measured just after removing the product from the oil bath and after cooling. The surface of fried products was measured by SLM and characterized by area-scale fractal analysis.

## **III.2. Materials and methods**

### **III.2.1. Materials**

Two main product categories were studied. Formulations were either based on potato flakes (PF) (7% w.b. moisture content, Alimentos Unisur, Chile) or on wheat flour constituents, which will be referred as PF- and G-based product categories (the latter representing gluten). In order to get a strict control of the gluten content in the dough, it was decided to work with a restructured matrix made of native wheat starch (NS) (8% w.b. moisture content) and vital wheat gluten (G) (7% w.b. moisture content) instead of wheat flour. Both of these ingredients were obtained from Asitec S.A., Chile. Methylcellulose (MC) (4% w.b. moisture content, Sigma M0512, Sigma–Aldrich, USA) was added as additional ingredient and high oleic sunflower oil (Camilo Ferrón, Chile) was used as frying medium.

### **III.2.2. Product formulation**

Samples were prepared ensuring the same water content in the dough,  $40 \pm 0.6\%$  (w.b.). The amount of water added depended on the initial water content of the ingredients and was adjusted to ensure that all different products contained the specified amount. To determine the amount of water that had to be added, the exact water content of ingredients was determined experimentally by drying in a forced-air oven at  $105^{\circ}\text{C}$  to constant mass (LDO-080F, Labtech, Korea).

Dry mixture formulations are summarized in Table III-1. In formulating the PF-based product category, PF were studied alone and with each of the two additional ingredients (MC and NS). Formulations of wheat-flour-based products contained either 8% or 12% gluten (% d.b.). These blends were studied alone and with 10% (d.b.) of MC added to the blend, and these products belong to the G-based products category.

**Table III-1:** Dry mixture blends of G- and PF-based products categories, expressed in terms of the components' proportions (proportions exclude ingredients' water content). The formulation of gluten-based products consisted of wheat vital gluten (G) and NS blends to emulate wheat flour, and MC as additional ingredient. The formulation of potato-flake-based products consisted of potato flakes (PF) as the main ingredient and native wheat starch (NS) and methylcellulose (MC) as additional ingredients.

	Formulation	Potato flakes (% d.b.)	Gluten (% d.b.)	Native starch (% d.b.)	Methylcellulose (% d.b.)
G-based	8G	-	8	92	-
	12G	-	12	88	-
	8G+MC	-	90		10
		-	8	92	
	12G+MC	-	90		10
		-	12	88	
PF-based	PF	100	-	-	-
	PF+MC	90	-	-	10
	PF+NS	90	-	10	-

### III.2.3. Sample preparation

PF-based products were prepared by mixing the dry ingredients for 2 min using a 5K5SS food mixer (KitchenAid, USA), equipped with a K5AB flat beater. To form the dough, distilled water was gradually added for 1 min to the specific dry mixture blend, until the water content (w.b.) reached 40%; the blend was then mixed for another minute. In these products, all the water was added at 15°C. In G-based products, water was added according to the protocol described by Gazmuri and Bouchon (2009). Half of the water was gradually added at 15°C while mixing for 1 min. After mixing for 1 extra minute, the remaining water was added. This water fraction was heated at 90°C, and was also poured while mixing for 1 min. The blend was then mixed for 1 extra minute. The dough was then wrapped in a plastic bag for 1 h at room temperature (20°C). After dough formation, it was kneaded to ensure homogeneity, laminated to the required thickness using a dough sheeter (DOYON-LSB516, Canada), and cut into 4x4 cm<sup>2</sup> squares. The exact thickness of the sheeted dough ranged from 2 to 2.3 mm, and was determined by controlling the weight of the chips to 4.7 ± 0.03 g in order to ensure the same solids content for each sample.

### **III.2.4. Frying**

The samples were fried at  $170 \pm 2^\circ\text{C}$  until a final moisture content of  $2 \pm 0.5\%$  (w.b.) was reached in a 5 L capacity deep-fryer (Somela-535T, Santiago, Chile), equipped with an external temperature control system (PID + Autotuning, Veto, Chile). The fryer was filled with 4 L of oil that was preheated for 2 h prior to frying (Blumenthal, 1991) and was discarded after 90 min of frying time. Throughout the frying process, five chips were placed in a basket and held in position with a wire grid to prevent them from floating. The frying time ranged from 6 to 7 min, depending on the product formulation. When frying was completed, the products were removed from the fryer, and the cooling period began.

### **III.2.5. Analytical methods**

*Surface oil content* (SO) corresponds to the amount of oil that can be easily removed from the surface of the product. It was determined, as described by Bouchon et al. (2003), by immersing each sample during 2 s in 150 mL of petroleum-ether (Winkler, Santiago, Chile) at room temperature, weighing the remaining oil after solvent evaporation under vacuum. Surface oil was removed after 2 s of cooling (the lowest reliable time that allowed moving a sample from the frying basket to the beaker with petroleum-ether) and after allowing drainage for 10 min at room temperature ( $20^\circ\text{C}$ ), holding the samples in a vertical position, so that excessive surface oil could drain off. The resulting solution was transferred to a 250 mL round bottom flask (Quickfit-BDH, Poole, UK) that had been previously dried and weighed. Finally, the extracted oil was collected by evaporating the solvent under vacuum (0.7 bar) using a rotary evaporator (BÜCHI Rotavapor R-124, Switzerland). The flasks containing the extracted oil were then dried to constant mass, by heating in a convective hot air oven at  $105^\circ\text{C}$ , cooled in a desiccator and weighted (Bouchon et al., 2003).

*Penetrated oil content* (PO) was determined after SO removal. The samples were ground and transferred into single-thickness cellulose extraction thimbles (33x80 mm, Toyo Roshi Kaisha, Ltd., Japan.). A clean, dry round bottom flask (250 mL) was

weighed and 200 mL of petroleum-ether were added to the flask. Extraction was carried out for 4 h using a soxhlet apparatus (60°C) and the solvent was removed using a rotary evaporator. The flasks containing the extracted oil were then dried to constant mass, cooled in a desiccator and weighted (AOAC, 1995; Bouchon et al., 2003).

*Total oil content* (TO) was determined as the sum of SO and PO. Fat content of the samples prior to frying was neglected. Solids content was determined by drying the defatted samples, using a forced-air oven at 105°C for 24 h until a constant mass was reached (AOAC, 1995).

*Moisture content* of the samples was determined before and after frying on each experiment to verify the moisture content of  $40 \pm 0.6\%$  and  $2 \pm 0.5\%$  w.b., respectively. This was carried out by air drying 3 g of ground sample at 105°C until constant mass was reached (AOAC, 1995).

To test for reproducibility of oil content results, five batches were prepared, sheeted, and fried for each formulation. Two additional batches of each product formulation were prepared for surface analysis.

### **III.2.6.Surface analysis**

#### **III.2.6.1. Surface measurement**

The topographic surface measurements were carried out using a UBM (Solarius Development, Sunnyvale, California, USA) scanning laser microscope (SLM) equipped with a triangulation laser height sensor (Keyence LC-2210, Osaka, Japan). Positioning tables moved the sample under the sensor, tracing at a speed of 0.5 mm/s. The sensor measured the heights at a frequency of 40 kHz. The measurements covered regions of  $5 \times 5 \text{ mm}^2$  and consisted of heights,  $z$  ( $\mu\text{m}$ ), at 10  $\mu\text{m}$  intervals in the  $x$  and  $y$  directions.

For each product formulation, two samples fried in different batches were collected. Three regions were measured on each sample, so that six measurements were obtained for each product. All products were superficially defatted before surface measurement



by immersing them in 150 mL of petroleum-ether for 30 s immediately after frying. The topographies of the measured surfaces were saved digitally for later analysis.

### III.2.6.2. Surface characterization

The measured surface topographies were characterized by using an area-scale fractal analysis. In this method, the apparent area of a measured surface is calculated by a series of virtual tiling exercises, covering the measured surface in a patchwork fashion with triangular patches (Figure III.1). The area of the patches represents the scale of observation. The tiling exercises are repeated with patches of progressively smaller areas to determine the apparent area as a function of the scale of observation. The apparent area at each scale is calculated as the number of triangular patches times the area of the patches; this calculation is normalized by dividing it by the projected area of the tiled region to determine a relative area. Consequently, the minimum relative area is one. Later, an area-scale plot is constructed as a log-log plot of the relative area versus the areal scale of observation. Detailed description of the method is available in Brown et al. (1993) and ASME B46 (2002).

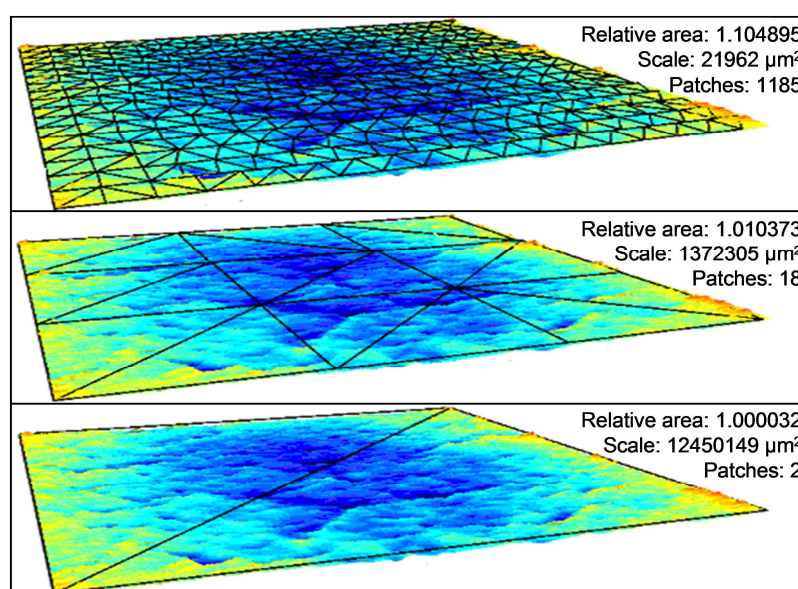


**Figure III.1:** : Diagram showing a sequence of three tiling exercises on a gluten-based product (12G) measured at 10  $\mu\text{m}$  sampling interval over a 5x5 mm<sup>2</sup> surface region. From the bottom to the top, the size of the triangular patch, or scale, decreases progressively, and the relative area increases.

Area-scale relations were calculated using SFRAX® software ([www.surfract.com](http://www.surfract.com)). Relative area as a function of scale was used as surface roughness descriptor.

### **III.2.7. Digital image acquisition**

Fried products were photographed using a color digital camera (PowerShot A70, Canon, USA) mounted inside a box impervious to light and internal black surfaces, with a uniform D65 light system to visualize macroscopic characteristic, as explained in Gazmuri and Bouchon (2009).

### **III.2.8. Statistical analysis**

Oil contents were compared using Duncan's multiple-range test with a confidence level of 95% using Statgraphics Plus software version 5.1 (Manugistic Inc., Rockville, MD, USA).

A scale-based F-test of significance was applied to the relative areas to determine the scales over which two surfaces have different relative area. As described by Jordan and Brown (2006) the relative areas of each scale (determined from measurements from two different samples) are treated as samples from two populations. The mean square ratio (MSR) is calculated for each scale and is subsequently plotted as a function of the scale. A threshold value of MSR is determined for a certain confidence level, depending on the number of measurements. The two populations, and therefore the two surfaces, are discernible over those scales where the MSR exceeds the threshold value. The scale-based F-test was executed using SFRAX® software with a confidence level of 99% for the comparison of pairs of six measurements, giving a threshold MSR value of 8.01.

Scale-based correlation developed by SFRAX® software was applied in order to determine the scales of best correlation of the surface and the total oil content of each product category. As explained by Briones et al. (2006), when the relative area of the surface at a specific scale is considered as the topographic characterization parameter (surface roughness descriptor), then the regression coefficient ( $R^2$ ) between a property related to that surface and the relative area can be calculated. These regression

coefficients are plotted for a series of scales. If a scale sensitive functional correlation to the property exists, then the  $R^2$  values could be low and perhaps erratic at larger scales, then increase with decreasing scale until reaching a maximum before either decreasing or leveling off. The characteristic scale of interaction for the property and the surface will be the scale over which this maximum  $R^2$  is reached (Brown and Siegmann, 2001; Cantor and Brown 2009).

### **III.3. Results and discussion**

Prior to frying, the characteristics of PF- and G-based dough presented clear qualitative differences. The PF-based dough was strong, elastic, and hard to sheet; whereas, the G-based dough was soft, brittle and easy to sheet. Important macroscopic differences between both product categories could be identified, as shown in the digital images presented in Figure III.2 (left-hand side), where a PF-based product appeared to be a darker brown and its surface more irregular when compared to a G-based product. Differences at a microscopic level were also evident, as can be seen in Figure III.2 (right-hand side), where measurements with the SLM have been used to construct topographic maps. In broad terms, more topographic irregularities can be observed in the PF-based product.

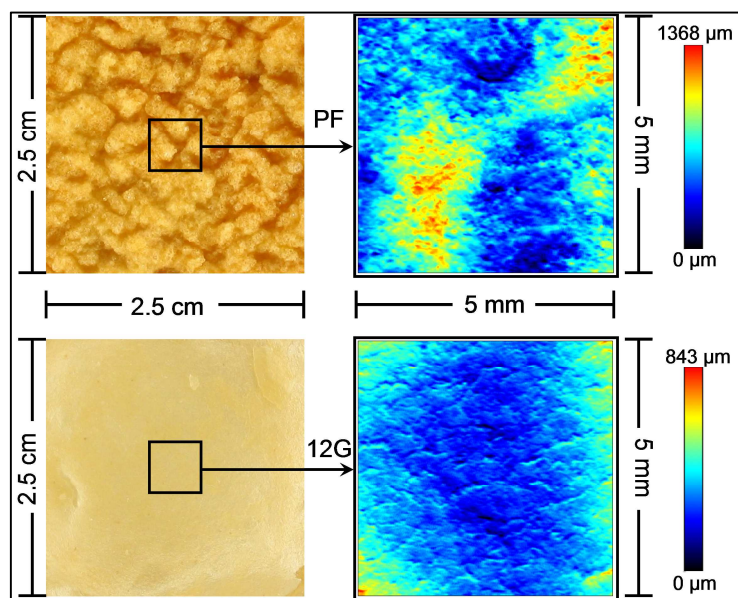


**Figure III.2:** Photographs of the surface (left) and representation of the measured topography (right) of deep-fat fried potato-flake-based product (PF on top) and gluten-based product (12G at the bottom). Each surface measure was acquired with a 10  $\mu\text{m}$  sampling interval on x and y directions. Note that the color scales that represent the z dimension are different in the two products.

### III.3.1. Surface topography

The area-scale fractal analysis uses the relative areas that are calculated from the virtual tiling exercise presented in Figure III.1. As can be observed, and as generally occurs, when the size of the triangular patch, or scale of observation decreases, the relative area increases. At the larger scales, the relative areas are often near one and therefore the surface can be described as smooth. At the finer scales, the relative area often deviates significantly from one, and the surface can be considered to be rough (Brown et al., 1993). When two surfaces are compared, increase in the relative area value at a certain area-scale is associated with the higher degree of irregular geometry and roughness.

Area-scale plots of G-based products are presented in Figure III.3. It is observed that the relative areas for all formulations are close to the value of one when the area-scale is higher and that differences between them are only revealed at smaller scales. An

overview of this plot indicates that the 8G product (uppermost curve) is roughest, followed by 12G and 8G+MC products and that the smoothest surface is the 12G+MC product (lowest curve). The effect of gluten content and MC addition on surface topography can be examined. The inclusion of MC in the formulation diminishes surface roughness in products containing either 8% or 12% d.b. gluten. This can be noticed when comparing the relative areas of 12G and 12G+MC products as well as those from 8G and 8G+MC. Furthermore, higher gluten content in the formulation implies a lower roughness, regardless of MC addition. This can be noted when comparing 8G+MC with 12G+MC as well as 8G with 12G products.

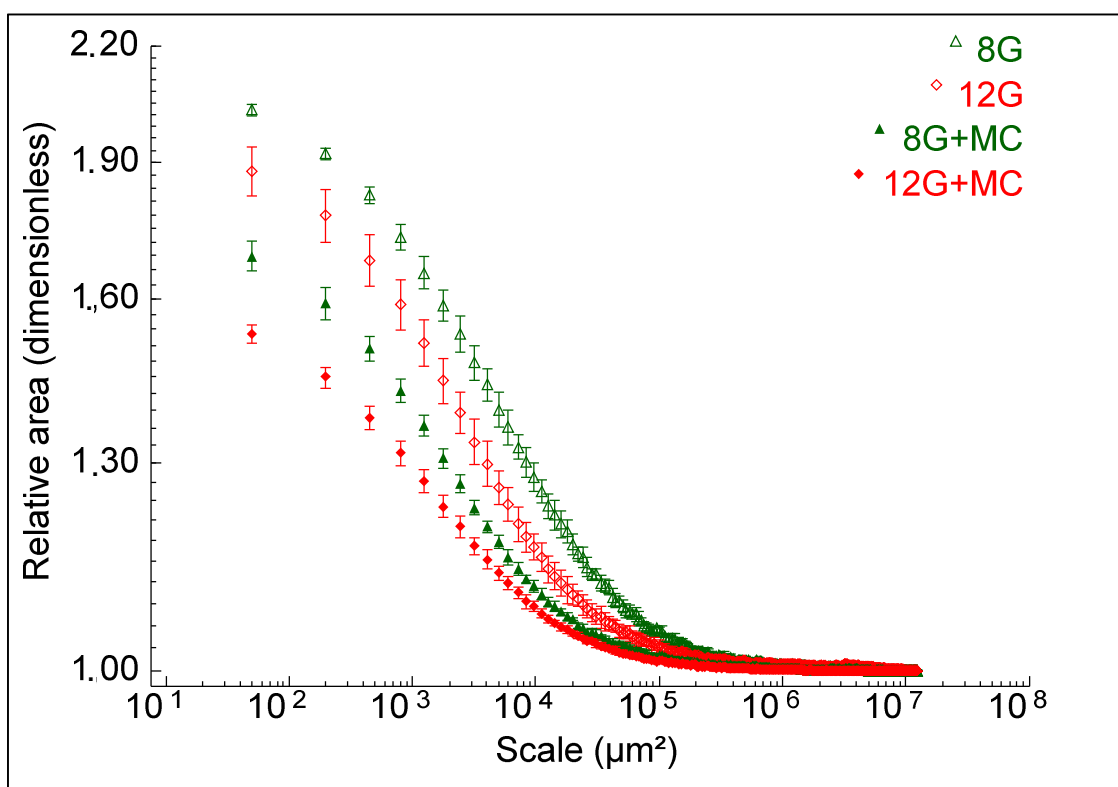


**Figure III.3:** Area-scale plots of gluten-based products. Relative area values correspond to the mean of six measures  $\pm$  standard deviation at each scale of observation. Larger relative areas indicate greater surface roughness.

The ranges of scales of observation over which the surfaces of the aforementioned pair-wise comparisons differ were determined using a scale-based F-test. Results are

summarized in Table III-2. This range is of interest, since it can advance the understanding of surface- related phenomena. For example, this information can provide an idea of the range of scales of protuberances over which oil absorption and/or drainage may be affected. Furthermore, this information can be useful for designing surfaces with tailor-made characteristics for topographically dependent interactions (Brown and Shipulski, 1994) or to get an indication of the effective area of transport phenomena for modeling purposes.

**Table III-2:** Scales of discrimination of G- and PF-products categories determined by scale-based F-test of significance with 99% confidence when comparing six measures of two surfaces for each pair-wise comparison.

	Pairwise comparison		Range of scales of differentiation ( $\mu\text{m}^2$ )
	(rougher)	(smoother)	
G-based	8G	12G	50 - $10^5$
	8G+MC	12G+MC	50 - $5 \cdot 10^4$
	8G	8G+MC	50 - $3 \cdot 10^5$
	12G	12G+MC	50 - $10^7$
PF-based	PF	PF+MC	50 - $8 \cdot 10^5$
	PF	PF+NS	50 - $5 \cdot 10^5$
	PF+MC	PF+NS	200 - 2000

Area-scale plots of PF-based products are shown in Figure III.4. The product made from whole PF developed the roughest surface during frying, followed by PF+MC and PF+NS. The addition of MC or NS to the formulation diminished the roughness of the surface significantly, as evidenced when comparing the relative areas of PF with PF+MC products and PF with PF+NS products. The ranges of scales of observation, over which the surfaces of PF-based products can be discriminated, according to scale-based F-test analysis, are summarized in Table III-2. Products with MC addition seem only slightly rougher than those with NS addition. In fact, even though surfaces of PF+MC and PF+NS products can be discriminated, the differences are restricted to a low range of scales (200-2000  $\mu\text{m}^2$  interval).

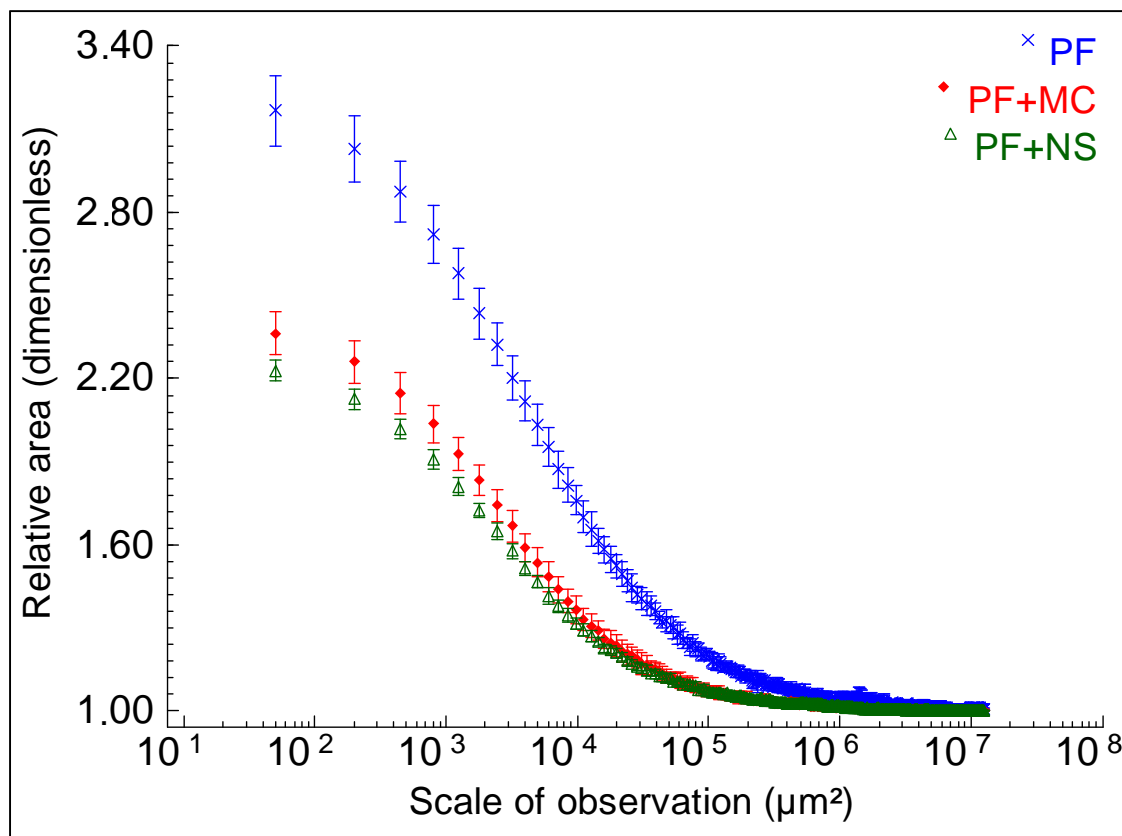


**Figure III.4:** Area-scale plots of potato-flake-based products. Relative area values correspond to the mean of six measures  $\pm$  standard deviation at each scale of observation. Larger relative areas indicate greater surface roughness.

In conclusion, the surface topographic analysis showed that PF-based products are significantly rougher in comparison to the G-based products. This highlights the importance of an appropriate selection of food ingredients for product formulation, since the nature of its main components, or food building blocks, clearly determines the distinctive characteristics of the final product.

### III.3.2. Total oil content

The total oil contents of G- and PF-based products after immediate (2 s) and 10 min of cooling are shown in Figure III.5. Total oil content after 10 min of cooling corresponds to the oil content at equilibrium, that is, when the competition between drainage of oil from the surface and suction of oil within the crust has ceased. In

preliminary experiments, it was observed that there is no change in the oil content after 10 min of cooling.

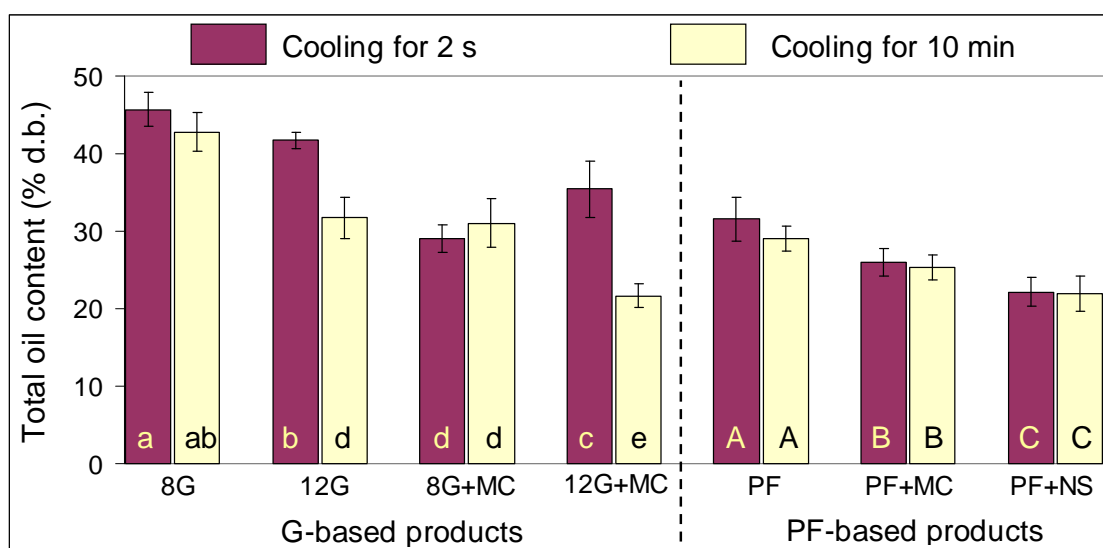


**Figure III.5:** Total oil (TO) content of formulated products after two cooling times, 2 s and 10 min. Values correspond to the mean of 5 measures  $\pm$  standard deviation. The same letter inside two bars indicates no significant differences in TO content between G-based products (lowercase letters) and between PF-based products (uppercase letters).

As Figure III.5 illustrates, an increase in the amount of gluten in the formulation decreases oil content. Oil content of 12G products is 25.8% lower than oil content of 8G products, after cooling for 10 min. This finding is consistent with previous reports by Gazmuri and Bouchon (2009), where the film-forming capacity of gluten makes the dough more elastic and less permeable to oil absorption.

The effect of increased gluten on reducing oil uptake is also found when comparing products with MC addition. After cooling for 10 min, 12G+MC products absorbed 30.1% less oil than 8G+MC products. Incorporation of MC also lowered the oil content of the products and more pronounced with higher portion of gluten. After cooling for 10 min, 12G+MC products contained 31.7% less oil than 12G products, whereas 8G+MC products contained up to 27.6% less oil than 8G products. The effect of MC addition in



oil uptake reduction has been attributed to the high water-binding capacity of MC and related thermogelation properties (Pinthus et al., 1992; Sanz et al., 2004).

As Figure III.5 indicates, the product containing pure PF as dry ingredient presented the highest final oil content at equilibrium. Incorporation of MC lowered the oil content by 13.1%, and higher oil content reduction (24.5%) was observed when NS was added into the formulations. Certainly, MC and NS addition, may also affect the crust inner structure, affecting key parameters such as mean pore size and permeability, which also play an important role. These aspects should be analyzed in future studies.

Within each product category, a good agreement between oil content at equilibrium and surface characterization was found. G-based products that developed rougher surfaces during deep-fat frying retained more oil after the process (Figures III.3 and III.5). Specifically, the addition of MC and the increase of gluten content in the formulation reduced surface roughness and decreased oil content. A similar behavior is observed when PF-based products are analyzed (Figures III.4 and III.5), where the effect of adding MC and NS resulted in both surface roughness and oil absorption reduction. As a result, it can be concluded that there is a direct relationship between oil retention and surface roughness within each product category, which could be linked to a larger available area for oil deposition, as suggested by Saguy and Pinthus (1995).

In order to support the relationship between total oil content and surface roughness, a scale-based correlation test was applied to PF- and G-based products (Figure III.6). The  $R^2$  for PF- and G-based product categories shows erratic behavior at largest scales of observation, where the mean relative areas are low (Figures III.3 and III.4). At smaller scales,  $R^2$  increases regularly to about 0.9. Within this range of scales, a candidate scale of interaction for each product category could be found, where  $R^2$  reaches a maximum. These are indicated in the plot. As can be noted, these candidate scales of interaction of PF-based products and G-based products are  $1793 \mu\text{m}^2$  and  $19,920 \mu\text{m}^2$ , respectively. The plots of total oil content versus the relative area at the selected scales of interaction of both products categories are shown in Figure III.7. The agreement between total oil

content and relative area is close to 90% when analyzing G-based products or PF-based products, separately, indicating a good correlation between surface topography and the amount of oil that is retained by fried products of the same product category.

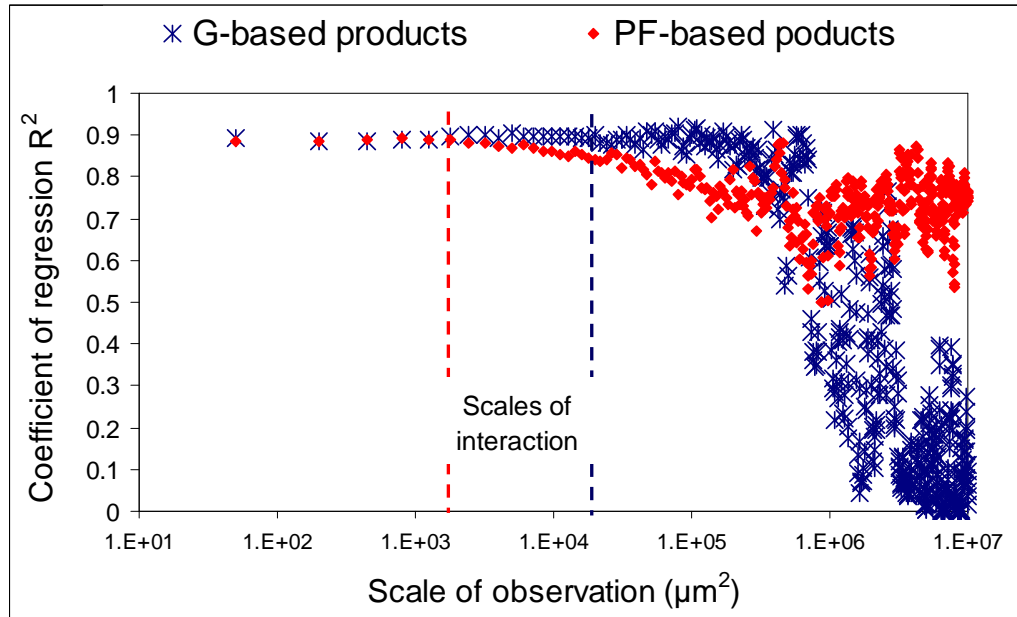


**Figure III.6:** Results of scale-based correlation test applied to potato-flake-based products and gluten-based products. Least squares regression coefficients ( $R^2$ ) for relative area as a function of total oil content are plotted versus the scale of observation. Possible scales of interaction for each product category are indicated in the plot.

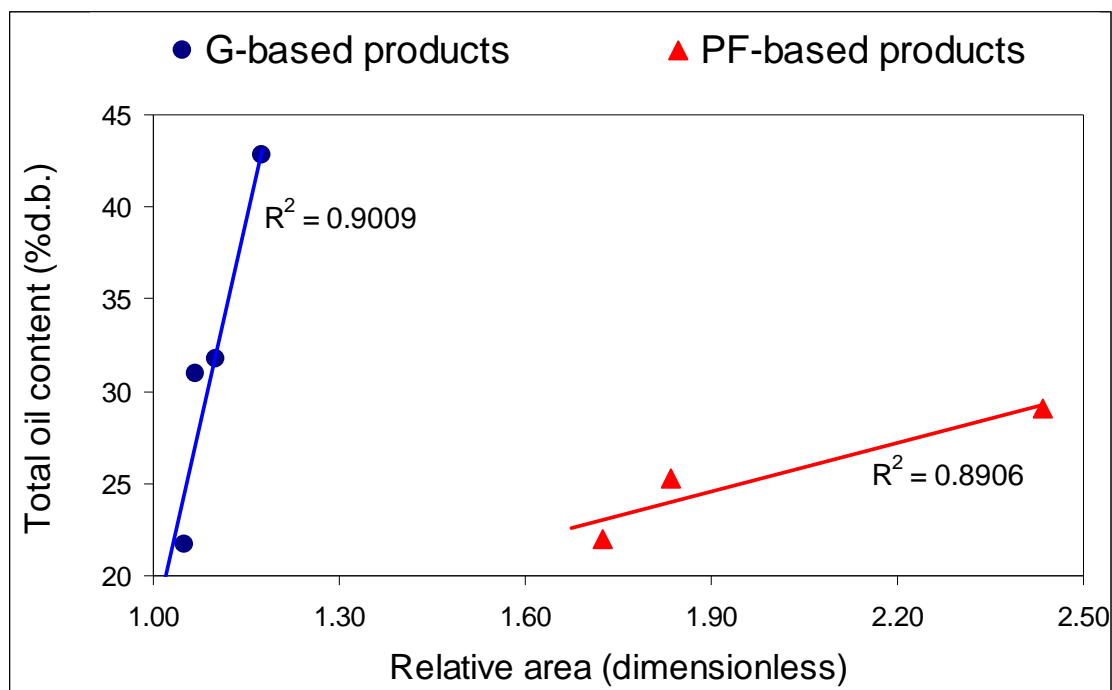


**Figure III.7:** Total oil content vs. relative area of potato-flake-based products and gluten-based products at candidate scales of interaction of  $1793 \mu\text{m}^2$  and  $19,920 \mu\text{m}^2$ , respectively. Least squares regression coefficients ( $R^2$ ) are shown.

Even though it was possible to find a relationship between oil content and surface roughness within a specific product category, it is not possible to extend this conclusion across products of different categories. PF-based products are rougher than G-based products, but they retained less oil. These results are in agreement with those obtained by Thanatuksorn et al. (2005) and by Rubnov and Saguy (1997), who examined the relationship between oil content and surface roughness in wheat-flour-based and PF-based products, respectively. In both studies, surface roughness was characterized using the same approach, i.e. deriving an apparent fractal dimension from the sample contours of scanning electron microphotographs. When results from both studies are compared, it can be observed that wheat-flour-based products contain higher oil content than PF-based products having the same surface roughness. Conversely, PF-based products having similar oil content to wheat-flour-based products are rougher.

This shows that the relationship is restricted to products with similar compositions, and that the surface irregularity is not the only factor that is affecting oil absorption. In fact, the balance between oil in the crust and residual surface oil is a result of the competition between capillary suction into the crust and drainage along the surface of the product, while the product cools down. Consequently, the micro-structure (mean pore size, connectedness, and permeability) of the crust, which is formed while the product is cooking in the frying oil, is a critical factor and is intimately related to the nature of the matrix (Bouchon et al., 2001). Also, the wetting properties and the hydrophobic nature may play an important role in oil absorption (Blumenthal, 1991; Pinthus and Saguy, 1994).

Total oil was determined just after removing the product from the oil bath, and after 10 min of cooling, in order to understand how fast the different food matrices attained equilibrium. As can be seen in Figure III.5, only products with high gluten content (12G and 12G+MC products) showed a significant difference in oil content after 2 s of cooling, whereas no differences were found in products with lower gluten content. That is, drainage occurred extremely rapidly in products with low gluten content (<2 s) and was delayed in products with higher gluten content. Also, no significant drainage after 2 s of cooling was detected in PF-based products.

### **III.3.3. Penetrated and surface oil contents**

In order to get a better understanding of oil absorption during cooling, it was decided to analyze the relative behavior of penetrated oil and surface oil at the two cooling times. To do so, the oil fractions were determined after 2 s and 10 min of cooling. Both were divided by the total oil content at equilibrium (after 10 min of cooling), in order to get information about the internal distribution of the oil inside each product in relation to the final oil content. The results are shown in Figures III.8 and III.9. From both figures it can be noticed that the sum of penetrated oil and surface oil fractions of 12G and 12G+MC products at the beginning of the cooling period exceeds by far 100%, since excessive oil drainage occurs after cooling for 2 s, as mentioned in the previous section.

As can be seen from penetrated oil results (Figure III.8), more than 50% of the final oil content has already penetrated inside G-based products just after 2 s of cooling (ranging from 53.5 up to 96.4%). That is, most of the oil seems to penetrate the structure during the immersion period or just after cooling begins. As described earlier, most of results found in the literature have reported that oil would penetrate mostly during the cooling period. However, Thanatuksorn et al. (2005) reported that oil would be mainly absorbed during the immersion period, in a work that focused on wheat-flour-based products, similar to those studied here. This behavior could be related to the characteristics of the porous network developed by G-based products during frying, which may influence the capillary flow of oil within the product. G-based matrixes may develop small pores during frying, which may increase the capillary pressure, because of the inverse relationship between both parameters (Bouchon and Pyle, 2005). During the immersion period, the capillary pressure could even exceed the inner pressure of the product, especially in dry pores, being able to drive oil within the structure during this stage. Certainly, the inner micro-structure of the product should be further analyzed to validate this statement. On the other hand, in PF-based products only approximately 30% of the final oil content penetrates the structure after cooling for 2 s. Most of the oil remains at the surface and is absorbed after some cooling takes place. This behavior is in accordance with results reported by Ufheil and Escher (1996) and Moreira et al. (1997) in potato slices and tortilla chips, respectively.

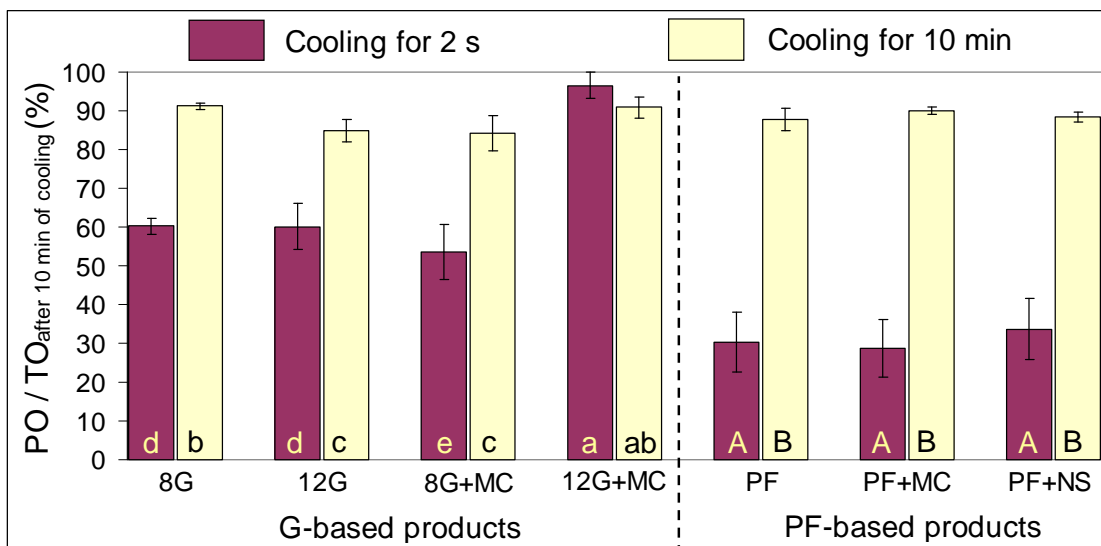


**Figure III.8:** Penetrated oil (PO) content of formulated products, at two cooling times, expressed as a fraction of total oil (TO) content after 10 min of cooling, or final TO content. Values correspond to the mean of 5 measures  $\pm$  standard deviation. The same letter inside two bars indicates no significant differences in PO content between G-based products (lowercase letters) and between PF-based products (uppercase letters).

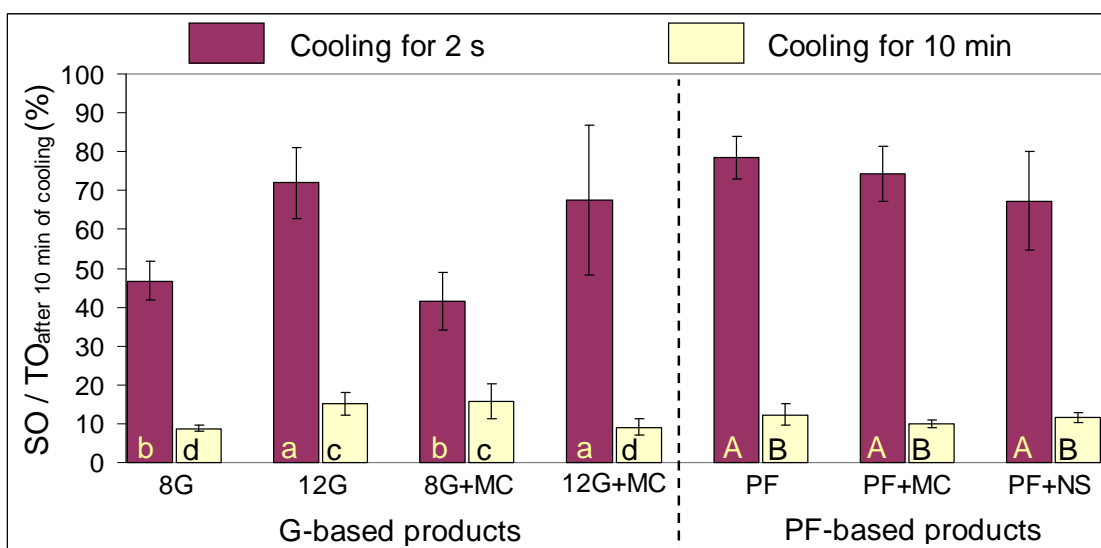


**Figure III.9:** Surface oil (SO) content of formulated products, at two cooling times, expressed as a fraction of total oil (TO) content after 10 min of cooling, or final TO content. Values correspond to the mean of 5 measures  $\pm$  standard deviation. The same letter inside two bars indicates no significant differences in SO content between G-based products (lowercase letters) and between PF-based products (uppercase letters).

### **III.4. Discussion and Conclusions**

Laser scanning microscopy technique allowed an adequate measurement of the surface of fried products, which were then successfully characterized and discriminated by area-scale fractal analysis. This methodology allowed studying the relationship between surface roughness and oil uptake in potato-flake- and gluten-based products. Within each product category, a good agreement between oil content at equilibrium and surface roughness was found. In gluten-based products, the formulations that developed rougher surfaces during deep-fat frying retained more oil. Specifically, the addition of methylcellulose and the increase of gluten in the formulation reduced surface roughness and decreased oil content. Similarly, in potato-flake-based products, formulations with higher roughness absorbed more oil. In this product category addition of methylcellulose and native wheat starch resulted in both surface roughness and oil absorption reduction.

Even though it was possible to find a linear relationship between oil content and surface roughness within a specific product category, it was not possible to extend this conclusion across the different product categories investigated. Potato-flake-based products were rougher than gluten-based products, but they did not retain more oil. Further, gluten-based products absorbed most of the oil during frying, whereas potato-flake-based mostly absorbed oil during cooling. Certainly, surface roughness is a key factor in oil absorption, but other food-related properties, such as the microstructure of the crust, which is formed while the product is being fried, as well as the wetting properties of the food matrix, may explain differences among product categories and should be analyzed in future studies.

#### **IV. Microstructural characterization of deep-fat fried formulated products using confocal scanning laser microscopy and a non-invasive double staining procedure**

##### **ABSTRACT**

The aim of this work was to characterize the inner microstructure of different fried formulated products to understand its relationship to oil absorption. Two product categories, which were either based on potato-flakes or wheat gluten, were analyzed. A non-invasive double staining procedure to perform a two channel observation using confocal scanning laser microscopy was set-up. The dough was directly stained during preparation with fluorescein-5-isothiocyanate (FITC), laminated and fried in oil stained with Nile red. Thereafter, samples were observed without further intrusion. Pore size, porosity and oil were quantified using image analysis. A direct relationship between porosity and oil absorption was found in gluten-based products, but, no relationship was detected in potato-flakes-based ones. Further, gluten-based products were less porous than potato-flakes-based products, but did not retain less oil. Parameters such as pore tortuosity and/or connectivity, as well as oil wettability, might explain such differences. In addition, the developed microscopy technique developed herein may be used in other food systems.

**Keywords:** Deep-fat frying, formulated products, internal microstructure, confocal scanning laser microscopy, image analysis, porosity, fluorophore; oil absorption; gluten; starch; potato flakes; methylcellulose.

##### **IV.1. Introduction**

The significance of microstructure in deep-fat frying has been greatly recognized when studying oil absorption mechanisms (Dueik and Bouchon, 2011). In fact, fried-food microstructure is a combination of both surface and inner features, which play different but key roles in oil absorption. Surface topography has a major role in oil drainage during post-frying cooling, whereas the crust inner structure defines product



permeability and the available space for oil deposition (Moreno et al., 2010). As a matter of fact, the equilibrium struck between surface drainage and oil penetration during cooling, which may well be mediated by capillary forces, has been found to determine the final oil content of the product (Bouchon et al., 2003). This agrees with previous studies that have pointed out that the micro-structure of the crust region, which is formed while the food is cooking in the frying oil, is the single most important product-related determinant of the final oil uptake into the product (Pinthus et al., 1995; Bouchon et al., 2001).

Due to the critical importance of crust microstructure, different studies have focused on the measurement of crust porosity, the most common porous media descriptor. As reviewed by Ngadi et al. (2008), intrusion porosimetry and pycnometry have been by far the most commonly used methods to quantify porosity in fried foods. One of the drawbacks of these methodologies is that results are strongly dependent on the experimental conditions used, which are difficult to standardize, restricting the possibility to compare results from different studies. An important advantage of intrusion porosimetry though, is that it allows the calculation of pore size, pore size distribution and pore surface area. However, calculations require some considerations, such as the conception of cylindrical shaped pores, which may be an unrealistic assumption. Thus, results must be cautiously understood. Recently, Dueik et al. (2012) determined the pore size distribution of fried vegetables using N<sub>2</sub> adsorption at cryogenic temperatures. Even though they were able to quantify the different structures adequately, samples had to be defatted before analysis and the technique only allowed quantification of nanopores ( $\approx < 30$  nm).

Another possibility is to quantify the porous structure through the analysis of visual images acquired by non-destructive imaging techniques. Kawa and Moreira (2001) obtained digital images of tortilla chips microstructure using environmental scanning electron microscopy (ESEM), after product breakage, without further preparation. They were able to quantify through image analysis the pore size distribution, obtaining pore sizes between 8 and 278  $\mu$ m. X-ray micro computed tomography (X-ray micro-CT) has

been also used to quantify the pore structure of fried food, such as French fries (Miri et al., 2006) and fried breaded chicken nuggets (Adedeji and Ngadi, 2011), after minimal sample preparation. Using this technique, porosity and pore size distribution, as well as other descriptors such as connectivity and shape, have been determined. Both ESEM and X-ray micro-CT were used to distinguish the solid matrix from the void space. However, through these techniques, it was not possible to clearly distinguish empty pores from those filled with oil, and to identify the different components of the solid matrix.

Confocal scanning laser microscopy (CSLM) has been increasingly used in food science to observe the inner microstructure of a food matrix due to its capability to obtain optical sections of rather thick samples without the need of physical sectioning (Dürrenberger et al., 2001; Lorén et al., 2007). In fried foods, CSLM has been mainly used to observe non-invasively the internal distribution of oil within fried potatoes by staining the oil prior to frying with Nile Red, a fluorescent, thermo-resistant and fat-soluble dye (Pedreschi and Aguilera, 2002; Bouchon et al., 2003; Achir et al., 2010). CSLM has also been used to observe the structure of fried potato tissue after staining the raw sample with Congo Red (Pedreschi and Aguilera, 2002) or after staining the fried sample with fluorescein-isothiocyanate, also known as FITC (van Loon et al., 2007). Also, deep-fat fried chicken drumsticks have been observed (Mukprasirt et al., 2000), after fixation with paraformaldehyde and glutaraldehyde. Recently, Adedeji et al. (2011) used CSLM to observe the fat distribution inside the coating of fried chicken nuggets after adding Nile Blue A, to stain the oil inside the product after frying. They were able to quantify the porosity, the percentage of fat and the pore size distribution, distinguishing pores ranging from 1.2 to 550  $\mu\text{m}$ . However, post-frying labeling may produce artifacts in the samples, such as the smearing of oil, which may interfere in related results.

CSLM may be also used to simultaneously observe more than one component inside a food matrix (Lorén et al., 2007). This can be accomplished if the components of interest exhibit distinguishable fluorescent spectra. This may be achieved by detecting the auto-fluorescence of particular components (if they are auto-fluorescent) or by

staining with selective fluorescent probes (van de Velde, 2003). Achir et al. (2010) used this approach to observe the microstructure of potatoes fried in stained oil. They were able to distinguish the oil from the potato cells, by detecting the natural fluorescence of phenolic compounds of cell walls under UV light.

In order to get a deeper understanding of the relationship between food microstructure and oil absorption, the study of formulated/fabricated products may be a good option. These products not only have the advantage of uniformity, in contrast with raw materials such as potatoes, whose heterogeneity can cause major methodological problems (Baumann and Escher, 1995), but they may also allow investigating the oil uptake capacity of different formulations. In fact, the different components derived from raw agricultural materials can be used as food “building blocks”, which may be combined and processed into controlled formulated products to enable the study of structure related phenomena, such as oil absorption during frying. This approach has been used by some authors in order to determine the influence of surface roughness in the final oil content of fried products (Rubnov and Saguy, 1997; Bouchon and Pyle, 2004; Thanatuksorn et al., 2005). In order to get a better understanding of this phenomenon, Moreno et al. (2010) studied the relationship between surface roughness and oil uptake in fried formulated products with a wide range of oil absorption capacities, which were either based on wheat gluten and starch or potato flakes. They concluded that within each product category, products with higher surface roughness retained more oil. However, this relationship could not be extended when comparing products of different categories. Potato-flake-based products were rougher than gluten-based products, did not retain more oil. In accordance, they suggested that the microstructure of the crust could explain such differences and should be examined in future studies.

In order to get a good understanding of the effect of crust microstructure in oil absorption in different product categories, it would be of interest to develop a non-invasive procedure that would allow multichannel CSLM observation of key components with minimal intrusion. An alternative would be the direct inclusion of the

fluorescent probe in the formulation, during product preparation, as shown by de Hoog and Tromp (2005) in baking studies. This procedure could well be coupled to the frying in stained oil. In accordance, the aim of this work was to develop a non-invasive double staining procedure to perform a two channel observation using CSLM, in order to differentiate and characterize the food matrix and the oil deposition through image analysis, to understand the relationship between inner microstructure and oil absorption capacity.

## **IV.2. Materials and methods**

In order to understand the effect of internal microstructure in oil absorption, seven dough-like products were formulated from different combinations using either potato flakes (PF) or wheat gluten (G), with native wheat starch (NS) and/or methylcellulose (MC).

### **IV.2.1. Materials**

PF (7% w.b. moisture content, Alimentos Unisur, Chile), G (7% w.b. moisture content, Asitec S.A., Chile), NS (8% w.b. moisture content, Asitec S.A., Chile) and MC (4% w.b. moisture content, Sigma M0512, Sigma-Aldrich, USA) were used in the formulations, whereas high oleic sunflower oil (Camilo Ferrón, Chile) was used as frying medium. Nile Red (72485, Sigma Aldrich, USA) was used to stain the frying oil and fluorescein-5-isothiocyanate (FITC) (Fluka, Switzerland) was used to stain the solid matrices.

### **IV.2.2. Product formulation**

Two products categories were formulated according to Moreno et al. (2010): PF-based and G-based products. Their composition (d.b.) and nomenclature are presented in Table IV-1.

**Table IV-1:** Composition of raw formulated products and relevant parameters of the fried dough (170°C), including: porosity determined by pycnometry ( $\epsilon_p$ ), porosity determined by image analysis ( $\epsilon_{ia}$ ) and penetrated oil content determined by image analysis ( $PO_{ia}$ ).

	Product	Composition (d.b.)	$\epsilon_p$ (%) <sup>*</sup>	$\epsilon_{ia}$ (%) <sup>**</sup>	$PO_{ia}$ (%) <sup>**</sup>
G-based	<b>8G</b>	8% G + 92% NS	26,8	40.3 ± 2.9 <sup>a</sup>	26.3 ± 2.5 <sup>A</sup>
	<b>12G</b>	12% G + 88% NS	23,8	30.4 ± 3.8 <sup>b</sup>	19.4 ± 2.6 <sup>B</sup>
	<b>8G + MC</b>	90% 8G + 10% MC	15,0	21.8 ± 2.4 <sup>c</sup>	10.4 ± 1.7 <sup>C</sup>
	<b>12G + MC</b>	90% 12G + 10% MC	14,0	17.6 ± 1.9 <sup>d</sup>	6.7 ± 1.9 <sup>D</sup>
PF-based	<b>PF</b>	100% PF	62,3	56.0 ± 6.5 <sup>e</sup>	7.1 ± 1.5 <sup>D</sup>
	<b>PF + NS</b>	90% PF+ 10% NS	61,6	57.7 ± 9.0 <sup>e</sup>	8.3 ± 4.7 <sup>D</sup>
	<b>PF + MC</b>	90% PF+ 10% MC	57,3	52.8 ± 5.0 <sup>e</sup>	9.5 ± 5.3 <sup>D</sup>

\* Mean values of two measurements.

\*\* Mean values ± standard deviation for G-based products (n=9) and PF-based products (n=18). Equal superscripts indicate no significant differences in  $\epsilon_{ia}$  (lowercase) and in  $PO_{ia}$  (uppercase).

### IV.2.3. Product preparation

The procedure used to prepare the products is the one described by Moreno et al. (2010), with few modifications to ensure sample staining. Most important steps are shown in Figure IV.1. First, the dry formulations described in Table IV-1 were mixed for 2 min using a K50-KPM50 food mixer (KitchenAid, USA). Thereafter, stained distilled water (0.01% FITC (w/w)) was gradually added to the specific dry mixture blend, until 40% (w.b.) moisture content. In PF-based products, all the water was added at 15 °C. In G-based products, half of the water was added at 15 °C, and the other half was added at 90 °C. Stained water was used during dough preparation to identify the solid matrix during CSLM observation, without further intrusion. The stained solution was prepared at room temperature (20 °C) under agitation with a magnetic stirrer during 1 h and was added to the dry mixture as specified, according to Moreno et al. (2010). The stained dough was laminated using a dough sheeter (DOYON-LSB516, Canada), and cut into square shaped chips of 4x4 cm<sup>2</sup> to be fried. The thickness was controlled by weight (4.7 ± 0.03 g/chip) in order to ensure the same solids content in each sample.

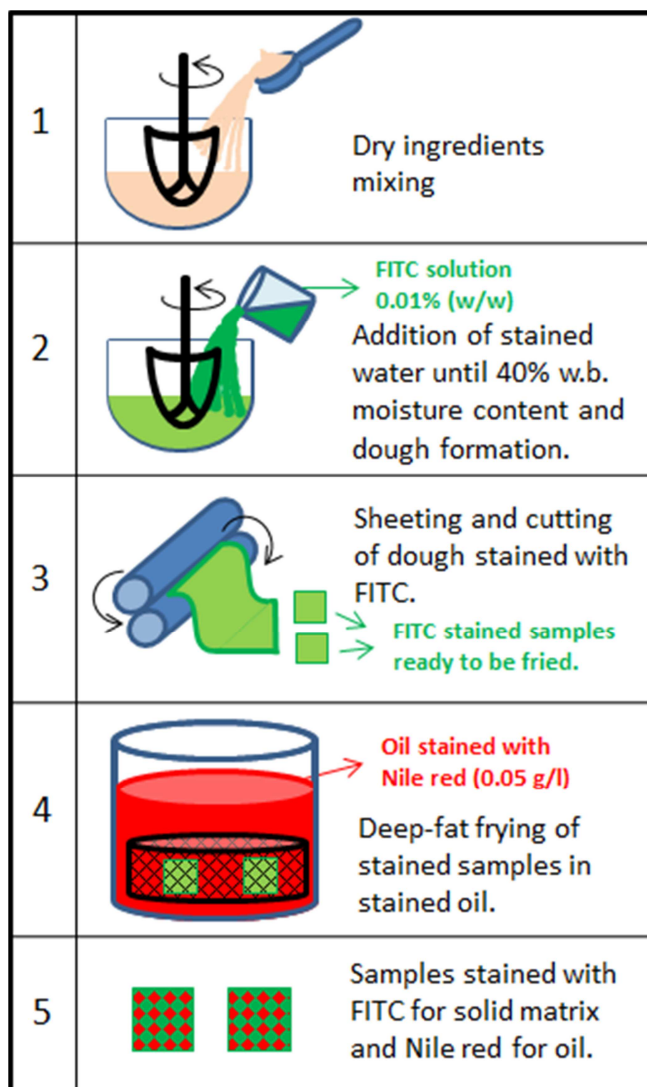


Figure IV.1: Dough preparation and staining protocol.

The products were fried at  $170 \pm 2$  °C until bubble end point ( $2 \pm 0.5\%$  moisture content w.b.) in a 5 l capacity deep-fryer (Somela-535T, Santiago, Chile), equipped with an external temperature control system (PID+Autotuning, Veto, Chile), as described in Moreno et al. (2010). In order to identify the oil inside the matrix, the frying oil was previously stained with Nile Red (0.05 g/l), according to Bouchon et al. (2003). After frying in stained oil, the products were allowed to cool for 10 min at room temperature to be finally stored in a desiccator up to CSLM observation.

#### **IV.2.4. Microstructural observation**

Inner microstructure was observed in an IX81 motorized inverted CSLM (FluoView1000, Olympus, Japan) in its fluorescent mode using 2 channels. One channel was used to observe the FITC-stained solid matrix, after exciting at 488 nm with the Argon laser. The other channel was used to observe the Nile-red-stained oil, after exciting at 543 nm with the Helium/Neon laser. Emissions were collected between 505 and 525 nm and over 560 nm, respectively. Digital image files were acquired using a 10x magnification objective lens (0.3NA) over regions of 512x512 pixels<sup>2</sup> with a resolution of 0.259  $\mu\text{m}/\text{pixel}$  in x and y directions. Image acquisition was performed with a pinhole size of 50  $\mu\text{m}$  when collecting the FITC emission and with a pinhole size of 90  $\mu\text{m}$  when collecting the Nile red emission. Each focal plane was obtained after averaging 4 acquisitions and 10 to 15 focal planes were scanned in the axial direction, using a step size along the z-axis of 1  $\mu\text{m}$  in G-based products and a step size of 5  $\mu\text{m}$  in PF-based products. Gray-scale intensity images (16 bit) were acquired for each channel. Thus, it was possible to obtain a final image at each focal plane, which resulted from the combination of two separated images from each channel.

#### **IV.2.5. Image restoration**

In order to remove noise and enhance the contrast of the acquired image, a deconvolution restoration process was performed (Swedlow, 2007). In general terms, deconvolution attempts to recover the original object, which is distorted due to the passage of the light through the optical path. To do so, the distortion at each point is characterized by a point-spread function (PSF), which can be estimated from known imaging parameters such as the numerical aperture of the objective lens, the light wavelength, the refraction index of the media and the microscope type. Deconvolution involves the convolution of the acquired image with the inverse of the PSF to obtain an estimate of the original object. Image deconvolution was performed with Huygens Essential 3.7 software (Scientific Volume Imaging, Netherlands, [www.svi.nl](http://www.svi.nl)), which

estimates the PSF of the observation with each channel and uses it to deconvolve them independently.

#### **IV.2.6. Image visualization**

The deconvolved intensity images of each channel were combined to create RGB composite images, where the green colored regions represented the FITC-stained solid matrix, the red colored regions represented the Nile-red-stained oil and the black regions represented the empty pores. Two different representations of confocal images will be shown in this paper: 1) focal planes of inner sections using ImageJ software (Rasband, 1997) and 2) 3D rendering using Huygens Essential 3.7 software. Images were then filtered with a median filter (3x3 pixels) and contrast was adjusted.

#### **IV.2.7. Image segmentation**

Images were segmented using the threshold color plugin available in ImageJ software, which enables image segmentation based on color composition in different color spaces. Segmentation was performed by thresholding the images in the CIE Lab color space. First, a threshold using the lightness coordinate (L) was performed. L values that fell below the intensity limit (L threshold) corresponded to the dimmest region of the image and were considered as empty pores, whereas the remaining pixels were considered as occupied regions. In order to smooth features, eliminate isolated pixels and fill small holes, opening (erosion followed by dilation) and closing (dilation followed by erosion) morphological operations were performed after empty pores detection. An example of a segmented image, showing empty pores, using this protocol in a G-based product is shown in Figure IV.2B.

After empty pores segmentation, images were thresholded using the red-green chromaticity coordinate ("a" coordinate) to differentiate the oil (red regions) from the solid matrix (green regions). In an analogous manner, all pixels with an "a" value below the threshold were considered as part of the solid matrix, whereas the remaining pixels were considered as regions containing oil. Similarly, opening and closing morphological



operations were performed after thresholding. An example of a segmented image, showing the oil location, using this protocol in a G-based product is shown in Figure IV.2C. Since oil is located in the void space within the structure, oil containing regions were considered as pores filled with oil. After empty pores and oil segmentation, the solid matrix was extracted from the original image as shown in Figure IV.2D.

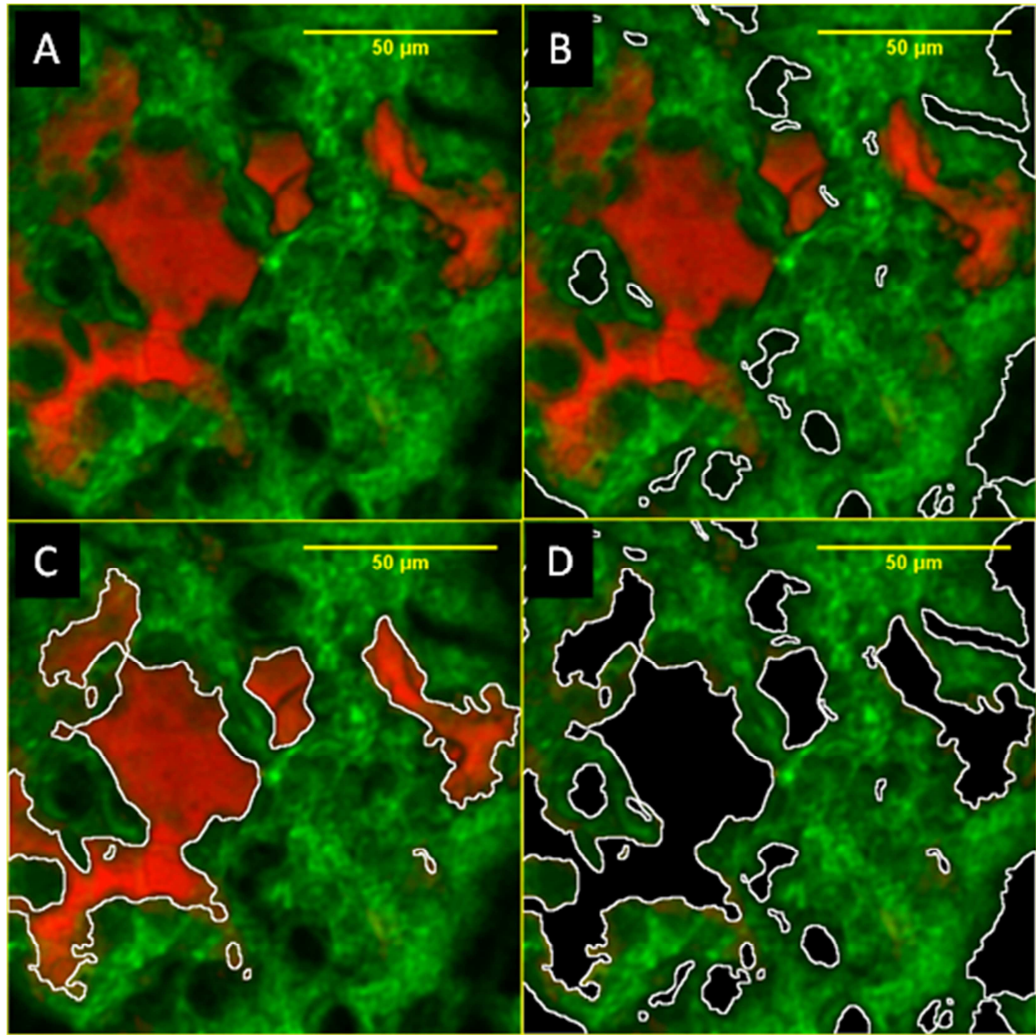


**Figure IV.2:** Example of image segmentation procedure performed in a focal plane of a 12G product: (A) Original image, (B) Empty pores outlined after segmentation using “L” coordinate thresholding, (C) Pores filled with oil outlined after segmentation using “a” coordinate thresholding, (D) Segmented solid matrix. In this image:  $PO_{ia} = 20.4\%$  and  $\epsilon_{ia} = 30.4\%$ .

#### **IV.2.8. Image analysis**

Segmented images were used to calculate the porosity (as a percentage) by image analysis (ia) according to Equation IV.1, which considers that pores can be either empty or filled with oil.

$$\varepsilon_{ia} = \frac{\text{Area of empty pores} + \text{Area of pores filled with oil}}{\text{Total image area}} \times 100 \quad \text{Equation IV.1}$$

This oil fraction corresponds to penetrated oil (PO), as referred by Moreno et al. (2010), since, as revealed by CSLM, it is located within the structure of the matrix. In accordance,  $PO_{ia}$  was defined as the fraction of the image that is occupied by the oil, determined through image analysis, according to Equation IV.2:

$$PO_{ia} = \frac{\text{Area of pores filled with oil}}{\text{Total image area}} \times 100 \quad \text{Equation IV.2}$$

Pore diameter of empty or filled pores was defined as the average of the maximum and the minimum Feret's diameter, that is, the mean caliper diameter (Dullien, 1979)

In addition the pore area fraction was defined as:

$$\text{Pore area fraction} = \frac{\text{Pore area}}{\text{Total area occupied by pores of the same type}} \times 100 \quad \text{Equation IV.3}$$

In Equation IV.3, the pore type can be either “filled with oil” or “empty”, since the pore area fraction is calculated independently for each pore category. Results are plotted as the cumulative pore area fraction v/s the pore size.

#### **IV.2.9. Porosity by pycnometry**

Porosity measurements using pycnometry were conducted in order to compare results with those obtained by image analysis. To do so, samples were defatted using soxhlet extraction during 8 h. Porosity was obtained according to Equation IV.4:

$$\varepsilon_p = 1 - \frac{\rho_b}{\rho_s} \quad \text{Equation IV.4}$$

Where  $\varepsilon_p$  refers to the porosity determined by pycnometry (p) (dimensionless),  $\rho_b$  to the bulk density ( $\text{kg}/\text{cm}^3$ ) and  $\rho_s$  to the solid density ( $\text{kg}/\text{cm}^3$ ).

Bulk density ( $\rho_b$ ) was determined as the ratio between the weight of the defatted sample (0.5-1 g approximately) measured in a GR 200 analytical balance (AND, USA) and its volume, which was determined by volume displacement of n-heptane in a glass pycnometer with an accuracy of 0.05 ml, as described by Ngadi et al. (2008).

Solid density ( $\rho_s$ ) was determined as the ratio between the weight of the defatted grinded sample measured in the analytical balance (1.5 g approximately) and its volume. The volume of the sample was measured with an ULTRAPYC 1200e gas pycnometer (Quantachrome Instruments, USA) operated with nitrogen at 19 psi. The volume of the solids was determined after 9 pulses of outgassing, and as the resultant of three runs of measurement for each sample, following recommendation from the manufacturer. Porosity measurements were performed in duplicate.

#### **IV.2.10. Statistical analysis**

In order to identify significant differences between the obtained results of  $\varepsilon_{ia}$  and  $PO_{ia}$  for different formulations, the values were compared using the non-parametric method of Kruskal-Wallis for median comparison with a confidence level of 95% using Statgraphics Plus software version 5.1 (Manugistic Inc., Rockville, MD, USA).

### **IV.3. Results and discussion**

#### **IV.3.1. Fluorescent labeling**

The combination of different fluorescent probes and staining methodologies in food research is not trivial and is an open field to explore (van de Velde et al., 2003). Therefore, as a contribution to this field, the main criteria for the selection of fluorophores and procedures will be described next.

Fluorophore selection was based on components affinity and based on absorption and emission spectra distinction. After an extensive literature review and preliminary experiments, FITC and Nile Red were selected. In addition, an experimental protocol was set-up, as explained in Figure IV.1, to minimize artifacts inclusion prior CSLM observation. FITC was diluted in distilled water, which was directly added to the dry mix to form the dough, avoiding additional steps. This procedure has been used to observe bread dough without perceiving any effect neither in dough quality (Weegels et al., 2003) nor in its rheology (Jekle and Becker, 2011). FITC was selected because it can stain starch (de Hoog and Tromp, 2005; Peighambardoust et al., 2006; Primo-Martín et al., 2007) and gluten (Bugusu et al., 2002; Lee et al., 2001), the main components of PF and G-based products (Moreno et al., 2010). According to Tromp et al. (2001), the affinity of FITC is strongly related to hydrophobicity, that is, the probe molecules tend to accumulate in hydrophobic regions, such as gluten rich domains, but they can also stain starch if local accessibility is ensured. The proper concentration of the fluorescent probe was determined during preliminary experiments. The resistance of FITC to high temperature processing has been observed after baking at 235°C (Primo-Martín et al., 2007) and frying at 170°C, as revealed during preliminary experiments. Nile red was selected as a fluorescent probe because it is a fat soluble and thermo-resistant dye, and because its fluorescent spectrum is well distinguishable from that of FITC.

### IV.3.2. Qualitative analysis of inner microstructure

In order to provide a general idea of both product categories, digital images of G-based (8G+MC) and PF-based (PF+NS) products are presented in Figure IV.3. As can be noted, the differences between G-based and PF-based products are evident under the naked eye, and should be reflected at the microscopic level. In order to explore the internal microstructure of the matrices, different observations using CSLM were performed in all samples. Some of the acquired images are shown in Figures IV.4 and IV.5. In all observations, an adequate contrast between the empty pores (black), the oil (red) and the solid matrix (green) was observed. Figure IV.4 shows representative focal planes of the different G-based formulations. As can be noted, 8G and 12G products seem to accumulate a higher amount of oil within the structure, which accumulates in bigger continuous domains, compared to products that contain methylcellulose (8G+MC and 12G+MC). This observation is consistent with results reported by Moreno et al. (2010), who determined a decrease in penetrated oil in G-based products when MC was added. Differences in oil content between 8G and 12G or between 8G+MC and 12G+MC are not as evident. Additional quantitative image analysis is required to carry out proper comparisons, as will be presented in the next section.

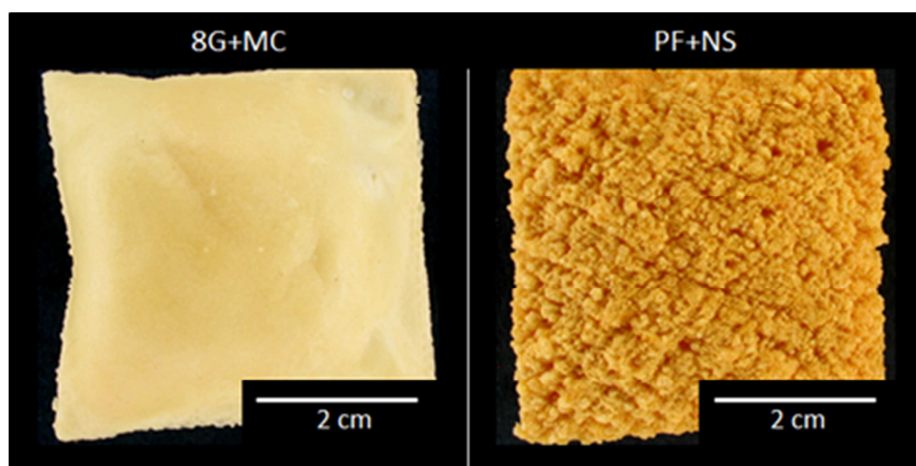


**Figure IV.3:** Digital photographs of unstained 8G+MC (left) and PF+NS (right) fried products (170°C).

PF-based products have larger geometrical features than G-based products, as can be observed at macro and microscale. Figure IV.5 shows two focal planes of each PF-based product to illustrate the differences that might be found when observing two distinct focal planes of the same formulation, which is also a consequence of the larger geometrical patterns. In general terms, it can be observed that the oil inside PF-based products can be either located inside small elliptical pockets or accumulate in irregularly shaped spaces of different sizes. Regarding the empty pores, they can be found in a wide range of sizes, as holes in a continuous region or forming foam-like structures. Pores in PF-based products seem larger than those found in G-based products, however, no conclusions about the difference in the inner microstructure between PF-based formulations can be deduced after qualitative observation. Quantitative analysis is required as will be discussed next

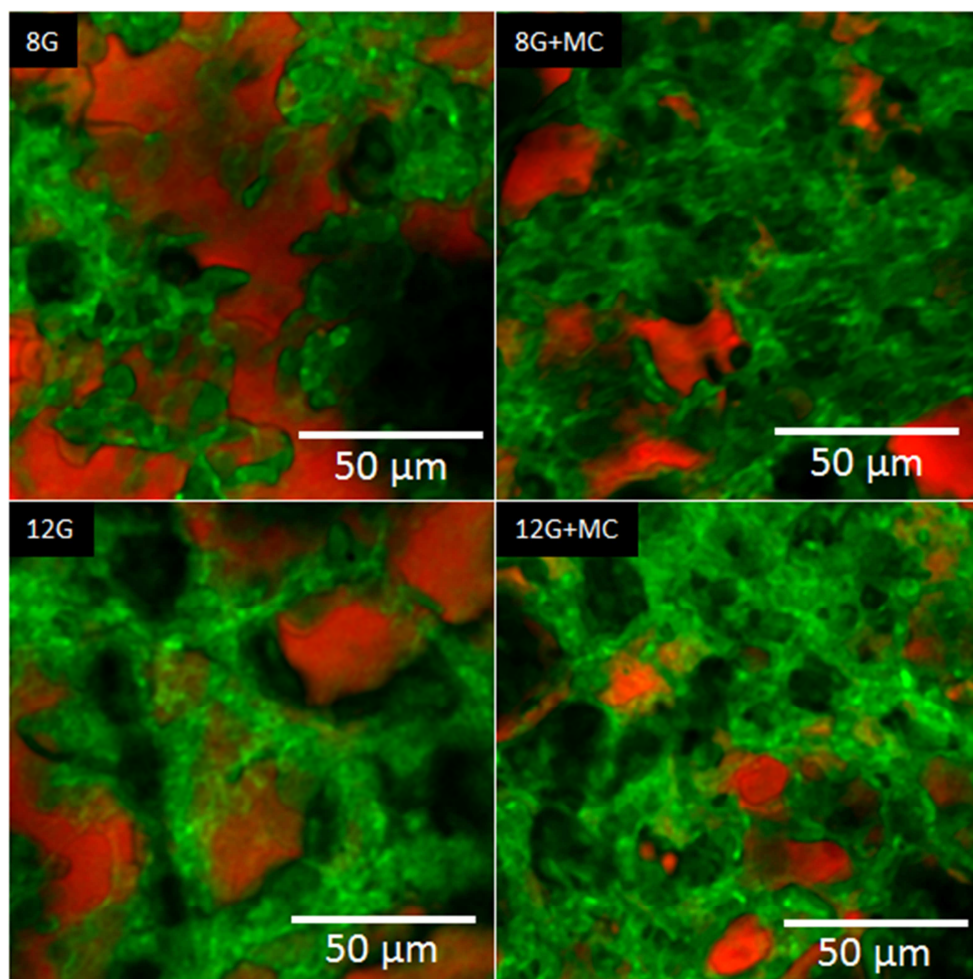


**Figure IV.4:** Focal planes of G-based products where the solid matrix (green), the oil (red) and the empty pores (black) can be observed.



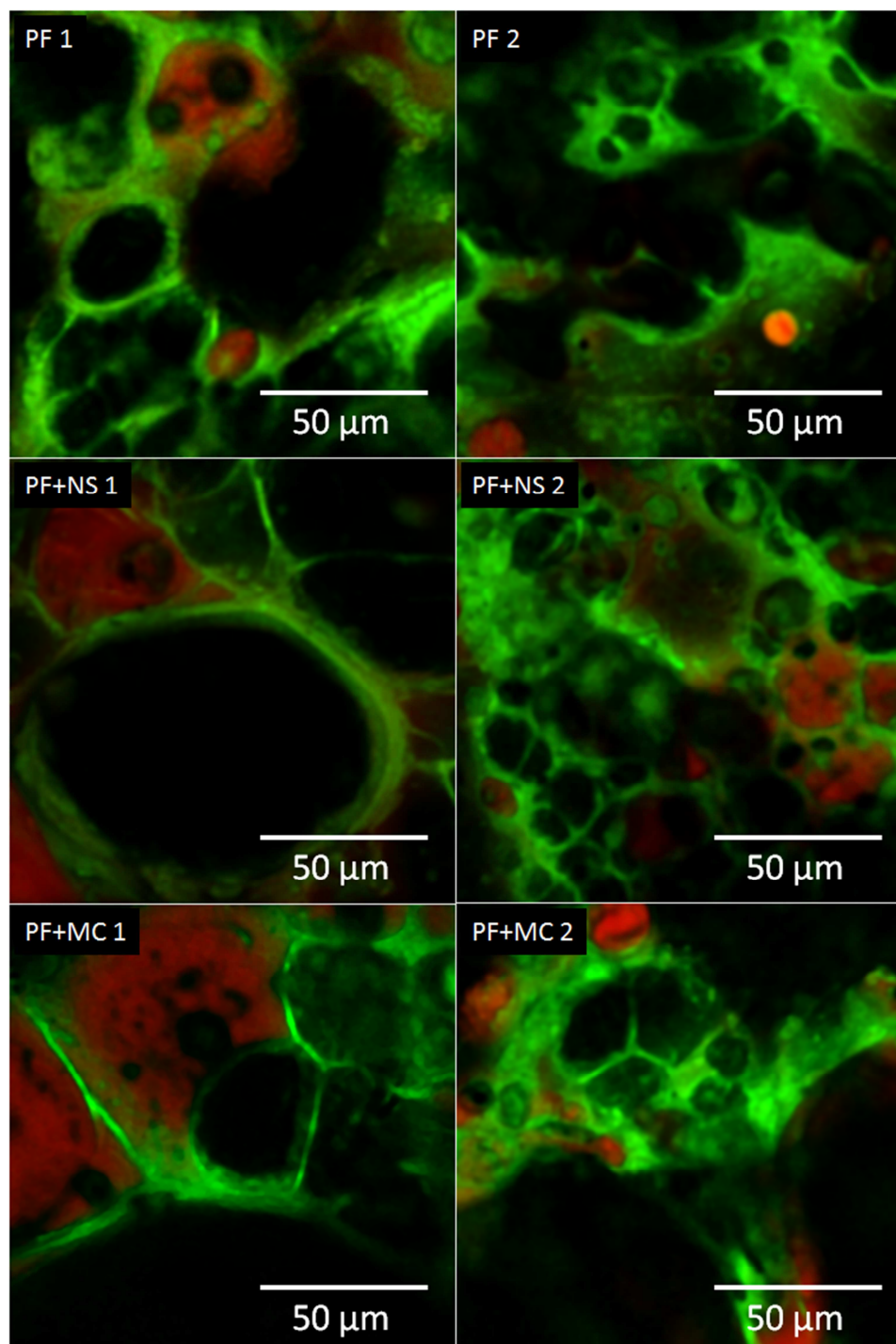


**Figure IV.5:** Focal planes of PF-based products where the solid matrix (green), the oil (red) and the empty pores (black) can be observed.



### **IV.3.3. Quantitative analysis of inner microstructure**

In order to quantify the microstructural features observed in confocal images, porosity and penetrated oil were determined by image analysis ( $\epsilon_{ia}$  and  $PO_{ia}$ ), as shown in Table IV.1. As can be seen from  $\epsilon_{ia}$ , G-based products are less porous than PF-based products. This means that the space occupied by empty pores and pores filled with oil in G-based products is smaller than in PF-based products, confirming qualitative observations. Regarding each product category, all G-based products presented different porosity values. In accordance to qualitative observation (Figure IV.4), G-based products with MC addition (8G+MC and 12G+MC) are less porous than products without MC (8G and 12G). Even though the differences between 8G and 12G or between 8G+MC and 12G+MC products were not evident in confocal images, the statistical analysis of the quantitative information indicates that the products with 8% gluten are more porous than those with 12% gluten, either with or without MC addition. On the other hand, no significant differences in porosity were identified in PF-based formulations after image analysis.

In order to understand the relationship between oil absorption and inner microstructure,  $\epsilon_{ia}$  values were plotted against the amount of oil that actually penetrated inside the structure, the  $PO_{soxhlet}$  fraction, determined by Moreno et al. (2010) (Figure IV.6). As can be seen, in G-based products, more porous matrices tend to retain more oil inside their structure, as revealed by the linear relationship ( $R^2=0.9261$ ). This behavior was not observed in PF-based products. No significant differences in porosity were identified between PF-based products through image analysis, however, according to Moreno et al. (2010), all PF-based products showed significant differences in  $PO_{soxhlet}$ . Regarding results of  $PO_{ia}$  (Table IV.1), significant differences between all G-based products were determined, but again, no differences were found between PF-based products. According to these results, G-based products with MC addition (8G+MC and 12G+MC) retained less oil than products without MC (8G and 12G), and products with

8% gluten retained more oil than those with 12% gluten, either with or without MC addition.

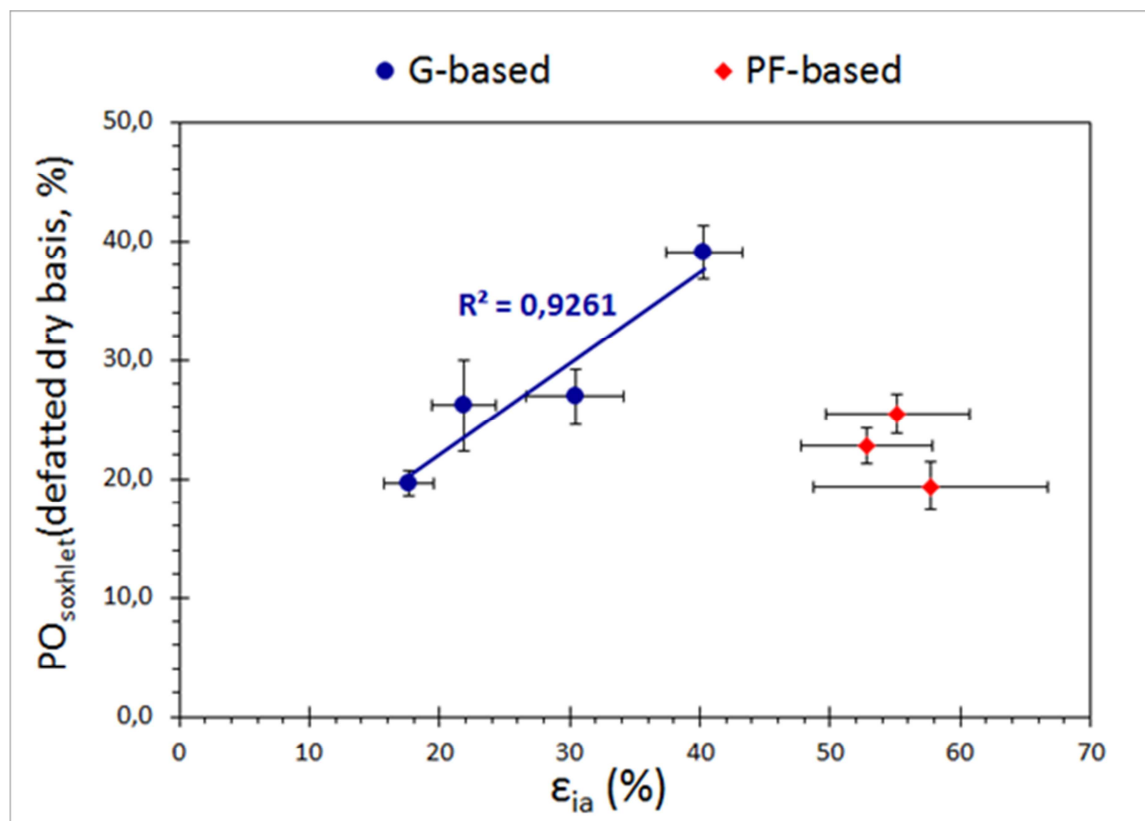


**Figure IV.6:** Penetrated oil content determined by soxhlet extraction (PO<sub>soxhlet</sub>) v/s porosity determined by image analysis (ε<sub>ia</sub>) of fried products. Least squares regression coefficient (R<sup>2</sup>) is shown for G-based products. Oil content values were taken from Moreno et al. (2010). Mean values ± standard deviation are presented.

In order to test the ability of the image analysis protocol developed in this study, ε<sub>ia</sub> and PO<sub>ia</sub> values were contrasted with results obtained using pycnometry (ε<sub>p</sub>) and soxhlet extraction standard tests, correspondingly. Two plots are presented in Figures IV.7 and IV.8, which show the relationship between ε<sub>ia</sub> and ε<sub>p</sub>, and between PO<sub>ia</sub> and PO<sub>soxhlet</sub>, respectively. Regarding porosity calculations (Figure IV.7), both methods ranked the products in a similar manner, and a strong relationship between the mean values determined by each technique was found (R<sup>2</sup>=0.9345). The relationship between PO<sub>ia</sub>

and  $PO_{\text{soxhlet}}$  was weaker ( $R^2=0.8238$ ), since no significant differences were found in  $PO_{\text{ia}}$  in PF-based products whereas  $PO_{\text{soxhlet}}$  was statistically different in all products. The relationship between  $PO_{\text{ia}}$  and  $PO_{\text{soxhlet}}$  in G-based products was stronger ( $R^2=0.8732$ ), since both methods ranked the products in the same manner.

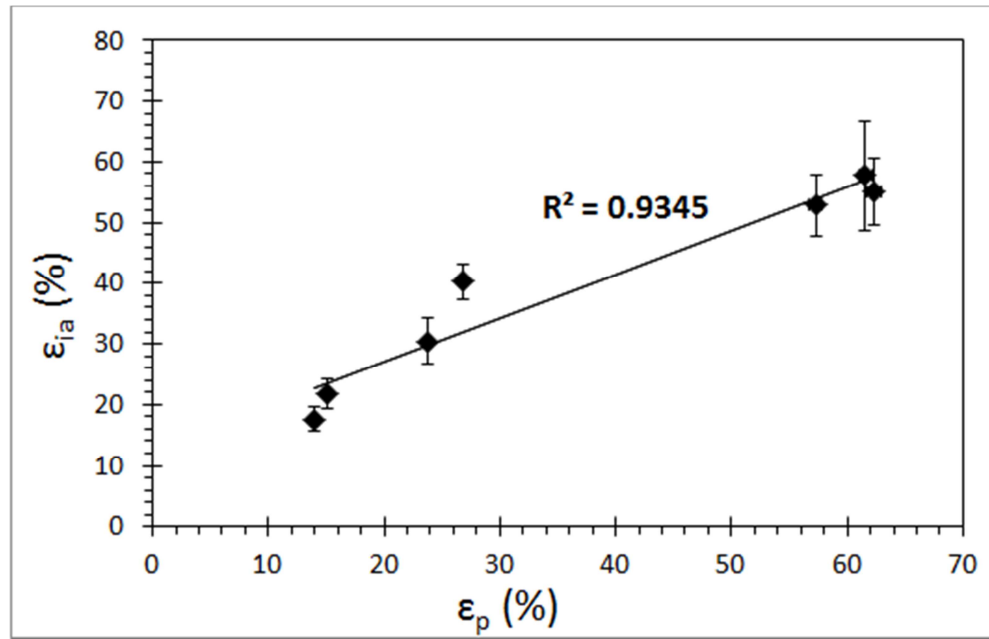


**Figure IV.7:** Mean values of porosity determined by image analysis ( $\epsilon_{ia}$ ) v/s mean values of porosity determined by pycnometry ( $\epsilon_p$ ) Least squares regression coefficients ( $R^2$ ) for all 7 formulated products are shown. Mean values  $\pm$  standard deviation are presented for  $\epsilon_{ia}$ . Mean value together with maximum and minimum measurements are presented for  $\epsilon_p$ .

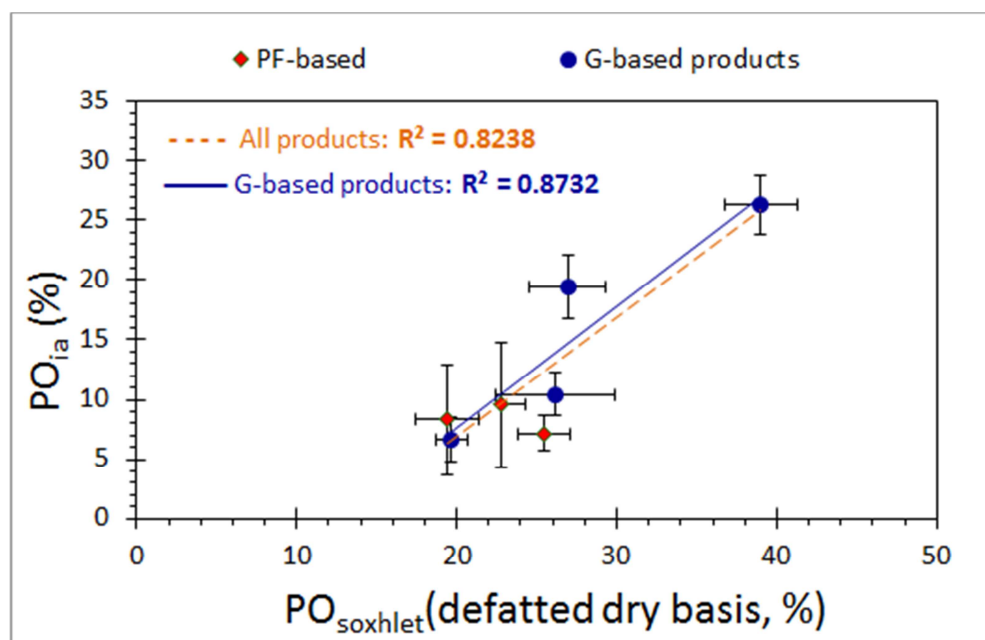


**Figure IV.8:** Mean values penetrated oil determined by image analysis ( $PO_{ia}$ ) v/s PO determined by soxhlet extraction ( $PO_{soxhlet}$ ) of formulated products. The values of PO by soxhlet extraction were taken from Moreno et al. (2010). Least squares regression coefficients ( $R^2$ ) for all 7 formulated products (green) and G-based products (blue) are shown. Mean values  $\pm$  standard deviation are presented.

As observed in confocal images, PF-based products presented a wider range of pore sizes compared to G-based products, which ranged from 0.7 to 156  $\mu\text{m}$  compared to 0.7-85  $\mu\text{m}$ , respectively. To get a better understanding of oil location, empty pores and pores filled with oil were analyzed independently in each product. Results are summarized in Figures IV.9 and IV.10, where the cumulative pore area fraction of empty and filled pores is plotted against the pore size for each fried formulated product. Overall, the range of pore size in G-products with MC (8G+MC and 12G+MC) is smaller than the one found in products without MC (8G and 12G), both in filled and empty pores (Figure IV.9). Particularly, pores filled with oil in formulations with MC addition are smaller ( $\approx < 40 \mu\text{m}$ ) compared to 8G and 12 G formulations (up to 80  $\mu\text{m}$ ). When comparing pores filled with oil and empty ones in each G-based product, even though some different patterns are observed, no clear distinctions can be derived, compared to PF-products where two clear clusters can be identified (Figure IV.10). In products without MC addition (8G and 12G), the cumulative area fraction of pores of a certain size filled with

oil is slightly higher than the one of empty pores, particularly in 8G products. This would indicate that in this type of products the oil might locate in slightly larger pores. However, when MC is added to the 12G formulation, an opposite situation is observed. On the other hand, when MC is added to the 8G formulation the difference between the cumulative area fraction of empty and filled pores of the same size does not show a clear pattern.

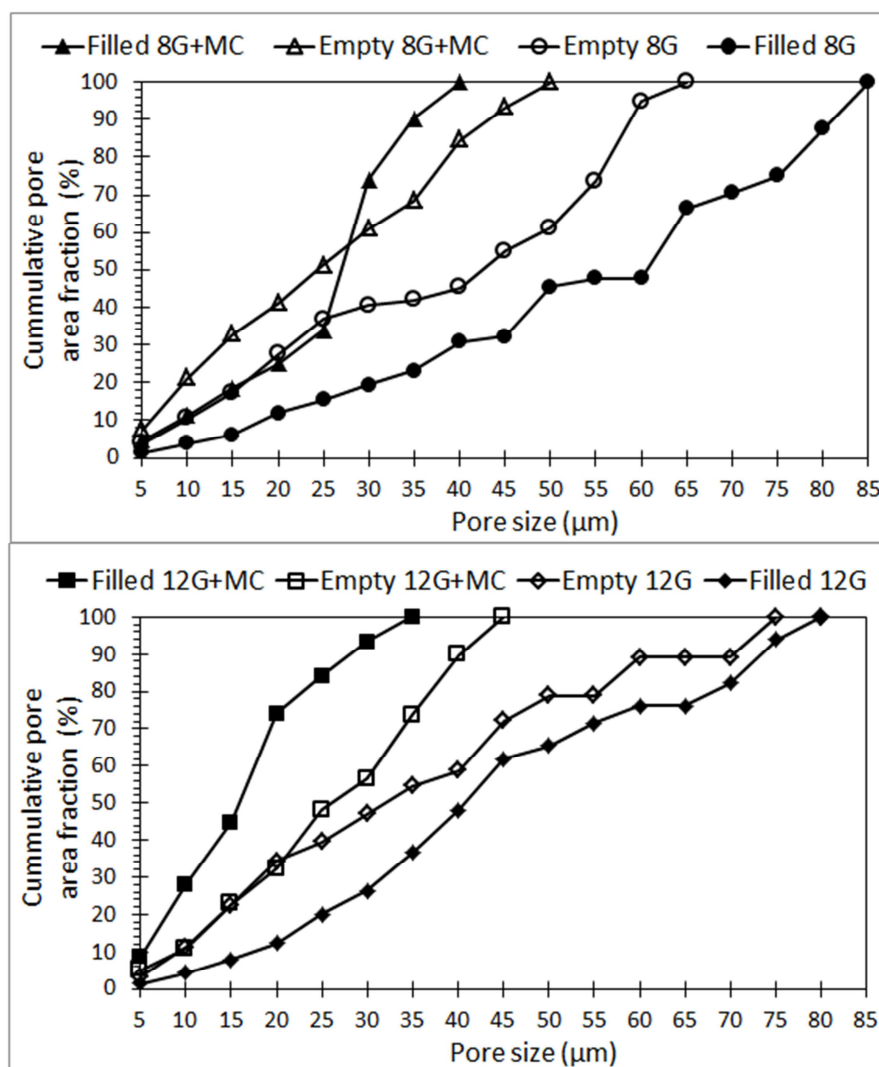


**Figure IV.9:** Cumulative pore area fraction v/s pore size of pores filled with oil (Filled) and empty pores (Empty) of G-based products. Results include all the pores measured for 9 focal planes.

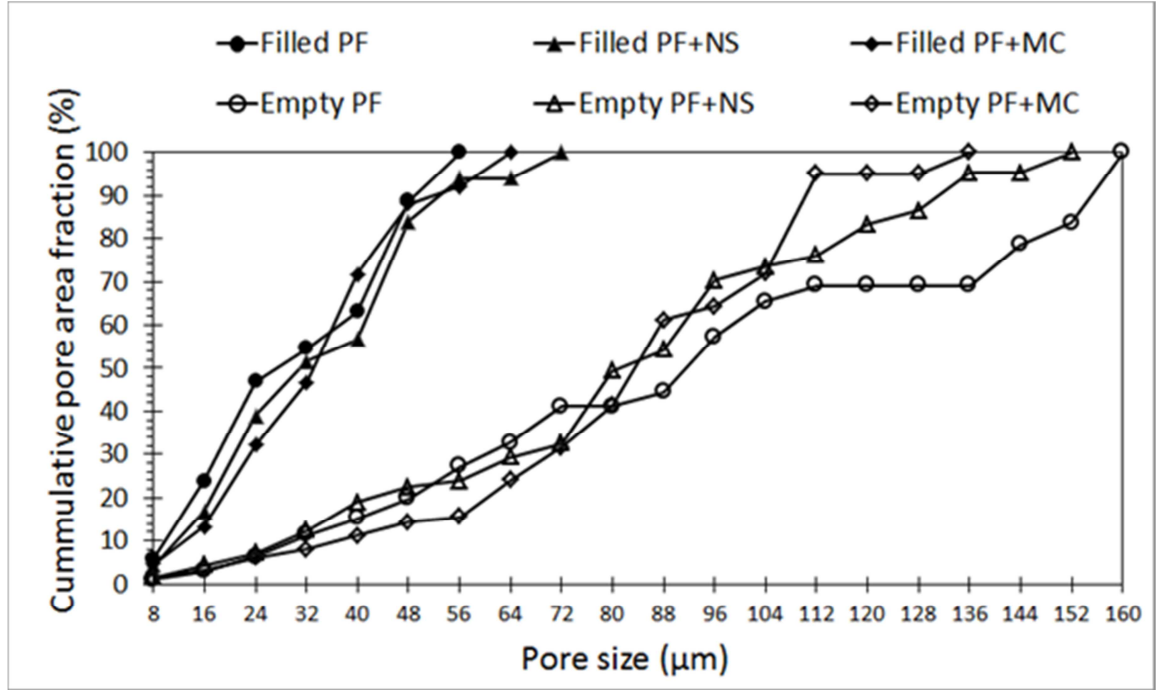


**Figure IV.10:** Cumulative pore area fraction v/s pore size of pores filled with oil (Filled) and empty pores (Empty) of PF-based products. Results include all the pores measured for 18 focal planes.

As shown in Figure IV.10, no main differences can be observed in the cumulative area fraction of pores filled with oil between PF-based products. In addition, no main differences are observed in small empty pores, whereas some differences can be observed in larger pores ( $\approx > 100 \mu\text{m}$ ). It can be noticed that oil is located in pores smaller than  $80 \mu\text{m}$ , while empty pores present a wider range of sizes. Approximately, half of the void area available corresponds to pores smaller than  $80 \mu\text{m}$ . Finally, the micro-volume of the different products was also studied, as shown in Figure IV.11, where some 3D renderings are presented. These upper views present the structure of the porous network with or without oil, and help to confirm from a different perspective the wider range of pore sizes in PF-products reported earlier.

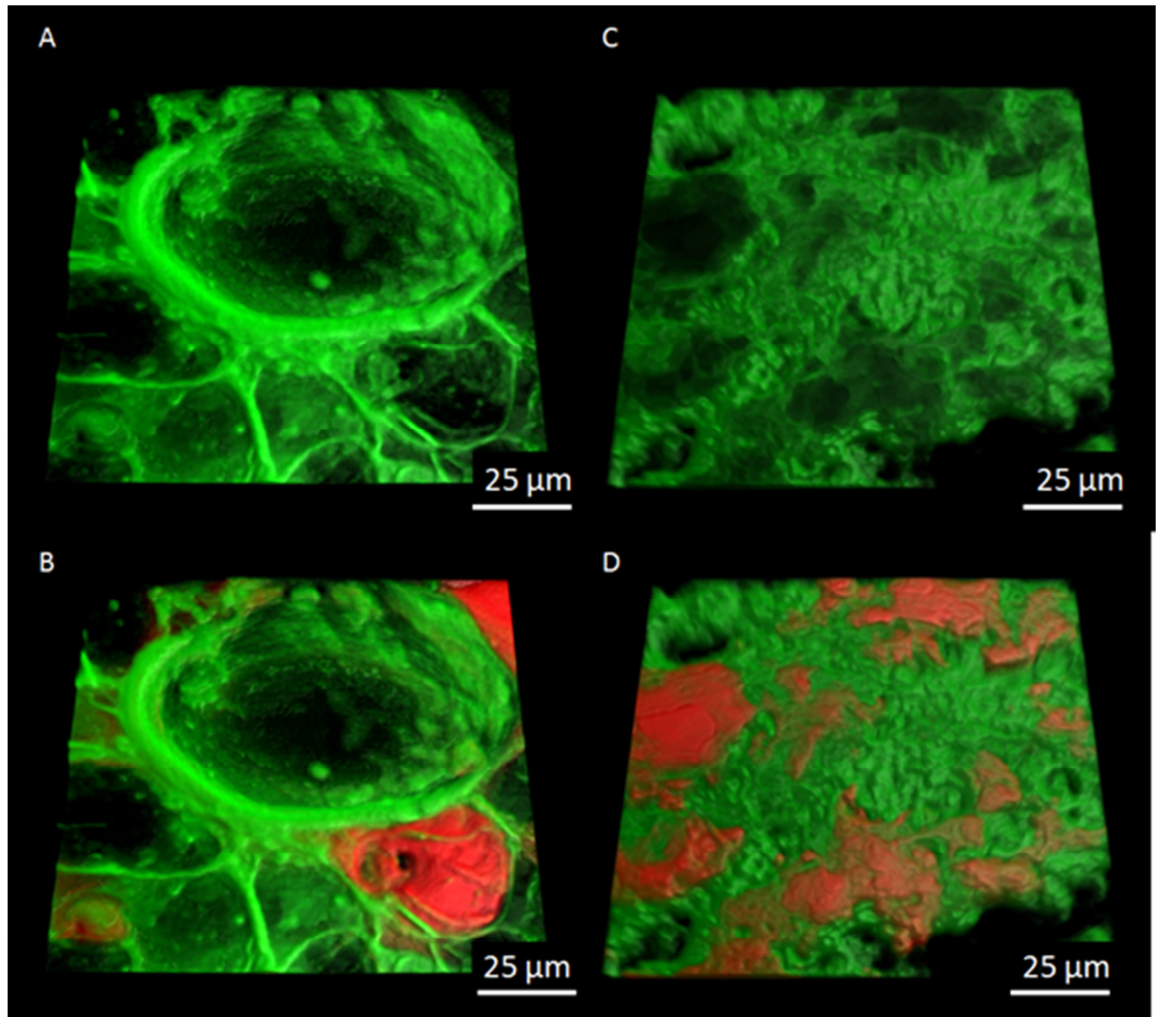


**Figure IV.11:** Three-dimensional rendition of PF (left) and G (right) based products. A and C: Upper view of the solid matrix (green) showing the porous structure without oil. B and D: Oil (red) located inside the pore structure of the solid matrix.

#### **IV.4. Conclusions**

The double fluorescent labeling procedure combined with the multichannel CSLM observation protocol developed in this work, showed to be a reliable methodology to observe and analyze the inner microstructure of fried gluten- (G) and potato-flakes- (PF) based formulated products. The technique allowed a non-invasive characterization of the food matrix and the oil deposition through image analysis, which gave valuable knowledge to understand the relationship between the inner microstructure and the oil

absorption capacity. Further, results from traditional instrumental analysis such as oil content (using soxhlet extraction) and porosity (using pycnometry) were successfully related to those derived from image analysis, thus, the latter could be used as a good proxy in future studies.

Regarding product microstructure, both product categories showed important differences in their inner structure, oil content and distribution, highlighting the importance of product formulation in the final characteristics of fried foods. PF-based products were more porous than G-based products and presented a wider range of pore sizes. In G-based products, an increase in gluten content and the addition of methylcellulose tended to reduce porosity and oil content as revealed by image analysis. Thus, considering results reported herein and those previously reported by Moreno et al. (2010), who focused on the relationship between surface roughness and oil absorption, it can be concluded that in G-based products, rougher and more porous structures retain more oil. However, in PF-based products even though there was a relationship between surface roughness and oil absorption, no differences in penetrated oil were observed after image analysis in this study. Further, no effect in porosity, determined either through image analysis or through pycnometry, was detected after the addition of either native starch or methylcellulose. Therefore, no clear relationship between inner porosity and oil absorption can be derived in this product category. In addition, G-based products were less porous than PF-based products, but did not retain less oil inside their structure. Additional parameters such as pore tortuosity and/or connectivity might explain such differences. Also the chemical affinity between the solid matrix and the oil could explain this behavior, since oil wetting can highly affect its absorption. In accordance, further analysis are required and discussed in future studies



## **V. Understanding the relationship of structural, textural and wetting related parameters with oil uptake in deep-fat fried formulated products**

### **ABSTRACT**

The oil absorption phenomenon in deep-fat fried foods has been focus of several studies, but it still remains unclear. This work aimed to quantify different characteristics of two groups of fried formulated products to understand their importance to the amount of oil retained after deep-fat frying and their influence in the mechanism of oil migration into the products. The fried products were characterized by their geometrical features, their chemical affinity with oil (by contact angle measurements in their restructured surfaces), and their hardness (by fracture force measurements). No clear relationship between the amount of oil retained by the products and their geometry was perceived, but some changes during frying could be relevant to the dynamic of oil penetration. There might be a relationship between the hardness of the products and the oil absorption mechanism, since harder products tend to retain less oil. The measurement of contact angles between oil and restructured food surfaces allowed to discriminate between the products under study, and helped to explain why some products retained less oil despite their larger geometrical features, since they had less chemical affinity with oil. The conclusions pointed to the complexity of attributing oil absorption only to one or two key parameters. Is the combination of factor the one that actually defines oil absorption, so the challenge is to find how the different combinations contribute to the oil absorption phenomenon, and use that knowledge to design novel fried products by an engineering formulation approach.

Keywords: Deep-fat frying, formulated products, wetting, texture, oil absorption, macrostructure.

### **V.1.Introduction**

Oil content is a key quality attribute in deep-fat fried food. During the process, the product is cooked and dehydrated inside a hot oil bath ( $\approx 160\text{-}190\text{ }^{\circ}\text{C}$ ), suffering several

complex physical and chemical reactions. Most of the experimental evidence shows that oil would mainly penetrate within the product after being removed from the oil bath, when it begins to cool down (Bouchon et al., 2001, Bouchon et al., 2003, Moreira et al., 1997, Ufheil and Escher, 1996). The mechanism of oil migration has been suggested to be mainly driven by capillary action into the voids created due to water evaporation and/or due to the physical expansion of the matrix, but, it may be also driven by the pressure gradient generated by the condensing vapor inside the product when a sufficient amount of un-evaporated water remains inside the structure (Mellema, 2003). In accordance, Bouchon and Pyle (2005) expressed the pressure difference needed to initiate oil infiltration during post-frying cooling ( $P_{\text{atm}} - P_{\text{pore}} > 0$ ) as a function of capillary pressure ( $P_c = 2\sigma_{\text{og}}\cos\theta/r$ ) and vapor pressure. A schematic diagram showing the capillary penetration phenomena in a cylindrical pore when having different arrangements is shown in Figure V.1.

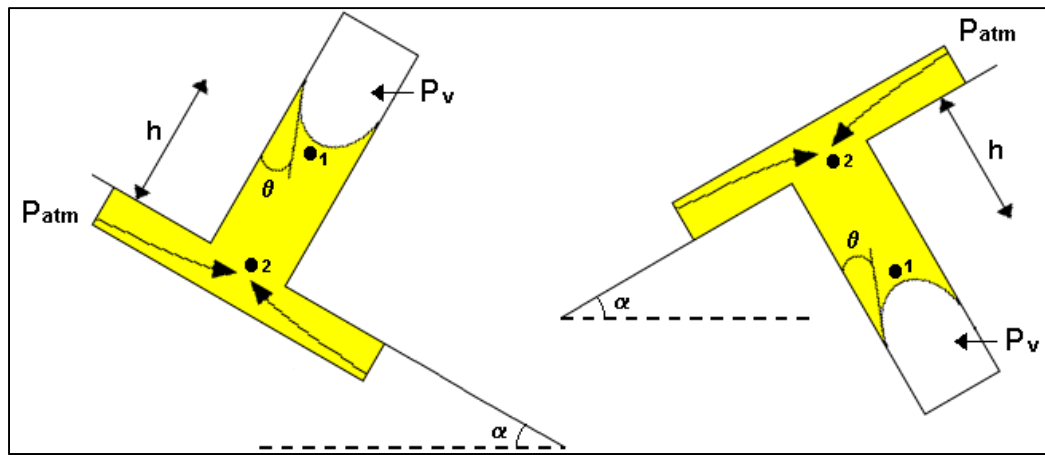


**Figure V.1:** Schematic diagram showing the capillary penetration phenomena when having different arrangements. Left: Upward configuration, the action of gravity restricts capillary penetration. Right: Downward configuration, the action of gravity enhances capillary penetration; from Bouchon and Pyle (2005).

If a reference datum plane ( $h=0$ ) was set at the bottom of each of the capillaries, the expression for the total driving force, that is the piezometric pressure difference, for a

capillary with an upward (+ $rg h \cos \alpha$ ) or a downward (- $rg h \cos \alpha$ ) orientation, could be represented by Equation V.1 (Bouchon and Pyle, 2005).

$$\Delta P^* = P_2^* - P_1^* = P_{atm} - P_{pore} = P_{atm} - \left( P_v - \frac{2 \sigma_{og} \cos \theta}{r} \pm \rho g h \cos \alpha \right) \quad \text{Equation V.1}$$

Where:

$P_2^*$  = Piezometric pressure at the bottom of the capillary, [Pa]

$P_1^*$  = Piezometric pressure at the liquid side of the meniscus, [Pa]

$P_v$  = Vapor pressure, [Pa]

$P_{atm}$  = Atmospheric pressure, [Pa]

$P_{pore}$  = Pore's pressure, [Pa]

$r$  = Radius of the capillary, [m]

$\sigma_{og}$  = Interfacial tension between oil and gas inside the capillary pore, [N.m-1]

$\theta$  = Contact angle (between oil and solid inner pore wall), [Rad]

$\rho$  = Oil density, [kg.m-3]

$g$  = Acceleration due to gravity, [m.s-2]

$h$  = Oil penetration distance, [m]

$\alpha$  = Angle between normal and vertical axes, [rad]

Since the driving force depends importantly on vapor pressure, this is expected to occur after some cooling takes place. As  $P_{pore}$  decreases and vapor condenses the pressure difference is expected to induce oil suction. In thick samples and/or short frying times, the condensation mechanism should predominate, whereas in thinner samples and/or longer frying times moisture, content may diminish considerably (and therefore  $P_{pore}$ ), allowing oil absorption to begin earlier. In fact, Moreira and Barrufet (1998) explained the mechanism of oil absorption in tortilla chips during cooling exclusively in terms of capillary forces. According to the authors, the elevated frying temperature

diminishes the interfacial tension between the surrounding oil and the gas phase inside the capillary pore ( $\sigma_{og}$ ), thus, limiting oil penetration inside the food, according to Equation V.1. This is reverted when the food is removed from the oil, due to cooling, which increases the capillary pressure. However, recent experimental results have shown that some thin fried products formulated from wheat flour or blends made of wheat gluten and starch absorb an important amount of oil during the immersion period (Moreno et al., 2010; Thanatuksorn et al., 2005), challenging previous experimental results. This opens a discussion about the effect of product formulation in the mechanism of oil absorption during deep-fat frying.

When a fried product is removed from the frying bath, surface oil can either drain of the product, be pulled into the porous network or remain at the surface. Both the inner and the surface microstructure would determine the room available for oil deposition and would affect the competition between oil suction and drainage. In order to test this hypothesis, Moreno et al. (2010) and Moreno and Bouchon (2012) studied the relationship between the surface roughness and the inner microstructure in two product categories, which were either based on potato-flakes or on a gluten-starch blend. They found that within each product category, products with higher surface roughness retained more oil. However, this relationship could not be extended when comparing products of different categories, potato-flake-based products were much rougher than gluten-based products, and retained similar or less oil. Also, a direct relationship between porosity and oil absorption was found in gluten-based products. However, no relationship was detected in potato-flake-based products. Further, gluten-based products were less porous than potato-flake-based products but did not retain less oil inside their structure. Consequently it could be ask, which are the key parameters that will determine the mechanism and the amount of oil retained by fried products made of markedly different food ingredients? Since the nature of ingredients may be so different, other characteristics such as the affinity of the matrix with oil or product macrostructure could be as relevant as microstructural features.

Wetting is strongly related to the chemical affinity between the matrix and oil, and has been suggested as an important factor affecting oil absorption in the frying process (Dana and Saguy, 2006). The term wetting refers to an interfacial phenomenon related to the ability of a fluid to spread over a surface, and can be characterized by the contact angle between the fluid and the surface when the interacting forces are in balance and a state of equilibrium is achieved (Kubiak et al., 2011). This equilibrium can be represented by Young's equation (Equation V.2), which reflects the horizontal force balance between the interfacial tensions acting at the contact line of the solid, liquid (oil in this case) and gas phases when a drop of a liquid rests on a surface (Katoh, 2005):

$$\sigma_{sg} = \sigma_{so} + \sigma_{og} \cos \theta \quad \text{Equation V.2}$$

Where:

$\sigma_{sg}$  = Interfacial tension between solid and gas [N/m]

$\sigma_{so}$  = Interfacial tension between solid and the oil [N/m]

$\sigma_{og}$  = Interfacial tension between oil and gas [N/m]

$\theta$  = Contact angle (between liquid drop and solid surface) [rad]

Equation V.2 is valid for an ideally rigid, flat, smooth, chemically homogeneous, insoluble and nonreactive solid surface (Dullien, 1979, Giljean et al., 2011, Kubiak et al., 2011), characteristics that are not commonly observed in food surfaces.

The wettability of surfaces can be strongly affected by surface roughness and, generally, the contact angle observed in rough surfaces differs from the value seen on ideal surfaces (Zhou and de Hosson, 1995). Surface roughness may increase the interfacial area, thus increasing the interface strength, or it can impair complete wetting leading to the presence of non-wetted regions, thus reducing the interface strength. The surfaces of fried foods are mainly rough, which makes it difficult to determine wettability. Even though there are some approximations to determine contact angles in

rough surfaces, they are mainly appropriate when the size of the surface features is small enough compared to the size of the drop (Giljean et al., 2011).

The macrostructure developed during frying is also a factor that can affect oil uptake. As described by Dana and Saguy (2006), the formation of large voids, cracks and fissures due to structure formation and water evaporation may foster oil penetration during the immersion period. They also suggested that these features are characteristics of reformed, battered and starchy products. Also, according to results reported by Kawas and Moreira (2001), it can be concluded that the degree of puffiness and diameter shrinkage is inversely related to the total oil content of tortilla chips with different levels of starch gelatinization before frying. Recently, Sobukola et al. (2012) measured the expansion of products formulated from wheat gluten and starch fried under different pressures, finding that it was inversely related to their oil content.

The resistance of fried foods to mechanical efforts, also referred as texture, is the reflection of their macro and microstructural arrangement, and may be strongly linked to product permeability to oil absorption. However, texture of fried products has been mostly studied from a sensory perspective, due to its relationship to crispness, an important quality parameter of fried foods (Miranda and Aguilera, 2006), and its relationship to oil absorption has not been of much attention. However, some authors have noticed an inverse relationship between oil uptake and the resistance to collapse due to mechanical effort (Pinthus et al., 1995; Krokida et al., 2001; Kita and Lisinska, 2005). Consequently, texture seems to be an important parameter to be analyzed when understanding the behavior of different formulated matrices during deep-fat frying. It is important to note though, that oil deposition within the structure may affect mechanical properties and consequently texture measurement (Krokida et al., 2001), thus, results must be carefully analyzed.

In accordance, the aim of this work is to understand the effect of the geometry (expansion), the texture and the affinity between the oil and the fried solid matrix, in oil

absorption of formulated matrices, which are either based on gluten and starch wheat, or potato flakes.

## **V.2. Materials and methods**

A set of seven formulated products was studied, which were divided in two main categories according to their main structural component: potato flakes and gluten.

### **V.2.1. Materials**

The ingredients used to formulate the dough were: potato flakes (PF, 7% w.b. moisture content, Alimentos Unisur, Chile), vital wheat gluten (G, 7% w.b. moisture content, Asitec S.A., Chile), native wheat starch (NS, 8% w.b. moisture content, Asitec S.A., Chile) and methylcellulose (MC, 4% w.b. moisture content, Sigma M0512, Sigma-Aldrich, USA). High oleic sunflower oil (Camilo Ferrón, Chile) was used as frying medium.

### **V.2.2. Product preparation**

The formulation of each product in a dry basis and its nomenclature were those used by Moreno et al. (2010) and are presented in Table V-1. As described by Moreno et al. (2010), the dry formulations were mixed for 2 min using a K50-KPM50 food mixer (KitchenAid, USA). The mix was hydrated up to 40% moisture (w.b.), using water at 15 °C in PF-based products, whereas in G-based products, half of the water was added at 15 °C, and the rest was added at 90 °C. The dough was sheeted and laminated until 2 mm thickness using a LSB516 dough sheeter (Doyon, Canada), to be finally cut into squares of 4x4 cm<sup>2</sup>, which were fried at 170 ± 2 °C until 2 ± 0.5% moisture content (w.b.), using a 5 l capacity deep-fryer (Somela-535T, Santiago, Chile), equipped with an external temperature control system (PID+Autotuning, Veto, Chile).

**Table V-1:** Dry basis formulations and nomenclature used throughout the study

Category	Denomination	Formulation (d.b.)
G-based	<b>8G</b>	8% G + 92% NS
	<b>12G</b>	12% G + 88% NS
	<b>8G + MC</b>	90% <b>8G</b> + 10% MC
	<b>12G + MC</b>	90% <b>12G</b> + 10% MC
PF-based	<b>PF</b>	100% PF
	<b>PF + MC</b>	90% PF+ 10% NS
	<b>PF + NS</b>	90% PF+ 10% MC

### V.2.3. Geometry measurement

The geometry of the fried products was quantified according to Figure V.2, measuring the maximum (e2) and minimum (e1) thickness of the samples, as well as their length (a) and width (b), using a Redline Mechanics screw Micrometer with an accuracy of 0.01 mm. Ten measurements were assessed in each fried formulated product.

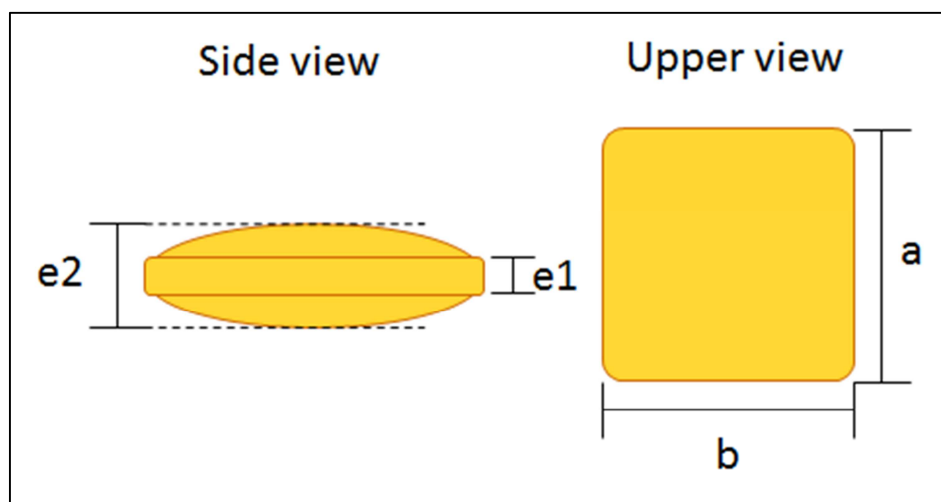


**Figure V.2:** Definition of geometrical parameters used to characterize product geometry; e1: minimum thickness, e2: maximum thickness, a: length, b: width.



#### **V.2.4. Texture measurement**

Texture measurement was assessed using a three-point bending test, as illustrated in Figure V.3. The speed of the bar was set at 10 mm/s and was kept constant. The maximum force (N) at the fracture point was used as a texture characterization parameter and was measured with a TA.XT2 Texture Analyzer (Texture Technologies Corp., USA). Ten measurements were performed in each formulated product, at room temperature (20°C), after cooling for 10 min after frying.

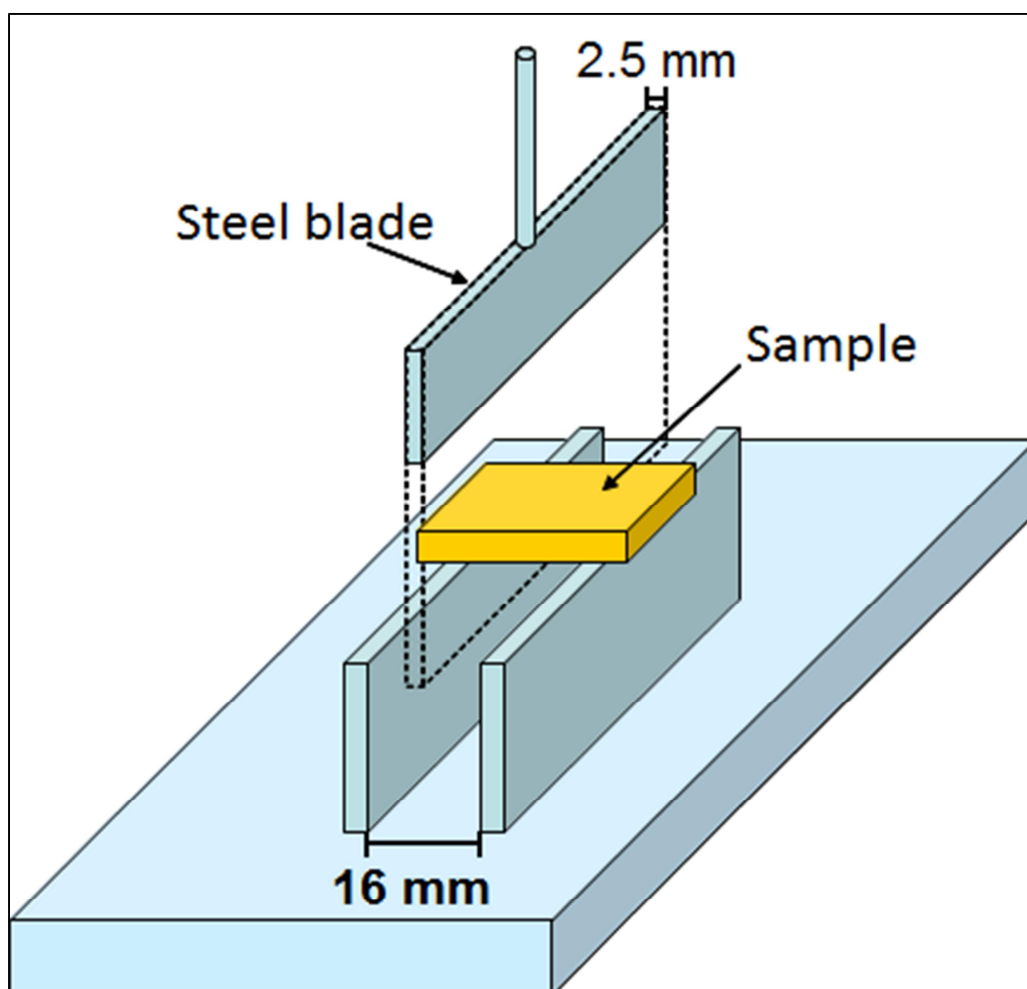


**Figure V.3:** Three point bending test set-up.

#### **V.2.5. Contact angle measurement**

As mentioned before, wetting and therefore, the contact angle, are highly dependent on surface local geometry, i.e. roughness. As determined by Moreno et al. (2010) all the fried formulated matrices under study presented significantly different surface roughnesses. Thus, in order to isolate the effect of wetting from the effect of surface roughness, a specific protocol was developed, according to Figure V.4. First, oil was removed from the fried sample using Soxhlet extraction with petroleum-ether at 60°C during 8 h. In the case of PF-based products, the whole sample was introduced inside the extraction thimble, whereas in G-based products, only the external crust was extracted. The defatted samples were placed under a fume cover, until solvent evaporation. Thereafter, they were submerged in distilled water at room temperature for 2 min in order to plastify the structure. The hydrated samples were placed between two clean glass slides to be slightly compressed using binder clips. The samples were kept at room conditions (20°, 35% RH) during 4 days and inside a desiccator with silica gel during the next 4 days, until they achieved 2% moisture (w.b.). Following this procedure a dry, defatted and flat surface was obtained. Finally, the glass slide was placed on a leveled surface and the static sessile drop method was used to measure the contact angle (Dullien, 1979).

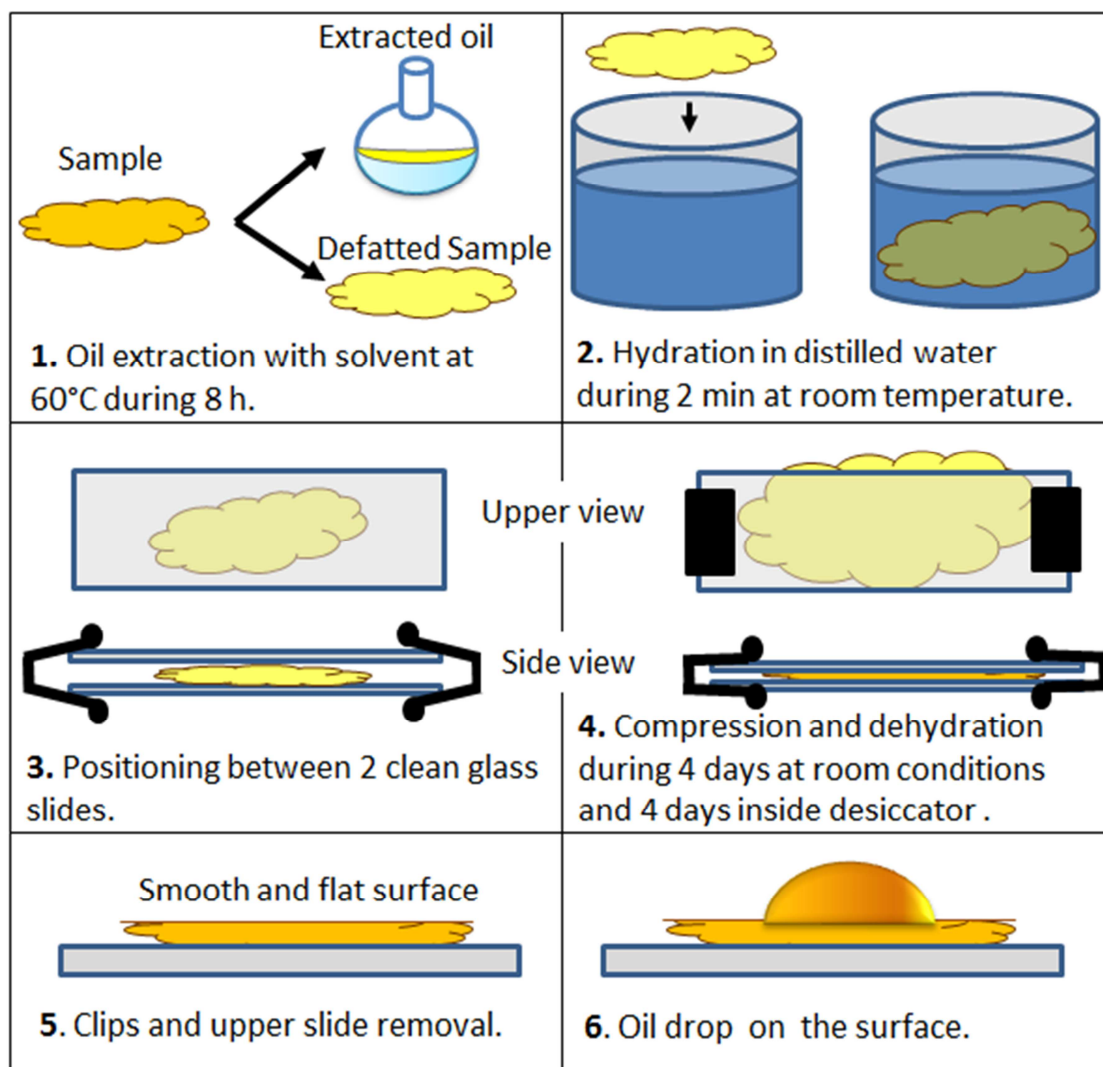


**Figure V.4:** Protocol used to measure the contact angle between the oil and the fried formulated matrix.

A Cool Snap Pro Color 289 digital camera (Photometrics Roper Division, Inc., Tucson, AZ, USA) was leveled and positioned to capture side-view images. An oil drop of 10  $\mu\text{l}$  was dispensed over the surface, using a micropipette (0.5-10  $\mu\text{l}$ ), Hirschmann Laborgeräte, Germany), just after taking the sample from the desiccator. Then, an image sequence at a rate of 10 frames/s was capture, which was stored in TIFF format. The equilibrium contact angle was measured after 10 s of drop deposition. The images were

segmented to isolate the oil drop from the background by thresholding using ImageJ software (Rasband, 1997).

#### **V.2.6. Digital image sequence acquisition of the frying process**

The frying process was performed at  $170 \pm 2^\circ\text{C}$  inside a glass beaker filled with oil heated in a heating plate connected to an external temperature control system (PID + Autotuning, Veto, Chile). A color digital camera (PowerShot A70, Canon, USA) was fixed in position and the samples were positioned between two metal grids to keep them within the field of view of the camera. Side view images were acquired every 5 s. Additional pictures of the fried product were also acquired.

#### **V.2.7. Statistical analysis and variables normalization**

Statistical analysis was conducted with Statgraphics Plus software version 5.1 (Manugistic Inc., Rockville, MD, USA). Maximum force results from texture and contact angle measurements were compared using Duncan's multiple-range test with a confidence level of 95%. The requisite of variance homogeneity was not satisfied for geometrical features, thus, they were analyzed using the non-parametric method of Kruskal-Wallis for median comparison with a confidence level of 95%.

### **V.3. Results and discussion**

In this section, the effect of deep-fat frying on product geometry, texture and oil surface-wetting of the different matrices together with their relationship with oil absorption is analyzed.

#### **V.3.1. Expansion kinetics and product geometry**

As can be observed in Figures V.5 and V.6, product expansion and thus product macrostructure was mainly formed during the first 15-20 s of frying. This is an important finding, which has not been previously reported, and was observed in all formulations. The process occurred as follows. At the beginning, the slices dropped to the bottom due to their dense structure. A mist of small bubbles leaving the matrix,

which probably corresponded to unbound water, immediately appeared. After few seconds ( $\approx 5$  s), a vigorous escape of big water bubbles occurred and the sample density quickly decreased due to dehydration and violent expansion, beginning to float. During the next 10-15 s, the samples reached their final size, to be further cooked and dehydrated. Consequently, most important macroscopic changes occurred during the first seconds of frying.

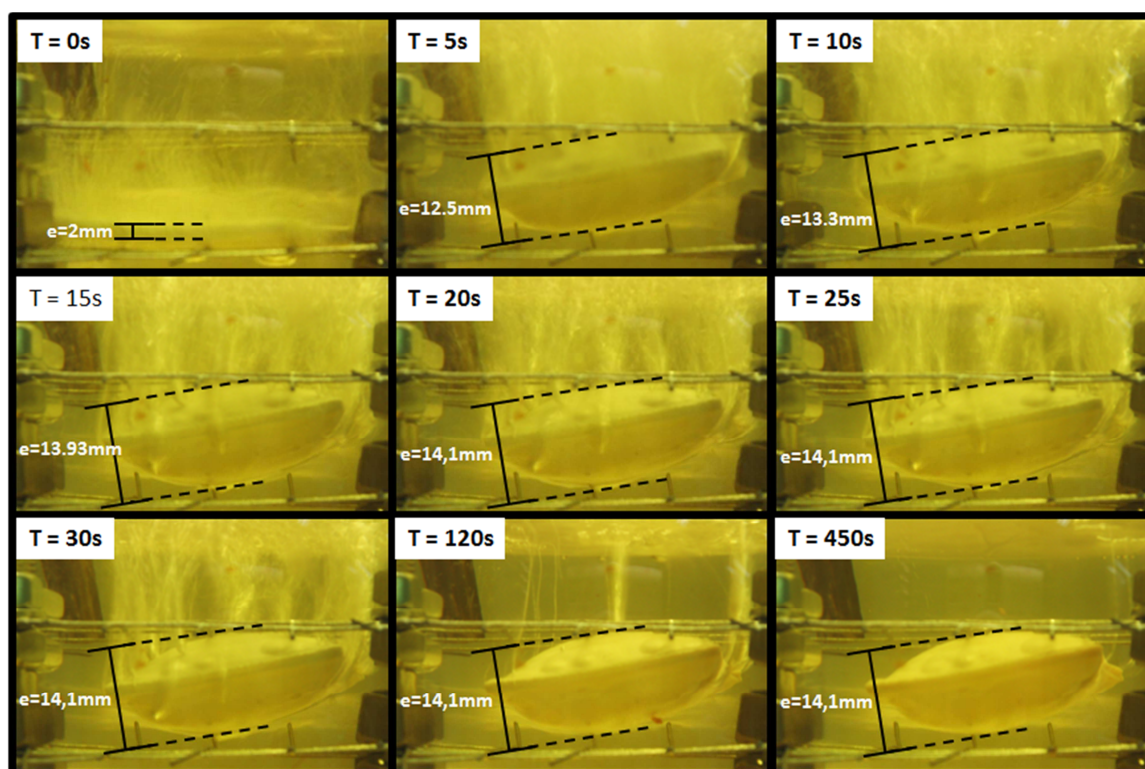


**Figure V.5:** Image sequence of a G-based product during frying at 170°C. The maximum thickness of the products determined by image analysis is also shown in each picture.

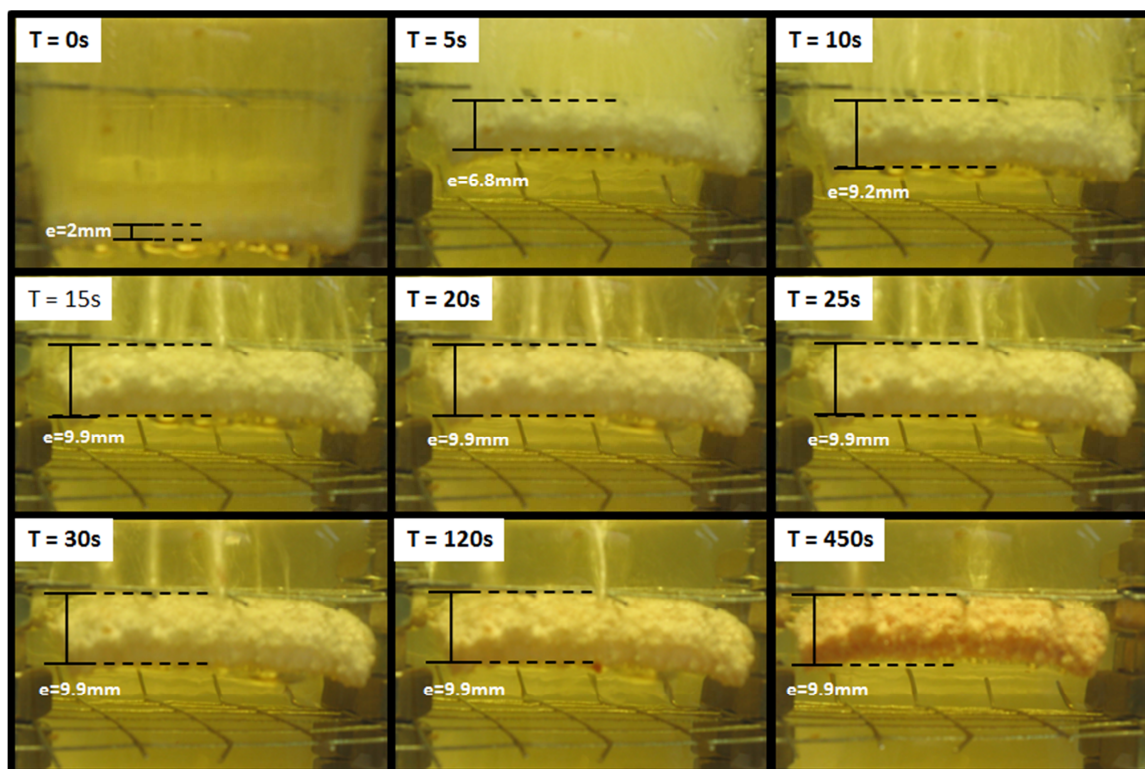


**Figure V.6:** Image sequence of a PF-based product during frying at 170°C. The maximum thickness of the products determined by image analysis is also shown in each picture.

In the case of G-based products, an external crust layer was formed (Figures V.7 and V.8). This external layer was extremely oily, whereas the inner layer contained a minimum amount of oil (Figure V.7). Even though the oil content was not measured, additional research using CSLM microscopy had shown that the inner region is virtually oil free (Moreno and Bouchon, 2011). The external crust was usually separated from the core by an empty space, suffering minimum expansion, and could either remain in the center (Figure V.8A) or attached to one of the external layers (Figure V.8B). In the case of PF-based products, no central layer was observed, and a thicker global crust was observed.



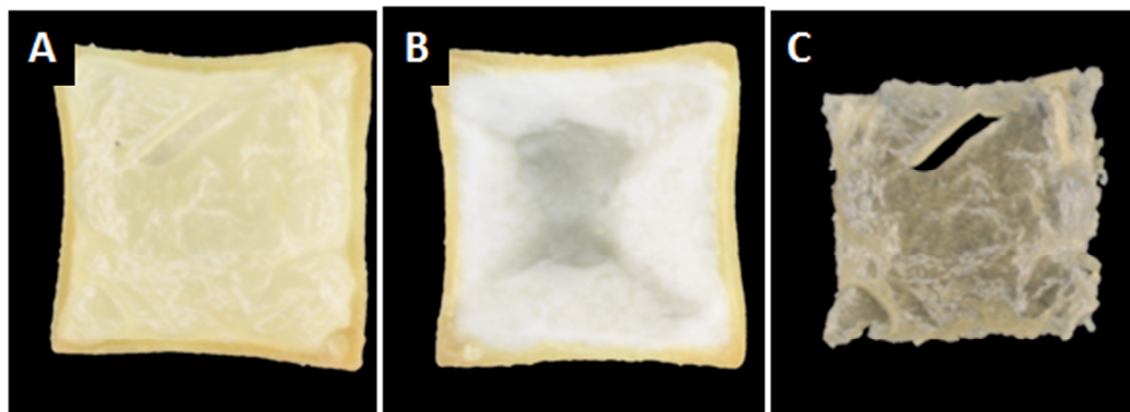









**Figure V.7:** Digital images of: (A) 8G fried product, (B) 8G interior and (C) 8G external crust.



**Figure V.8:** Cross sections of: (A) 12G, (B) 12+MC and (C) PF fried products.

Interestingly, the external crust in G-based products was observed to form during the first 15-20 s, when the products reached their final size. As reported by Moreno et al. (2010), in this product category an important amount of oil penetrated during the immersion period, before removing the product from the oil. Since oil is mainly located in that external layer, which dries faster than the inner portion (moving evaporation front as explained by Bouchon and Pyle, 2005), according to equation 1, it could be thought that the pressure within this porous outer layer could be low enough to allow oil penetration at an earlier stage. Thus, this oil fraction would probably penetrate through capillary action.

Additional geometry descriptors are presented in Figure V.9. Overall, after frying neither PF-based nor G-based products presented significant differences between length and width, thus, a general side “a” is reported. However, both product categories showed a rather different behavior. G-based products tended to suffer lateral shrinkage (length and width reduction), whereas PF-based products tended to keep, or even enlarge, their lateral size “a”. In G-based products MC helped to limit this shrinkage. Overall, shrinkage did not depend on gluten content.

8G	12G	8G+MC	12G+MC
			
e1 = $0.30 \pm 0.04$ cm <sup>a</sup> e2 = $1.71 \pm 0.33$ cm <sup>e</sup> a = $3.77 \pm 0.17$ cm <sup>A</sup>	e1 = $0.35 \pm 0.05$ cm <sup>a</sup> e2 = $1.69 \pm 0.22$ cm <sup>e</sup> a = $3.76 \pm 0.11$ cm <sup>A</sup>	e1 = $0.29 \pm 0.03$ cm <sup>a</sup> e2 = $0.90 \pm 0.17$ cm <sup>c</sup> a = $3.90 \pm 0.09$ cm <sup>B</sup>	e1 = $0.34 \pm 0.05$ cm <sup>a</sup> e2 = $1.03 \pm 0.29$ cm <sup>c</sup> a = $3.90 \pm 0.09$ cm <sup>B</sup>
PF	PF+MC	PF+NS	
			
e1 = $0.83 \pm 0.08$ cm <sup>c</sup> e2 = $0.98 \pm 0.09$ cm <sup>c</sup> a = $4.21 \pm 0.09$ cm <sup>D</sup>	e1 = $0.72 \pm 0.11$ cm <sup>b</sup> e2 = $1.06 \pm 0.16$ cm <sup>c</sup> a = $4.00 \pm 0.09$ cm <sup>C</sup>	e1 = $0.7 \pm 0.07$ cm <sup>b</sup> e2 = $1.39 \pm 0.13$ cm <sup>d</sup> a = $4.00 \pm 0.11$ cm <sup>C</sup>	

**Figure V.9:** Mean values  $\pm$  standard deviation (n=10) of geometrical parameters of fried formulated products. Side views of the products were illustrated by keeping the proportions to the actual measured geometrical parameters. Lowercase letters indicate significant differences in thickness (minimum and maximum thicknesses were compared together). Uppercase letters indicate significant differences in length.

Product expansion was quantified through the minimum (e1) and the maximum (e2) thickness. G-based products suffered a much higher maximum expansion (e2) than PF-based products, which in turn had a rather regular expansion (e1 was slightly lower than e2). The addition of MC significantly reduced the maximum thickness in G-based products, as well as their minimum thickness (e1), reflecting some capacity to preserve



the original shape in this product category. In PF-based products, no significant effect of MC addition in maximum thickness was observed, whereas the addition of NS significantly increased it. Overall, all products that contained NS suffered an important central expansion ( $e_2 \gg e_1$ ), since all G-based products contained NS in their formulation.

The main responsible for product expansion during frying is the resistance imposed by the solid matrix to water evaporation. The inner pressure build-up due to gas expansion, together with the viscoelastic behavior of the material, which suffers strong internal stresses, produces the expansion in the axial direction (Yamsaengsung et al., 2011). According to Bouchon and Pyle (2004), the low water holding capacity of NS allows a rapid initial vapor loss, which speeds up crust formation. This crust allows withstanding a higher pressure and precludes moisture loss, allowing starch gelatinization, and therefore, product expansion.

Figure V.10 shows the oil content of the fried food matrices obtained in a previous work (Moreno and Bouchon, 2010). Accordingly, in PF-based products category, less expanded products (PF and PF+MC products) showed a higher oil retention compared to the most expanded one (PF+MC), however no significant differences were found between them. The concave expanded structure may foster oil drainage after frying, thus, reducing oil absorption. Even though Moreno et al. (2010) did not determine any drainage during post-frying cooling, there could be an influence on oil drainage just upon removal of the product from the oil. In the case of G-based products, more expanded ones (8G and 12G), showed higher oil content. As shown earlier, these products had an external crust layer, which may be vulnerable to high levels of stretching, resulting in a highly permeable and brittle outer surface, where oil can easily infiltrate.

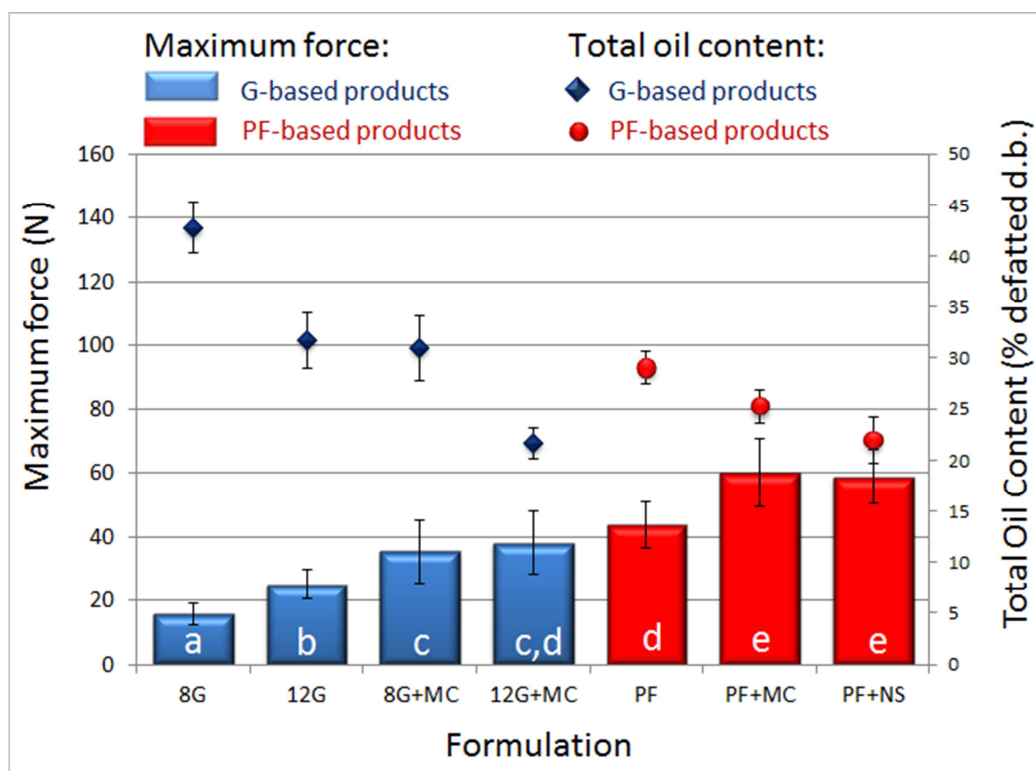


**Figure V.10:** Maximum force of fracture and total oil content of fried formulated products. Oil content values were taken from Moreno et al. (2010). Mean values of 5 measurements  $\pm$  standard deviation are shown for oil content. Mean values of 10 measurements  $\pm$  standard deviation are shown for maximum force. Different letters inside each bar indicate significant differences.

### V.3.2. Texture

The maximum force at the fracture point of the different fried matrices is shown in Figure V.10. In general terms, the force required to break PF-based products was higher than the one needed to break G-based products. The addition of MC increased the hardness in both PF- and G-based products, as well as NS addition in PF-based products. Hardness was also increased when raising the gluten content, but only in MC-free slices. A good correlation between maximum breaking force and oil content was determined in each product category, with an  $R^2$  of 0,8369 in G-based products and an  $R^2$  of 0,7235 in PF-based products. In the case of PF-based products, the tendency was not that clear, since no statistical difference in hardness between PF+MC and PF+NS was observed, despite their difference in oil content, but still the softer product (PF) retained the higher

amount of oil. To dig further into this relationship, it would be useful to quantify the texture of the product at frying temperatures, or at the beginning of the cooling period, when most of oil absorption takes place. According to experimental state diagrams from Cuq et al. (2003), gluten, native starch and pre-gelatinized starch could be in a rubbery state at frying temperatures (170°-190°C), even at a low moisture content, being prone to deformation. Models and studies, usually do not consider such deformation, which could be an interesting topic for future research.

### **V.3.3. Contact Angle**

Contact angle was measured on the defatted fried matrix, according to the protocol described in Figure V.4, to assess oil wetting of the fried structure, which is completely different from the raw laminated dough. An example of contact measurement is depicted in Figure V.11, which shows the surface prior to the measurement (A), the oil drop before (B) and after reaching equilibrium (C) and the segmented drop together with the contact angle.

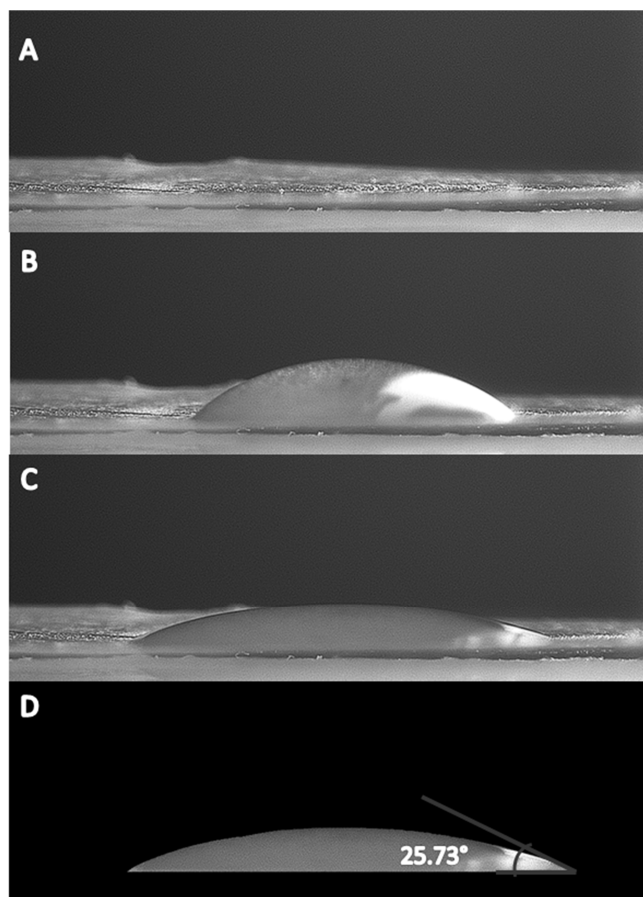


**Figure V.11:** (A) Photograph of the flat surface of a 12G defatted formulated product. (B) Advancing oil drop before reaching equilibrium. (C) Oil drop at equilibrium. (D) Segmented oil drop at equilibrium. The contact angle between solid-oil and oil-air interfaces is outlined and measured.

Results were plotted in Figure V.12. As can be seen, all values were lower than  $90^\circ$ , indicating that all surfaces were wetted, reflecting a good chemical affinity between the oil and the matrices. If the contact angle was larger than  $90^\circ$ , the matrix would be partially wetted and for high values, oil could even tend to move over the surface. In addition, according to Equation V.1, the capillary pressure ( $P_c$ ) would be negative, precluding oil penetration through capillary action.

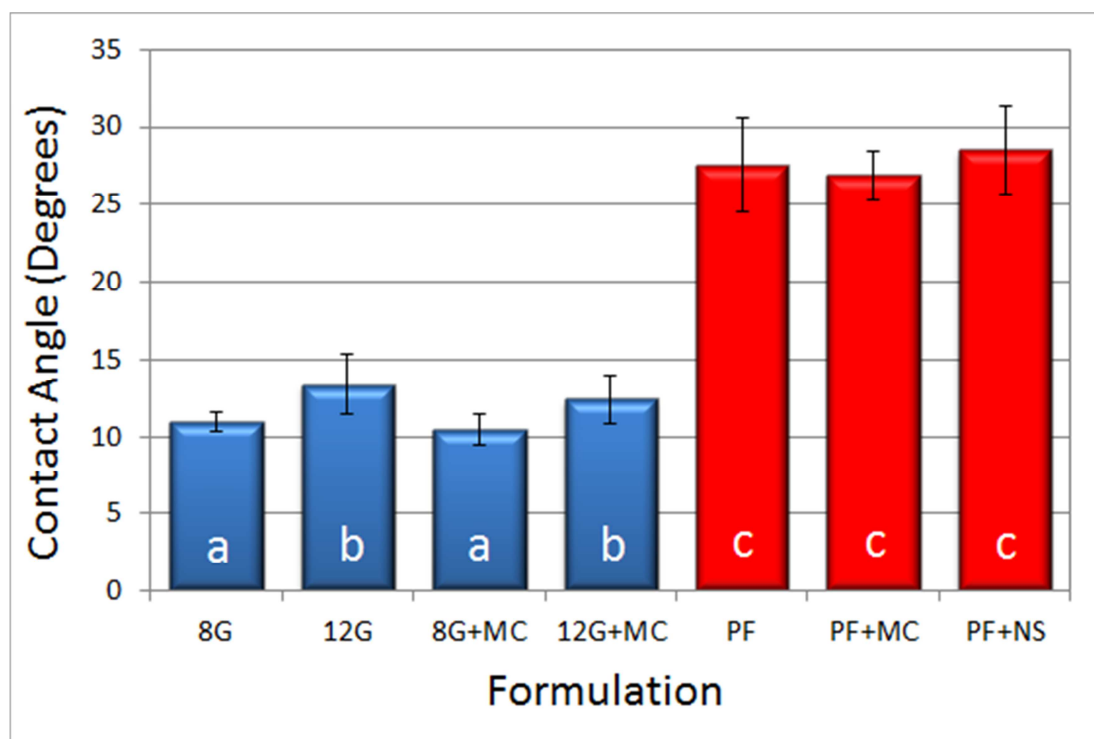


**Figure V.12:** Contact angle of fried formulated products. Mean values of 6 measurements  $\pm$  standard deviation are shown. Different letters inside each bar indicate significant differences.

Overall, in G-based products lower contact angle values were obtained compared to PF-based products, reflecting a better chemical affinity with oil. Pinthus and Saguy (1994) reported an expression (Equation V.3) to determine the interfacial tension between the food surface and the oil as a function of the contact angle and the interfacial tension between the oil and the gas ( $\sigma_{og}$ ):

$$\sigma_{so} = \frac{\sigma_{og}}{4} [1 - \cos \theta]^2 \quad \text{Equation V.3}$$

The same expression could be used to related PF- and G-based matrices with  $\sigma_{og}$ , according to Equation V.4:

$$\frac{(\sigma_{so})_{PF}}{[1 - \cos \theta_{PF}]^2} = \frac{\sigma_{og}}{4} = \frac{(\sigma_{so})_G}{[1 - \cos \theta_G]^2} \quad \text{Equation V.4}$$

Considering that contact angles of PF-based products are larger than contact angles of G-based products, and that both range between 0° and 90°C, the following relation can be stated:

$$\frac{(\sigma_{so})_{PF}}{(\sigma_{so})_G} = \frac{[1 - \cos \theta_{PF}]^2}{[1 - \cos \theta_G]^2} > 1 \quad \text{Equation V.5}$$

And finally:

$$(\sigma_{so})_{PF} > (\sigma_{so})_G \quad \text{Equation V.6}$$

According to Equation V.6, for contacts angles between 0° and 90°, there is a direct relationship between  $\sigma_{so}$  and the contact angle, when surfaces are wetted by the same liquid (oil). Accordingly, PF-based products should have a higher interfacial tension with oil ( $\sigma_{so}$ ), reflecting the lower wettability and their weaker chemical affinity.

The higher affinity between the oil and G-based matrices could explain to some extent the higher oil content of most G-based formulations compared to PF-based products. When studying the effect of product formulation within each product category, no significant differences in contact angle measurement were observed between PF-based products. That is, the addition of NS or MC to PF-based products did not affect the chemical affinity between the matrix and the oil, thus, this factor cannot explain differences in oil absorption in this product category. Also, no effect was observed when adding MC to G-based formulations. Differences were only noticed when the gluten content was varied. Formulations with higher gluten content, showed a slightly but significantly lower wettability. To some extent, these measurements are consistent with oil-uptake results, which showed a higher oil content of 12G compared to 8G products, as well as when comparing 12G+MC with 8G+MC samples.

#### **V.4. Conclusions**

The effect on oil absorption of product geometry, texture and oil wetting properties of different fried gluten- (G) and potato-flakes- (PF) based formulated products was analyzed.

Both product categories suffered most important macro-structural formation during the first 15-20 s, including product expansion. However, a clear distinction between both product categories was observed, in G-based products an external crust layer was formed, whereas in PF-products a thicker global crust was obtained. Overall, no clear relationship between the amount of oil retained by the matrices and their geometry was obtained. In PF-based products, the most expanded product (made of PF and native starch) showed the lowest oil content, a behavior that could be linked to the existence of a thick concave crust that might impair oil adherence upon removal of the product from the oil bath. On the other hand, in G-based products, most expanded products retained the highest amount of oil, probably as a consequence of the fast formation of the external crust, which was subjected to high levels of stretching increasing its permeable to oil absorption. In relation to texture, hardest products tended to retain less oil in each product category, reflecting the relationship between this parameter and oil permeability.

The measurement of contact angle between the oil and the different restructured food surfaces allowed discriminating between both product categories. The main conclusion derived from these results is that the tendency of PF-based products to retain less oil despite the larger geometrical features at the macro (roughness) and microscopic scales (porosity) compared to G-based products reported in previous studies, may be related to its lower chemical affinity with oil (e.i. higher contact angle). However, no significant differences in wetting were observed between the different PF-based formulations, despite their differences in oil uptake. Thus, other factors such as surface roughness, may explain such differences within this product category.

Certainly the amount of oil absorbed by fried formulated products, as well as the oil absorption mechanisms, depend on several factors, which are difficult to define.

However, as shown in this work, it is possible to identify some key factors in the light of phenomenological equations, which help understanding the behavior of different formulations. The combination of food ingredients is a good approach to design novel matrices to be fried. If chemical affinity with oil is combined with the building of hierarchical food structures at the nano- and micro-structural level, a more effective design of fried products using an engineering formulation approach could be achieved. Such concepts are currently under study by this research group.



## **VI. Discussion and Conclusions**

Throughout this work several microstructural characterization methodologies were successfully developed to understand the relationship between product microstructure and oil absorption in different formulated products. Two product categories, which were either based on potato-flakes (PF-based products), or wheat gluten and starch (G-based products) were laminated, fried and analyzed. These products showed the advantage of reproducibility, in contrast with raw materials such as potatoes, whose heterogeneity can cause major methodological problems. They also allowed successfully investigating the oil uptake capacity of different matrices. Formulation were based on such ingredients, but also the use of methylcellulose (MC) as well as the inclusion of added native wheat starch (NS), allowing the understanding of different food “building blocks”, in structure development and oil absorption phenomena.

Most of the methodologies that were developed along this work were effectively adapted to minimize artifact incorporation, to increase objectivity during observation. In the light of this approach the use of laser scanning microscopy together with the use of fractal analysis showed to be an instrumental technique to characterize surface roughness, allowing successful discrimination between the different product categories. Similarly, the development of a double fluorescent labeling procedure protocol combined with multichannel confocal scanning laser microscopy (CSLM) observation showed to be a reliable methodology to observe and analyze the inner microstructure of the different products.

Regarding surface metrology, it was found that the most reliable parameter to differentiate the surfaces of fried foods was the relative area, which was calculated from area-scale fractal analysis. Several parameters derived from area-scale fractal analysis were obtained, such as the smooth-rough crossover and the fractal dimension; however, the relative area was scale-sensitive and allowed adequate discrimination of fried surfaces through a range of relevant scales. In addition, it allowed studying the

relationship between surface roughness and oil uptake. In fact, it was found that within each product category, products with higher surface roughness retained more oil. Specifically, in G-based products the addition of MC and the increase of gluten in the formulation reduced surface roughness and decreased oil content. In PF-based products, addition of MC and NS resulted in both surface-roughness and oil-absorption reduction. However, the relationship between surface roughness and oil absorption could not be extended when comparing products of different categories. PF-based products were rougher than G-based products, but did not retain more oil for an equivalent roughness. In addition, it was found that G-based products absorbed most of the oil during frying, whereas PF-based mostly absorbed oil during cooling.

CSLM allowed the non-invasive characterization of the food matrix and the oil deposition through image analysis, giving valuable knowledge to understand the relationship between the inner microstructure and the oil absorption capacity of the matrices, to further understand the differences between product categories. In fact, both product categories showed important differences in their inner structure, oil content and distribution, making evident the key role of specific food building blocks in microstructure development, and thus, in the final characteristics of fried foods. PF-based products were more porous and presented a wider range of pore sizes than G-based products. Overall, a direct relationship between porosity and oil absorption was obtained in G-based products, but, no relationship was detected in PF-based products. In addition, G-based products were less porous but retained, in general, more oil.

Additional aspects, such as the understanding of the chemical affinity between the oil and the food matrix, as well as product expansion and texture were also examined and gave further knowledge about their effect in oil absorption. Importantly, thanks to in situ examination using digital recording, it was concluded that product categories suffered most important macro-structural formation during the first 15-20 s, including product expansion, but, a clear distinction between both product categories was observed. In G-based products an external crust layer was formed, which could be clearly identified from an internal layer, whereas in PF-products a thicker global crust was obtained. In

addition, a protocol was developed to measure the contact angle between the oil and the different restructured food surfaces, which allowed removing the effect of surface roughness from the measurement, as well as the discrimination between both product categories. Overall, it could be concluded that the tendency of PF-based products to retain less oil despite the higher surface roughness and porosity compared to G-based products reported in previous studies, could be related to some extent to its lower chemical affinity with oil, i.e. lower wetting. But, as no significant differences in wetting were observed between the different PF-based formulations, despite their differences in oil uptake, surface roughness can still explain differences within this product category.

Certainly, it would be ideal to have an explicit definition about the specific effect of key parameters in oil retention of formulated fried products. However, this is not trivial since it is not possible to work in a *ceteris paribus* system, i.e. keeping all parameters invariants after variation of one of them. As in many domains, this is difficult to achieve, since any modification either in the processing conditions, the formulation or the pre-treatment, among others, will have more than one consequence in the characteristics of the final product or associated transport phenomena. However, as shown along this work, it was possible to have a good distinction of most important factors affecting oil absorption, within a specific product category or when comparing different product categories, in the light of phenomenological equations, which help understanding the behavior of different formulations.

In order to have an overall perspective of most important factors analyzed during this Thesis, the parameters characterizing expansion, contact angle, hardness, relative area, porosity measured by image analysis, and oil uptake, were normalized according to Equation VI.1.

$$P_{i(0,1)} = \frac{P_i - P_{\min}}{P_{\max} - P_{\min}} \quad \text{Equation VI.1}$$

Where:

P<sub>i</sub> = Measurement of parameter P in product “i”

$P_{max}$  = Maximum value among all the measurements of parameter P

$P_{min}$  = Minimum value among all the measurement of parameter P

$P_i(0,1)$  = Normalized parameter P, which ranged between 0 and 1

Results were compiled in a spider map, as shown in Figure VI.1, in order to obtain a visual description of most important aspects defining each formulated product.

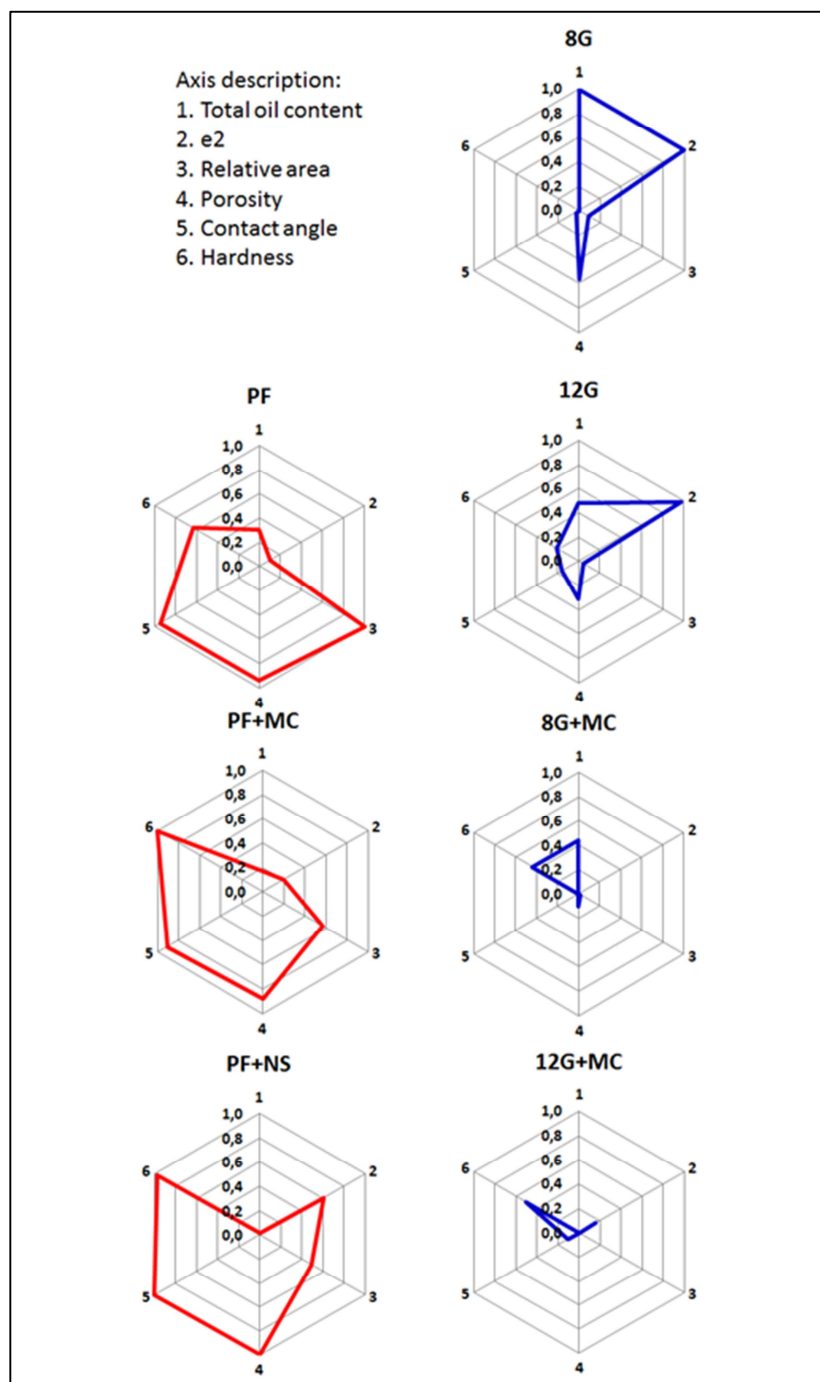


**Figure VI.1:** Spider map showing most important factors analyzed in Chapters II, III, IV and V. Each parameter was normalized between 0 and 1 with respect to the maximum and minimum value. Acronyms stand for their composition in a dry basis: PF (100% PF), PF+MC (90% PF + 10% MC), PF+NS (90% PF + 10% NS), 8G (8% G + 92% NS), 12G (12 G + 88% NS), 8G+MC (90% 8G mixture + 10% MC) and 12G+MC (90% 12G mixture + 10% MC).

This Figure allows observing at a glance the effect of food ingredients combination in most important quality parameters, highlighting the effect of constituents in defining food structure.

If chemical affinity with oil is combined with the building of hierarchical food structures at the nano- and micro-structural level, a more effective design of fried products using an engineering formulation approach could be achieved. This approach should go one step beyond, where in addition to the knowledge of raw ingredients properties and their effect when combined into different food matrixes, specific structuring processes could be implemented, in order to control to higher extent food properties.

There are several approaches that could be used in the future to introduce more “engineering” to food structuring, including the possibility to use nano-technology to create hierarchical structures or even fractal ones. For instance, through this kind of approach it could be possible to lead to the formation of a non-wettable surface, which could prevent oil absorption. This approach could be combined with the study of structure formation in situ during frying, by adapting specific microscopy techniques in the light of those developed here. To do so, the use of devices with thermal control to observe microstructural arrangements or to understand the development of textural properties in real time could be useful tools.

Another important aspect that could be considered when processing formulated fried foods is the possibility to design specific structures in which oil could be entrapped, reducing its bioaccessibility and/or its bioavailability during digestion. This imposes new challenges, such as the integration of new disciplines like medicine, nutrition and biological sciences, which certainly may help increase the impact of research, according to new health trends.

**References**

Achir, N., Vitrac, O. & Trystram, G. (2010). Direct observation of the surface structure of French fries by UV-VIS confocal laser scanning microscopy. *Food Research International*, 43(1), 307-314.

Adedeji, A. A. & Ngadi, M. O. (2011). Microstructural characterization of deep-fat fried breaded chicken nuggets using X-ray micro-computed tomography. *Journal of Food Process Engineering*, 34(6), 2205-2219.

Adedeji, A.A., Liu, L. & Ngadi, M.O. (2011). Microstructural evaluation of deep-fat fried chicken nugget batter coating using confocal laser scanning microscopy. *Journal of Food Engineering*, 102(1), 49-57.

Aguilera, J.M. (2005). Why food microstructure?. *Journal of Food Engineering*, 67, 3-11.

Aguilera, J.M. (2006). Food product engineering: building the right structures. *Journal of the Science of Food and Agriculture*, 86, 1147-1155.

Aguilera, J.M. & Gloria, H., (1997). Determination of oil in fried potato products by differential scanning calorimetry. *Journal of Agricultural and Food Chemistry* 45, 781-785.

Aguilera, J.M. & Stanley, D.W. (1999). Microstructural principles of food processing and engineering (2<sup>nd</sup> ed., pp. 413-423). Aspen Publishers Inc., Gaithersburg.

AOAC. (1995). *Official Methods of Analysis*, 16th ed. Association of Official Analytical Chemists, Washington, DC, Unites States.

## References

- Annapure, U.S., Singhal, R.S. & Kulkarni, P.R. (1999). Screening of hydrocolloids for reduction in oil uptake of a model deep fat fried product. *Food Processing and Preservation* 101, 217-221.
- ASME B46. (2002). US National Standard ASME B46.1, Surface Texture (Surface Roughness, Waviness and Lay). The American Society of Mechanical Engineers, New York, United States.
- Baumann, B. & Escher, E. (1995). Mass and heat transfer during deep fat frying of potato slices - I. Rate of drying and oil uptake. *Lebensmittel-Wissenschaft & Technologie*. 28, 395-403.
- Blumenthal, M.M. (1991). A new look at the chemistry and physics of deep-fat frying. *Food Technology* 45, 68-71.
- Bouchon, P. & Aguilera, J.M. (2001). Microstructural analysis of frying potatoes. *International Journal of Food Science and Technology*, 36, 669-676.
- Bouchon, P., Hollins, P., Pearson, M., Pyle, D.L. & Tobin, M.J. (2001). Oil distribution in fried potatoes monitored by infrared microspectroscopy. *Journal of Food Science*, 66(7), 918-923.
- Bouchon, P., Aguilera, J.M. & Pyle, D.L. (2003). Structure-oil absorption relationships during deep-fat frying. *Journal of Food Science*, 68(9), 2711-2716.
- Bouchon, P. & Pyle, D.L. (2004). Studying oil absorption in restructured potato chips. *Journal of Food Science*, 69(3), 115-122.



## References

- Bouchon, P. & Pyle, D.L. (2005). Modelling oil absorption during post-frying cooling. I. Model development. Transactions of the institution of chemical engineers Part C. Food and Bioproducts Processing, 83(4), 261-272.
- Briones, V., Brown, C.A. & Aguilera, J.M. (2006). Scale-sensitive fractal analysis of the surface roughness of bloomed chocolate. Journal of the American Oil Chemists' Society 83, 193-199.
- Brown, C.A., Charles, P.D., Johnsen, W.A. & Chesters, S. (1993). Fractal analysis of topographic data by the patchwork method. Wear 161, 51-61.
- Brown, C.A. & Shipulski, E.M. (1994). Concurrent engineering design of surface roughness using scale-area analysis. Manufacturing Science and Engineering, Book No. G0930A 68, 155-159.
- Brown, C.A. & Siegmann, S. (2001). Fundamental scales of adhesion and area-scale fractal analysis. International Journal of Machine Tools and Manufacture 41, 1927-1933.
- Bugusu, B.A., Rajwa, B. & Hamaker, B.R. (2002). Interaction of maize zein with wheat gluten in composite dough and bread as determined by confocal laser scanning microscopy. Scanning, 24(1), 1-5.
- Cantor, G.J. & Brown, C.A. (2009). Scale-based correlations of relative areas with fracture of chocolate. Wear 266, 609-612.
- Cuq, B., Abecassis, J & Guilbert, S. (2003). State diagrams to help describe wheat bread processing. International Journal of Food Science and Technology, 38, 759-766.

## References

- Dana, D. & Saguy, I.S. (2006). Review: Mechanism of oil uptake during deep-fat frying and the surfactant effect-theory and myth. *Advances in Colloid and Interface Science* 128-130, 267-272.
- Day, L., Augustin, M.A., Batey, I.L. & Wrigley, C.W. (2006). Wheat-gluten uses and industry needs. *Trends in Food Science and Technology* 17, 82-90.
- de Hoog, E.H.A. & Tromp, R.H. (2005). Confocal microscopy – A tool to study food ingredient functionality. In A.P. Riley (Ed.), *New developments in food policy, control and research*. Nova Science Publishers, Inc., New York. . (pp. 149-174).
- Dueik, V. & Bouchon, P. (2011). Development of healthy low-fat snacks: understanding the mechanisms of quality changes during atmospheric and vacuum frying. *Food Reviews International*, 27 (4), 408-432.
- Dueik, V., Moreno, M.C. & Bouchon, P. (2012). Microstructural approach to understand oil absorption during vacuum and atmospheric frying. *Journal of Food Engineering*, 111(3), 528-536.
- Dullien, F.A.L. (1979). *Porous Media Fluid Transport and Pore Structure*. Academic Press, Inc., San Diego.
- Dürrenberger, M.B., Handschin, S., Conde-Petit, B. & Escher, F. (2001). Visualization of food structure by confocal laser scanning microscopy (CSLM). *Lebensmittel-Wissenschaft und-Technologie*, 34(1), 11-17.
- Farkas, B.E., Singh, R.P. & Rumsey, T.R. (1996). Modeling heat and mass transfer in immersion frying. I. Model development. *Journal of Food Engineering*, 29, 211-226.

## References

- Gazmuri, A.M. & Bouchon, P. (2009). Analysis of wheat gluten and starch matrices during deep-fat frying. *Food Chemistry*, 115, 999-1005.
- Garayo, J. & Moreira, R.G. (2002). Vacuum frying of potato chips. *Journal of Food Engineering*, 55, 181-191.
- Giljean, S., Bigerelle, M., Anselme, K. & Haidara, H. (2011). New insights on contact angle/roughness dependence on high surface energy materials. *Applied Surface Science*, 257, 9631- 9638.
- ISO 25178. (2007). Geometrical product specifications (GPS)-Surface texture: Areal-Part 2: Terms, definitions and surface texture parameters.
- Jekle, M. & Becker, T. (2011). Dough microstructure: Novel analysis by quantification using confocal laser scanning microscopy. *Food Research International*, 44(4), 984-991.
- Jordan, S.E. & Brown, C.A. (2006). Comparing texture characterization parameters on their ability to differentiate ground polyethylene ski bases. *Wear* 261, 398-409.
- Kato, K. (2005). Contact Angle and Surface Tension Measurement. In S. Hartland (Ed.), *Surface and Interfacial Tension: Measurement, Theory, and Applications*. Surfactant Science Series vol. 119 (pp. 375-423). Taylor and Francis. New York.
- Kawas, M.L. & Moreira, R.G. (2001). Effect of degree of starch gelatinization on quality attributes of fried tortilla chips. *Journal of Food Science*, 66(2), 300-306.
- Keller, C., Escher, F. & Solms, J.A. (1986). Method of localizing fat distribution in deep-fat fried potato products. *Lebensmittel-Wissenschaft und Technologie* 19, 346-348.

## References

- Kita, A. & Lisinska G. (2005). The influence of oil type and frying temperatures on the texture and oil content of French fries. *Journal of the Science of Food and Agriculture*, 85(15), 2600-2604.
- Krokida, M.K., Oreopoulou, V., Maroulis, Z.B., & Marinos-Kouris, D. (2001). Viscoelastic behaviour of potato strips during deep fat frying. *Journal of Food Engineering*, 48, 213-218.
- Kubiak, K.J., Wilson, M.C.T., Mathia, T.G. & Carval, Ph. (2011). Wettability versus roughness of engineering surfaces. *Wear*, 271, 523-528.
- Lee, L., Ng, P. K. W., Whallon, J. H. & Steffe, J. F. (2001). Relationship between rheological properties and microstructural characteristics of nondeveloped, partially developed, and developed doughs. *Cereal Chemistry*, 78(4), 447-452.
- Lorén N., Langton, M. & Hermansson, A.-M. (2007). Confocal fluorescence microscopy (CLSM) for food structure characterization. In D.J. McClements (Ed.), *Understanding and controlling the microstructure of complex foods* (pp. 232-260). CRC Press, Boca Raton.
- Mellema, M. (2003). Mechanism and reduction of fat uptake in deep-fat fried foods. *Trends in Food Science and Technology* 14, 364-373.
- Minihane, A.M. & Harland, J.I. (2007). Impact of oil used by the frying industry on population fat intake. *Crit Rev Food Sci Nut* 47, 287-297.
- Miranda, M. & Aguilera, J.M. (2006). Structure and texture properties of fried potato products. *Food Reviews International*, 22, 173-201.

## References

- Miri, T., Bakalís, S., Bhima, S.D. & Fryer, P.J. (2006). Use of X-ray Micro-CT to characterize structure phenomena during frying. IUFoST, 13th World Congress of Food Science and Technology, Nantes, France.
- Moreira, R.G., Palau, J.E. & Sun, X. (1995). Deep-fat frying of tortilla chips: an engineering approach. *Food Technology*, 49, 146-150.
- Moreira, R.G. & Barrufet, M.A. (1998). A new approach to describe oil absorption in fried foods: a simulation study. *Journal of Food Engineering*, 35, 1-22.
- Moreira, R.G., Castell-Perez, M.E. & Barrufet, M.A. (1999). *Deep Fat Frying: Fundamentals and Applications*. Kluwer Academic/ Plenum Publishers, Dordrecht.
- Moreira, R.G., Sun, X. & Chen, Y., (1997). Factors affecting oil uptake in tortilla chips in deep-fat frying. *Journal of Food Engineering*, 31, 485-498.
- Moreno, M.C. & Bouchon, P. (2008). A different perspective to study the effect of freeze, air, and osmotic drying on oil absorption during potato frying. *Journal of Food Science* 73, E122-E128.
- Moreno, M.C., Brown, C.A. & Bouchon, P. (2010). Effect of food surface roughness on oil uptake by deep-fat fried products. *Journal of Food Engineering*, 101(2), 179-186.
- Moreno, M.C. & Bouchon, P. (2011). Microstructural analysis of deep-fat fried formulated products by confocal laser scanning microscopy (CLSM) and fluorescent labeling. In *Proceedings of the Eleventh International Congress on Engineering and Food*, Athens, Greece.
- Moreno, M.C. & Bouchon, P. (2012). Microstructural characterization of deep-fat fried formulated products. Submitted to *Journal of Food Engineering*.

## References

- Mukprasirt, A., Herald, T.J., Boyle, D. L. & Rausch, K. D. (2000). Adhesion of rice flour-based batter to chicken drumsticks evaluated by laser scanning confocal microscopy and texture analysis. *Poultry Science*, 79(9), 1356-1363.
- Ngadi, M., Adedeji, A.A. & Kassama, L. (2008). Microstructural changes during frying of foods. In S. Sahin, S.G. Sumnu (Eds.), *Advances in deep-fat frying of foods* (pp. 169-200). Contemporary Food Engineering Series. CRC Press, Boca Raton.
- Pedreschi, F., Aguilera, J.M. & Brown, C.A. (2000). Characterization of food surfaces using scale-sensitive fractal analysis. *Journal of Food Process Engineering* 23, 127-143.
- Pedreschi, F., Aguilera, J.M. & Arbildua, J.J. (1999). CLSM study of oil location in fried potato slices. *Microscopy and Analysis* 39, 21-22.
- Pedreschi, F. & Aguilera, J.M. (2002). Some changes in potato chips during frying observed by confocal laser scanning microscopy (CLSM). *Food Science and Technology International*, 8(4), 197-201.
- Peighambardoust, S.H., van der Goot, A.J., van Vliet, T., Hamer, R.J. & Boom, R.M. (2006). Microstructure formation and rheological behaviour of dough under simple shear flow. *Journal of Cereal Science*, 43(2), 183-197.
- Pinthus, E.J., Weinberg, P. & Saguy, I.S. (1992). Gel-strength in restructured potato products affects oil uptake during deep-fat frying. *Journal of Food Science* 57, 1359-1360.
- Pinthus, E.J., Weinberg, P.A. & Saguy, I.S. (1993). Criterion for oil uptake during deep fat-frying. *Journal of Food Science* 58, 204-205.

## References

- Pinthus, E.J., Weinberg, P. & Saguy, I.S. (1995). Oil uptake in deep fat frying as affected by porosity. *Journal of Food Science*, 60(4), 767-769.
- Pinthus, E.J. & Saguy, I.S. (1994). Initial interfacial tension and oil uptake by deep-fat fried foods. *Journal of Food Science* 59, 804-807.
- Primo-Martín, C., van Nieuwenhuijzen, N.H., Hamer, R.J. & van Vliet, T. (2007). Crystallinity changes in wheat starch during the bread-making process: Starch crystallinity in the bread crust. *Journal of Cereal Science*, 45(2), 219-226.
- Rasband, W.S. (1997). ImageJ, National Institutes of Health, Bethesda, Maryland, USA, <http://rsb.info.nih.gov/ij/>.
- Rubnov, M. & Saguy, I.S. (1997). Fractal analysis and crust water diffusivity of a restructured potato product during deep-fat frying. *Journal of Food Science*, 62(1), 135-137. 154.
- Saguy, I. S. & Dana, D. (2003). Integrated approach to deep fat frying: engineering, nutrition, health and consumer aspects. *Journal of Food Engineering*, 56, 143-152.
- Saguy, I.S. & Pinthus, E.J. (1995). Oil uptake during deep-fat frying: factors and mechanism. *Food Technology* 49, 142-145. 152.
- Sanz, T., Salvador, A. & Fiszman, S.M. (2004). Effect of concentration and temperature on properties of methylcellulose-added batters. Application to battered fried seafood. *Food Hydrocolloids* 18, 127-131.
- Singh, R.P. (1995). Heat and mass transfer in foods during deep-fat frying. *Food Technology*, 49,134-137.

## References

- Sobukola, O. P., Dueik, V. & Bouchon, P. (2012). Understanding the effect of vacuum level in structure development and oil absorption in vacuum-fried wheat starch and gluten-based snacks. *Food Bioprocess Technology*, DOI: 10.1007/s11947-012-0899-1.
- Swedlow, J.R. (2007). Quantitative fluorescence microscopy and image deconvolution. *Methods in Cell Biology*, 81, 447-465. *Digital Microscopy*, 3rd Edition.
- Thanatuksorn, P., Pradistsuwana, C., Jantawat, P. & Suzuki, T. (2005). Effect of surface roughness on post-frying oil absorption in wheat flour and water food model. *Journal of Science and Food Agriculture*, 85(15), 2574-2580.
- Tromp, R.H., van de Velde, F., van Riel, J. & Paques, M. (2001). Confocal scanning light microscopy (CSLM) on mixtures of gelatine and polysaccharides. *Food Research International*, 34(10), 931-938.
- Ufheil, G. & Escher, F. (1996). Dynamics of oil uptake during deep-fat frying of potato slices. *Lebensmittel–Wissenschaft und Technologie* 29, 640-644.
- van Loon, W.A.M., Visser, J.E., Linssen, J.P.H., Somsen, D.J., Klok, H.J. & Voragen, A.G.J. (2007). Effect of pre-drying and par-frying conditions on the crispness of French fries. *European Food Research and Technology*, 225(5-6), 929-935.
- van de Velde, F., Weinbreck, F., Edelman, M.W., van der Linden, E. & Tromp, R. H. (2003). Visualisation of biopolymer mixtures using confocal scanning laser microscopy (CSLM) and covalent labelling techniques. *Colloids and Surfaces B: Biointerfaces*, 31(1-4), 159-168.
- Varela, G. (1988) Current facts about the frying of food. In: Varela, Bender & Morton (eds.) *Frying of Food: Principles, Changes, New Approaches*, Chichester: Ellis Horwood.



## References

Yamsaengsung, R., Ariyapuchai, T. & Prasertsit, K. (2011). Effects of vacuum frying on structural changes of bananas. *Journal of Food Engineering*, 106, 298-305.

Weegels, P.L., Groeneweg, F., Esselink, E., Smit, R., Brown, R. & Ferdinando, D. (2003). Large and fast deformations crucial for the rheology of proofing dough. *Cereal Chemistry*, 80(4), 424-426.

Zhou, X.B. & de Hosson, J.Th.M. (1995). Influence of surface roughness on the wetting angle. *Journal of Materials Research*, 10, 1984-1992.